2017

Investigation of Voltage Stability of Wind Rich Electric Power Systems

Kanchana Amarasekara
University of Wollongong

School of Electrical, Computer and Telecommunications Engineering

Investigation of Voltage Stability of Wind Rich Electric Power Systems

Kanchana Amarasekara, BSc(Eng)

Supervisors

Dr. Lasantha G. Meegahapola, Prof. Sarath Perera and Dr. Ashish P. Agalgaonkar

This thesis is presented as required for the

Award of the Degree of

Doctor of Philosophy

of the

University of Wollongong

August 2017

Dedicated to my parents...

Declaration

I, Kanchana Amarasekara, declare that this thesis, submitted in partial fulfillment of the requirements for the award of Doctor of Philosophy, in the School of Electrical, Computer and Telecommunications Engineering, University of Wollongong, is wholly my own work unless otherwise referenced or acknowledged. The document has not been submitted for qualifications at any other academic institution.

Kanchana Amarasekara

Date: 31 August 2017

Abstract

With the increasing penetration levels of wind power generation in power systems around the world, it is imperative to understand the impact of wind generators on power system dynamics and stability. Wind generators have distinct characteristics compared to synchronous generators used in conventional power systems, such as the intermittency and limited predictability of wind resources, and utilisation of asynchronous power generators and power electronic converters, which partially or fully decouple the mechanical and electromagnetic dynamics. Due to these distinct characteristics, wind generators can affect stability of existing networks in relation to voltage stability, frequency stability and rotor angle stability. Through a critical review of existing literature related to these areas, it was identified that there are significant research gaps related to voltage stability in wind rich networks, which is the focus of the work presented in this thesis.

The main consequence of voltage instability is the inability to meet the reactive power demand of power systems. Voltage stability is affected by the reactive power support available in a network, where generators are the main reactive power sources. Therefore, with the increased penetration levels of wind power generation in power systems, it is important to investigate the capabilities of wind generators to support the voltage stability.

Voltage stability of a power system is usually assessed using steady-state methods such as PV curves, VQ curves and QV modal analysis. These steady-state methods which inherently require less computational capability can indicate the level of stability of a power system. Therefore, VQ curves and QV modal analysis tools are used in the preliminary investigations of voltage stability in wind rich networks presented in this thesis. The importance of accurate representation of the reactive power capabilities of wind generators in voltage stability studies was emphasised in the analysis. Test systems integrated with doubly-fed induction generator (DFIG) based variable-speed wind generators (VSWGs), modelled in DIgSILENT Power Factory, are used to investigate the impacts of voltage control strategy, reactive power capabilities and

loading levels of the VSWGs on steady-state voltage stability. Moreover, the impact of synchronous generators and, DFIG and full-converter wind generator (FCWG) based VSWGs on steady-state voltage stability are compared.

Typically, placement of VSWGs in power systems depends on the availability of the wind resources. However, there can be a number of possible connection options available for integration of a wind farm to an interconnected power system. In the next phase, a method is developed which can aid the decision on identifying the optimal location of VSWGs, considering steady-state voltage stability of a network. QV modal analysis tool is used to identify strong and weak areas of a power system in terms of voltage stability. Also, VQ curves are used in the analysis.

Voltage stability is a dynamic phenomenon which is affected by the generator and load dynamics, time dependent control actions of power system components such as, excitation system controller, over-excitation limiters (OXLs), under-excitation limiters (UELs), transformers with on-load tap changers (OLTCs), and the response of reactive power compensation devices. Steady-state analysis methods are not capable of incorporating the dynamics of these components and hence, the steady-state analytical methods are not sufficient to accurately evaluate the voltage stability of a network. Therefore, dynamic simulations with accurate dynamic models of power system components have to be conducted to obtain more conclusive results. This led to the examination of dynamic voltage stability of wind rich networks, which is detailed in the thesis. Dynamic voltage instability phenomenon is usually categorised into two types: short-term voltage instability and long-term voltage instability. This classification is based on the different time frames over which the voltage instability is observed, depending on various power system components responding at different time frames. It is important to consider both short-term and long-term voltage stabilities in voltage stability studies. Therefore, this thesis investigates the impact of VSWGs integrated to an electricity network on both short-term and long-term voltage stabilities.

Long-term voltage stability is considered in the first phase of the dynamic voltage

stability analysis. Using a dynamic model of a test system developed in DIgSILENT Power Factory, the impact of DFIG and FCWG based VSWGs on long-term voltage stability is investigated. With increasing penetration levels of the renewable power generators in power systems, some of the existing synchronous generators will normally be retired. Therefore, it is vital to note that VSWGs will be replacing some of the existing synchronous generators in power systems. This factor has been extensively considered in the long-term voltage stability analysis presented in this thesis, which investigate the behaviour and the impact of VSWGs to support a network under such conditions. Two common mechanisms which can drive a network to long-term voltages instability are considered, and impact of VSWGs on those types of long-term voltage stability is evaluated. Furthermore, the impact of connection point of VSWG based wind farms and the loading level on long-term voltage stability are examined. In addition, the impact of DFIG and FCWG based wind generators on long-term voltage stability are compared.

Conducting complete dynamic simulations on large networks requires considerable time, effort and computational capability. Already well developed direct methods exists, which are alternative methodologies to evaluate system stability without explicitly solving differential equations which represent system dynamics. These methods are generally developed using energy function based techniques. The practical application of most of these methods are limited mainly due to the limitations in application of the methodologies for large interconnected networks which are represented using detailed models. A novel energy function based method is developed in this thesis to examine long-term dynamic voltage stability, which overcomes the aforementioned limitations, using the conventional energy function approach. The application of this method to a large interconnected network is illustrated using Reliability and Voltage Stability (RVS) test system. The application of the proposed method to evaluate the long-term voltage stability of a wind rich network is also demonstrated. One of the main applications of this method could be in online voltage security assessment.

The last part of this thesis focuses on the impact of VSWGs on short-term voltage stability, which is the second category of dynamic voltage stability. The main driving force of short-term voltage instability is the behaviour of dynamic loads, such as induction motors. Therefore, a test system model which includes VSWGs and significant induction motor loads is used in the studies. Two common mechanisms which can drive a power system to short-term voltage instability are considered, and the impact of VSWGs on short-term voltage stability is examined. Impact of different loading level of VSWGs on short-term voltage stability is also examined. Moreover, the impact of DFIG and FCWG based VSWGs on short-term voltage stability are compared.

Acknowledgments

It is my pleasure to express my sincere gratitude to all those who helped me in numerous ways during my PhD candidature.

First, I wish to express my sincere gratitude to my principal supervisor, Professor Sarath Perera of University of Wollongong, for giving me the opportunity to pursue my postgraduate studies at the University of Wollongong and for his continuous support, guidance and encouragement. Thank you for being a great mentor to my academic, professional and career life.

Besides my principal supervisor, I would like to express my sincere gratitude to my co-supervisor Dr. Lasantha Meegahapola of RMIT University for his continuous guidance and encouragement. I highly appreciate his tremendous support to my research, being away from University of Wollongong during the latter part of my PhD candidature. Without your support and encouragement, I would not have been able to complete my thesis. I am also grateful to my co-supervisor Dr Ashish Agalgaonkar for his support, guidance and encouragement to complete this thesis.

This research has been conducted with the support of the Australian Government Research Training Program Scholarship, I wish to acknowledge the Commonwealth contribution in pursuing my postgraduate studies.

Also, I wish to thank all APQRC (Australian Power Quality and Reliability Centre) and SECTE (School of Electrical Computer and Telecommunication Engineering) staff for their generous support at various occasions. Very special thanks to all research colleagues at the APQRC and friends at the University of Wollongong for their friendships and great support.

Last, but not least, my heartiest gratitude goes to my husband, who moved to Wollongong with me sacrificing some of his own dreams, for his tremendous support, love and patience. I would like to extend my heartiest gratitude to my parents, brother and sister for their unconditional love and encouragement. You are my guiding lights and the pillars of my success.

List of Principal Symbols and Abbreviations

AVR	Automatic voltage regulator
DAE	Differential-algebraic-equations
DFIG	Doubly-fed induction generator
FACTS	Flexible alternating current transmission systems
FCWG	Full-converter wind generator
GSC	Grid-side converter
IEEE PES	Institution of Electrical and Electronic Engineering: Power and Energy Society
MSC	Machine-side converter
OLTC	On-load tap changer
OXL	Over-excitation limiter
PCC	Point of common coupling
PMU	Phasor measurement units
QSS	Quasi-steady-state
RSC	Rotor-side converter
RVS	Reliability and Voltage Stability
SVC	Static-VAr-Compensator
UEL	Under-excitation limiter
VSWG	Variable-speed wind generator
WRIG	Wound-rotor induction generator

β	pitch angle
Id_ref	d-axis current reference
Iq_ref	q-axis current reference
i_{rd}, i_{rq}	rotor current referred to stator
i_{sd}, i_{sq}	stator current
i_{sd}, i_{sq}	stator current
J	inertia constant
L_l	Stator leakage inductance
L_{ld}	d-axis damper winding leakage inductance
L_{lf}	rotor leakage inductance
L_{lq}	q-axis damper winding inductance
L_{ls}, L_{lr}	stator leakage inductance and rotor leakage inductance referred to stator
L_m	mutual inductance
L_{md}	d-axis magnetising inductance
L_{mq}	q- axis magnetising inductance
λ_{sd}, λ_{sq}	stator flux
λ_{rd}, λ_{rq}	rotor flux
P	generator active power measurement
P_ref	active power reference
Pt	mechanical(turbine) power
Qg_ref	grid-side converter reactive power reference

Qr_ref	rotor-side converter reactive power reference
Qref	reactive power reference
R_a	stator resistance
R_d	damper winding resistance
R_e	field winding resistance
R_r	rotor resistance
R_s	stator resistance
R_s, R_r	stator and rotor resistances
T_e	electromechanical torque
T_m	mechanical torque
Udc	DC link voltage
Vac	voltage at point-of-common coupling
v_{rd}, v_{rq}	rotor voltages referred to stator
Vs	stator voltage
v_{sd}, v_{sq}	stator voltages
ω	generator speed
ω_d	grid frequency
ω_{dA}	grid frequency - rotor electrical frequency
X_m	magnetising reactance
X_s	stator reactance
X_r	rotor reactance

Publications Arising from the Work Presented in this Thesis

1. H.W.K.M. Amarasekara, L. Meegahapola, A.P. Agalgaonkar, S. Perera, "Impact of Renewable Power Integration on VQ Stability Margin," in *Proc. Australasian Universities Power Engineering Conference (AUPEC 2013)*, Tasmania, Australia, October 2013

2. H.W.K.M. Amarasekara, L. Meegahapola, A.P. Agalgaonkar, S. Perera, "Investigation of Load Driven Long-Term Voltage Instability Phenomenon with Wind Generation," in *Proc. Australasian Universities Power Engineering Conference (AUPEC 2015)*, Wollongong, Australia, September 2015

3. H.W.K.M. Amarasekara, L. Meegahapola, A.P. Agalgaonkar, S. Perera, "Impact of Variable-Speed Wind Power Generators on Short-Term and Long-Term Voltage Stability," in *Proc. 14th International Workshop on Large-Scale Integration of Wind Power into Power Systems as well as on Transmission Networks for Offshore Wind Power Plants*, Brussels, Belgium, October 2015

4. H.W.K.M. Amarasekara, L. Meegahapola, A.P. Agalgaonkar, S. Perera, "Placement of Variable-Speed Wind Power Generators in Power Systems Considering Steady-State Voltage Stability," in *Proc. IEEE International Conference on Power System Technology (PowerCon) 2016* , Wollongong, Australia, September, 2016

5. H.W.K.M. Amarasekara, L. Meegahapola, A.P. Agalgaonkar, S. Perera, "Characterisation of Long-Term Voltage Stability with Variable-Speed Wind Power Generation," *IET Generation, Transmission and Distribution*, vol.11, no.7, pp.1848-1855, 2017.

Contents

List of Figures

List of Tables

Chapter 1

Introduction

1.1 Statement of the Problem

The global renewable energy penetration level is growing rapidly due to reasons such as the environmental concerns to develop clean energy, concerns for energy security and need for reduced energy prices. According to [1], it is estimated that renewables, including hydro-power provide 23.7% of the global electricity. The renewable energy generation levels in some countries, such as Germany, Scotland, Ireland, Denmark and Iceland are very high and it is reported that the instantaneous renewable power generation in some countries/regions, such as South Australia was 100% during certain periods [2–4]. Among different renewable energy sources utilised around the globe, wind power is one of the most widely used technologies. According to [5], wind power represents 15.6% of the total installed power capacity in Europe.

In conventional power systems, electrical power is generated using synchronous generators, driven by thermal turbines. However, with the increased wind power generation levels in the power systems, the traditional generation pattens are seen to be constantly changing. One major difference in wind power generation compared to conventional generation, is the intermittency and limited predictability. Wind power generation utilises asynchronous generators and/or power electronic converters. Wind power generators are usually located in the locations, where wind resources are available and, such sites are usually located far away from the load cen-

tres. In addition, the utilisation of power electronic converters and/or small power generators for wind generators will significantly affect the the system inertial response. Due to these distinctly different characteristics of wind power generation, it is imperative to investigate the impact of these generators on power system dynamics and stability. The investigations in the literature, such as [6–8] indicate that the wind power generation can affect the power system stability in all types including voltage stability, rotor angle stability and frequency stability. Furthermore, wind power generation can also affect the quality of power supply, system fault levels and protection systems [9].

Voltage Stability is defined as "the ability of a power system to maintain steady voltages at all buses in the system after being subjected to a disturbance from a given initial operating condition" [10]. As per the theoretical aspects associated with voltage stability phenomenon, the main consequence of voltage instability is the inability of power systems to meet the reactive power demand [11]. The voltage stability is affected by the reactive power support available in a power network, where generators are the main reactive power sources of the network. Therefore, with the increased penetration levels of wind power generation in power systems, it is important to investigate the capabilities of wind generators to maintain voltage stability. Factors, such as the location of wind generators far away from the load centers would also affect the voltage stability, as it can affect the network losses, hence the power flows.

Voltage stability of a power network is generally assessed by the steady-state methods, such as PV curves, VQ curves and QV modal analysis. These static methods require less computational capability which can indicate the level of stability of a power network. Therefore, these methods can be used for preliminary investigation of the voltage stability in wind rich networks. However, voltage stability is a dynamic phenomenon. The network voltage stability is affected by the generator and load dynamics, time dependent control actions of power system components such as, excitation system controller, over-excitation limiters (OXLs), under-excitation

limiters (UELs) and transformers with on-load tap changers (OLTCs), and the response of reactive power compensation devices. The steady-state analysis methods are not capable of incorporating the dynamics of these components and hence, the steady-state analysis methods are not sufficient to accurately evaluate the voltage stability of a network. Therefore, dynamic simulations with accurate dynamic models of the power system components have to be conducted to derive more conclusive results [12]. In such case, dynamic voltage stability analysis is essential to accurately assess the voltage stability of wind rich networks.

The dynamic voltage instability phenomenon is usually categorised into two types: short-term voltage instability and long-term voltage instability. This classification is based on the different time frames over which the voltage instability is observed, depending on differing responses associated with various power system components. The dynamic loads such as, induction motors can drive a power network to voltage instability in a few seconds after a fault. However, system components such as, OLTCs and OXLs have long term dynamics and they will respond typically over minutes following a disturbance. Due to these factors, it is important to consider both short-term and long-term voltage instabilities in voltage stability studies. It is imperative to investigate how inclusion wind generation to an electricity network impact both of these types of dynamic voltage instabilities.

Conducting complete dynamic simulations for large networks demands considerable time, effort and computational capabilities. In the past, researchers have developed various direct methods for dynamic stability analysis of power networks. These are alternative methodologies to evaluate system stability without explicitly solving differential equations which represent system dynamics, which are generally developed using energy function based techniques. However, the practical application of most of these methods are limited mainly due to the limitations in application of the methodologies to large interconnected networks which are represented using detailed models. Therefore, developing novel direct methods for stability evaluation, which can be conveniently applied to large interconnected networks is highly

relevant in the case of evolving power systems.

Due to the growing renewable power penetration levels in power networks, system dynamics are rapidly changing and also, becoming less predictable and less reliable. Hence, real-time security assessment is very crucial in current power systems to maintain the stability and reliability. Real-time security assessment can be one of the applications of the direct methods. Due to these concerns, developing novel direct methods for voltage stability evaluation is highly relevant. Direct methods for dynamic voltage stability evaluation can also be used to verify the system responses derived from the dynamic simulations.

1.2 Research Objectives and Methodologies

The main aim of this thesis is to investigate the voltage stability in wind rich power networks addressing key research gaps. For the purpose of fulfilling the above aim, the following research gaps were identified, following an extensive literature review:

1. Most of the existing work in this topic is limited to steady-state voltage stability evaluation, and have not considered crucial system conditions and some important characteristics of the power system components. Variable-speed wind power generators (VSWGs), which are the the most commonly used wind generators have not been considered in most of the existing work, where the accurate characteristics will be crucial for deriving accurate conclusions.

2. Limited studies exist, which investigate the dynamic voltage instability in wind rich networks considering the complete dynamic models of VSWGs and other power system components.

3. Limited methods exist in the literature for direct voltage stability evaluation, which can be applied to wind rich power networks.

The main objectives of the proposed research are as follows:

- to conduct a complete investigation of steady-state voltage stability in networks with VSWGs by accurately representing the VSWGs and their characteristics;

- to investigate the impact of VSWGs on dynamic voltage stability considering both the short-term and long-term voltage stability phenomena, utilising complete dynamic models of a power network and dynamic simulations; and

- to develop a direct stability evaluation method for dynamic voltage stability assessment, which can be conveniently applied to large interconnected wind rich power networks.

Computer-aided modelling and simulation are the main approaches used in power system stability evaluation. In this research, well-known power system simulation tool DIgSILENT Power Factory was used for conducting simulation studies.

In the preliminary steady-state voltage stability assessment, well- known steady-state voltage stability analysis tools VQ curves and QV modal analysis are used. These methods are developed based on power flow studies. The accurate characteristics of VSWGs, synchronous generators, loads and other power system components are incorporated in the various simulations of the test systems.

In the dynamic voltage stability evaluation of wind rich networks, both short-term and long-term dynamic simulations were conducted using DIgSILENT Power Factory. In conducting dynamic simulations, appropriate dynamic models of important power system components, such as synchronous generators and their controllers, VSWGs, dynamic loads such as induction motors and, transformer OLTCs were utilised.

In the development of a direct method for dynamic voltage stability assessment, the corresponding basic mathematical model was verified using a simple two bus network, which was implemented in DIgSILENT Power factory using DIgSILENT simulation language(DSL). The proposed methodology was applied to a large interconnected network to verify the results of dynamic simulations in wind rich networks.

1.3 Outline of the Thesis

A brief summary of the contents in the remaining thesis chapters is provided in this section.

Chapter 2 provides a comprehensive review of the existing literature on the research topic and identifies research gaps which need to be filled through further research. It starts with a review of basics of wind power generation and various different generation technologies utilised to harness wind power. The basic theoretical aspects related to voltage stability and existing steady-state voltage stability tools are reviewed. The existing studies on steady-state analysis in wind rich networks are critically reviewed to identify the research gaps. The basics of the dynamic voltage instability phenomenon are reviewed with a comparative analysis of various different instability mechanisms which can lead a power network to dynamic voltage instability. The distinct methods available for dynamic voltage stability assessment are reviewed. The existing literature on energy function approach for voltage stability analysis as a direct method for voltage stability analysis is reviewed. The available literature on dynamic voltage stability analysis of wind rich networks is critically reviewed to identify the gaps in the existing work. In voltage stability studies, utilisation of suitable models of various power system components is crucial. Hence, the existing literature on developing suitable models of power system components for voltage stability studies is reviewed.

Chapter 3 presents the outcomes of steady-state voltage stability analysis of electricity networks containing VSWGs. VQ curves and QV modal analysis techniques are utilised in the steady-state voltage stability analysis. The steady-state voltage stability of a network with doubly-fed induction generator (DFIG) based wind generation is evaluated considering factors such as generator voltage control strategy and reactive power capabilities. Impact of the VSWGs and synchronous generators on power system voltage stability are compared. A method for placement of VSWGs in networks to improve the voltage stability is developed.

Chapter 4 investigates the impact of VSWGs on long-term voltage stability.

The dynamic models of the VSWGs utilised in this thesis are explained. A detailed long-term voltage stability analysis with DFIG and full-converter wind generator (FCWG) based VSWGs are conducted, utilising complete dynamic model of a test system and dynamic simulations. Two mechanisms, which can lead a network to long-term voltage instability are considered in the studies and the impact of DFIG and FCWG based wind generation on these two types of instabilities are investigated. Moreover, the behaviour of DFIG and FCWG based VSWGs on long-term voltage stability is compared. This chapter also evaluates the impact of different wind generator loading levels on long-term voltage stability. Furthermore, the impact of DFIG wind generation on long-term voltage stability in electricity networks containing induction motors is also evaluated.

Chapter 5 presents an alternative methodology for the verification of long-term dynamic voltage stability in power systems in general with some emphasis on wind rich systems. A novel energy function method for voltage stability evaluation is introduced for long-term dynamic voltage stability evaluation. The basic theoretical derivations of the proposed energy function approach are detailed using a simple two bus network. The extension of this method to a large network is explained using Reliability and Voltage Stability (RVS) test system. The application of the proposed method to evaluate the long-term dynamic voltage instability of a power network with wind generation is illustrated using some of the case studies presented in Chapter 4.

Chapter 6 investigates the impact of VSWGs on short-term voltage stability, which is one of the other sub-classifications of dynamic voltage stability. The impact of DFIG based wind generation on the short-term voltage stability is investigated considering two instability mechanisms which can lead a power system to short-term voltage instability. Impact of the loading levels of VSWGs on short-term voltage stability is examined. Moreover, the impact of DFIG and FCWG based wind generators on short-term voltage stability are compared.

Chapter 7 summaries the conclusions of the thesis and provides recommendations

for future work.

Chapter 2

Literature Review

2.1 Overview

This chapter presents a review of the literature related to wind power generation, different wind power generation technologies, voltage stability, methods for static and dynamic voltage stability evaluation, and the voltage stability analysis in power systems integrated with wind power generation. The existing work in these areas are critically reviewed to identify the gaps in the existing research with a view to conduct further research.

2.2 Wind Power Generation

2.2.1 Basics of Wind Power Generation

The mechanical power (in watts) harvested by a wind turbine (P_m) is given by (2.1) [7],

$$P_m = \frac{1}{2}\rho {v_w}^3 \pi r^2 C_p(\lambda) \tag{2.1}$$

where,

ρ - air density (kg/m^2)

r - radius of the blade (m)

v_w - wind speed (m/s)

C_p - performance coefficient

λ - tip speed ratio

The tip speed ratio is given by (2.2),

$$\lambda = \frac{\omega r}{v_w} \tag{2.2}$$

where ω is the rotor speed (radians/s). The C_p represents the power captured by the wind turbine from the available power in the wind. According to (2.1), the power captured by a wind turbine can be maximised by maximising C_p. However, C_p has a theoretical maximum of 0.593 governed by the Betz's law [7] and C_p depends on λ and blade pitch angle. Fig. 2.1 shows the typical variation of C_p with λ for a fixed pitch angle.

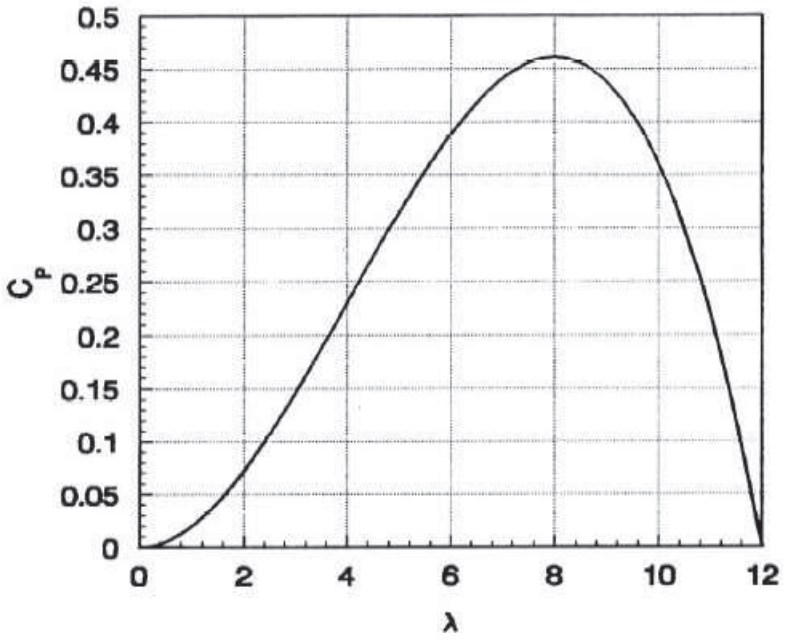

Figure 2.1: The variation of C_p with λ [13]

As shown in Fig. 2.1, performance coefficient peaks at a particular tip-speed ratio, hence if the rotor speed of the wind turbine is constant, C_p peaks only at

a particular wind speed. The early wind turbines equipped with squirrel-cage induction generators were operated at almost constant rotor-speed. Therefore, the performance coefficient and hence, the efficiency peaks at a particular wind speed. Therefore, the fixed-speed wind turbine generators do not operate at maximum efficiency at all wind speeds. Therefore, the focus of subsequent development of wind turbine generators was to improve the efficiency of power extraction of the wind turbines over a range of wind speeds which led to the development of variable-speed wind generators.

In VSWGs, the rotor speed is controlled with the wind speed to operate the wind turbine at maximum C_p to extract maximum power. Fig. 2.2 shows the variation of turbine output with the turbine speed and wind speed. The VSWGs are operated to extract maximum power over a range of wind speeds.

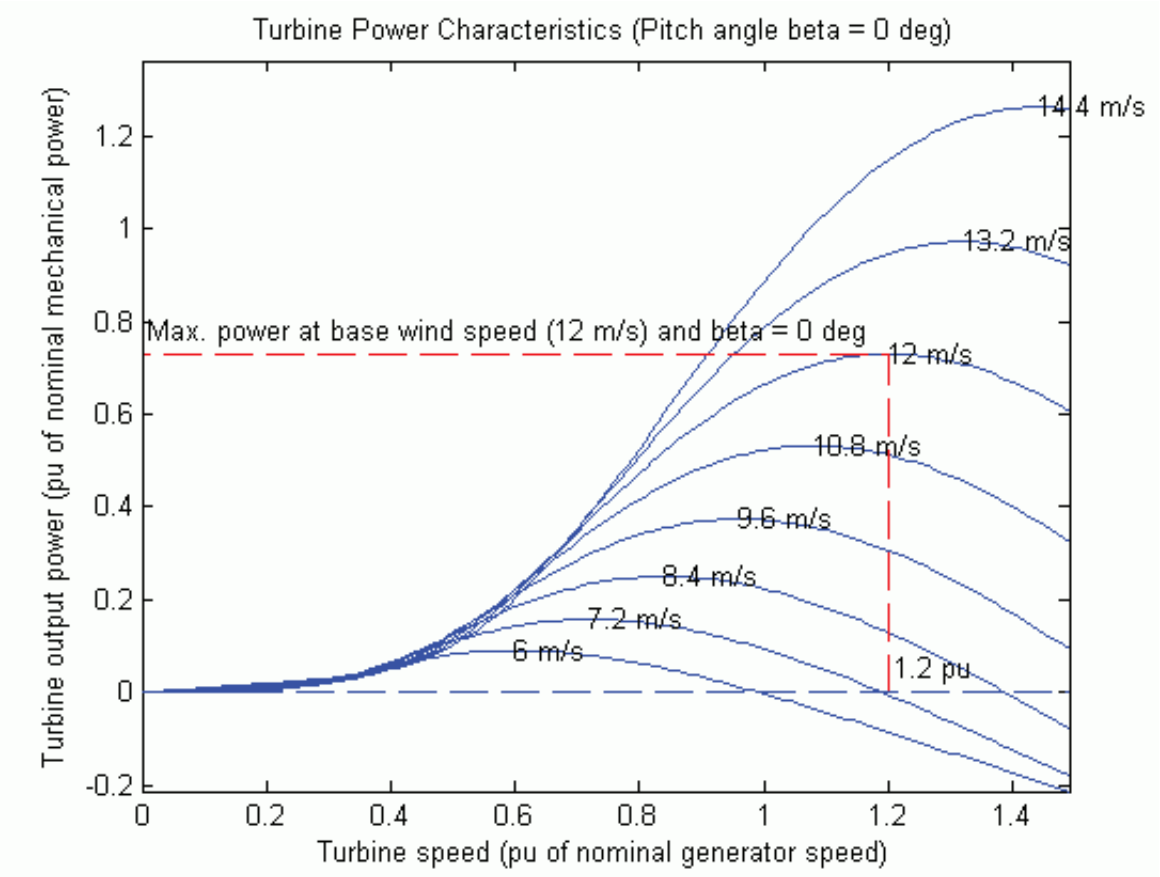

Figure 2.2: The variation of turbine output power Vs. turbine speed [14]

Modern wind turbines have a operating wind speed range depending on the wind turbine design. Fig. 2.3 shows the typical variation of power output of a wind turbine. Typically, there is a cut-in speed (about 5 m/s) above which the wind turbine will operate. For wind speeds above the cut-in speed up to the rated wind speed, the power output will increase. At wind speeds above the rated wind speed (rated power output), the pitch control will limit the output power. Wind turbine will completely cut-out beyond the cut-out wind speed (about 25 m/s).

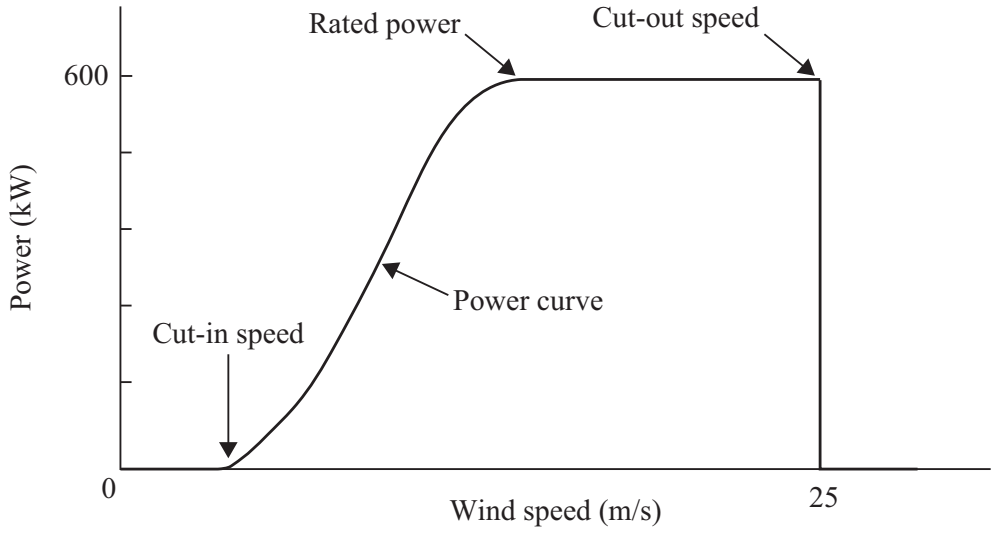

Figure 2.3: A typical power curve of a wind turbine (600 kW) [9]

2.2.2 Wind Power Generator Technologies

The commercially available wind generators are usually categorised in to four categories [7];

- **Type 1**: Squirrel-cage induction generator based fixed-speed wind generators

  Fig. 2.4 shows a schematic of a type 1 wind generator. This type represents the typical fixed-speed wind power generation based on squirrel-cage induction generator. The generator is directly connected to the grid. These type of induction generators can supply active power to the grid. However, they absorb reactive power from the grid for excitation. These wind generators

are usually equipped with capacitor banks at the point of common coupling (PCC) to compensate for the reactive power absorption from the grid, and to minimise the detrimental effects on the grid voltage [15].

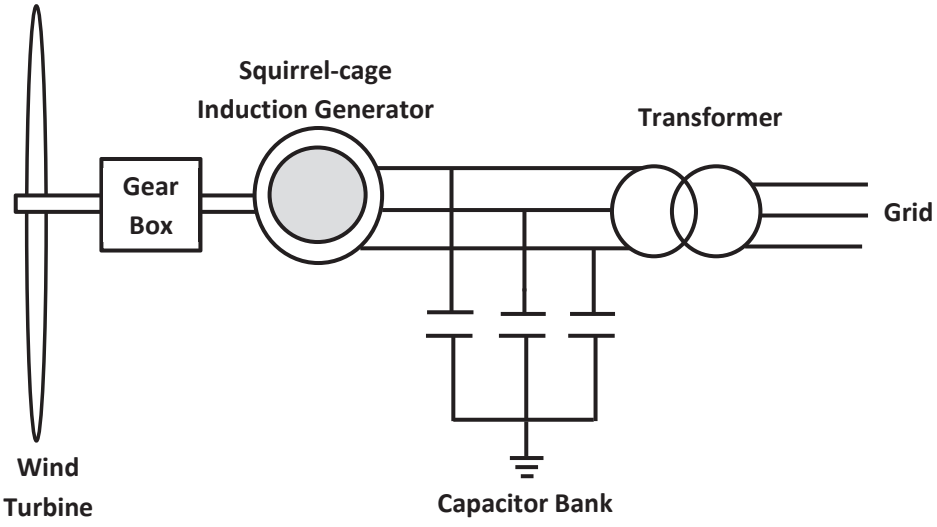

Figure 2.4: Schematic of type 1 wind generator

- **Type 2**: Wound rotor induction generator based wind generator with limited speed variation by utilising an external resistor

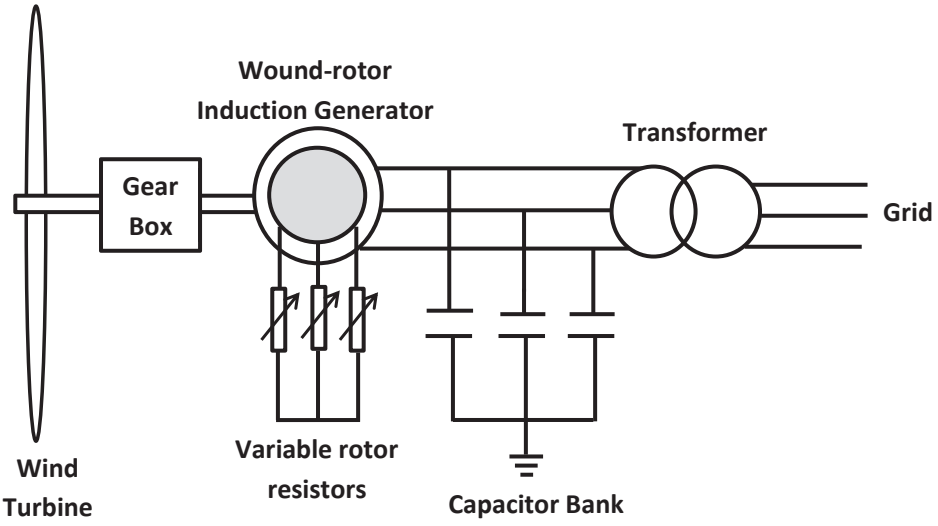

Figure 2.5: Schematic of type 2 wind generator

Fig. 2.5 shows a schematic of a type 2 wind generator, equipped with wound-

rotor induction generator and external variable rotor resistors. About 10% of speed variation is achieved by utiling the external rotor resistors and hence, these wind generators are partly variable-speed wind geneartors. These generators also consumes some reactive power from the grid and hence the capacitor banks are used at the PCC for reactive power regulation.

- **Type 3**: Doubly-fed induction generator based wind generators

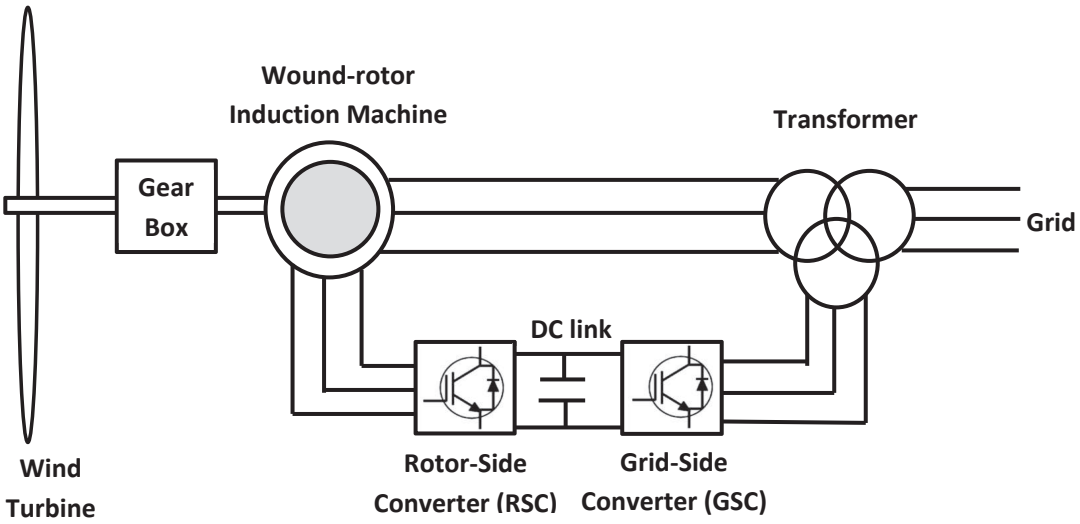

Figure 2.6: Schematic of type 3 wind generator

Fig. 2.6 shows a schematic of a type 3 wind generator. These variable-speed wind generators utilise a wound-rotor induction generators. The stator is directly connected to the grid and the rotor is connected to the grid via back-to back power electronic converters. Therefore, the net power output of the generator is the sum of power transfers through both the stator and the rotor. The back-to-back power electronic converters are usually, rated for 30% - 50% of the generator rating, depepending on the manufacturer. The machine can operate in both sub-synchronous and super-synchronous speeds. The active power is injected through the rotor to the grid during super-synchronous mode of operation and active power is absorbed by the rotor from the grid during the sub-synchronous mode of operation.

- **Type 4**: Permanent magnet synchronous generator or induction generator based full-converter wind generator

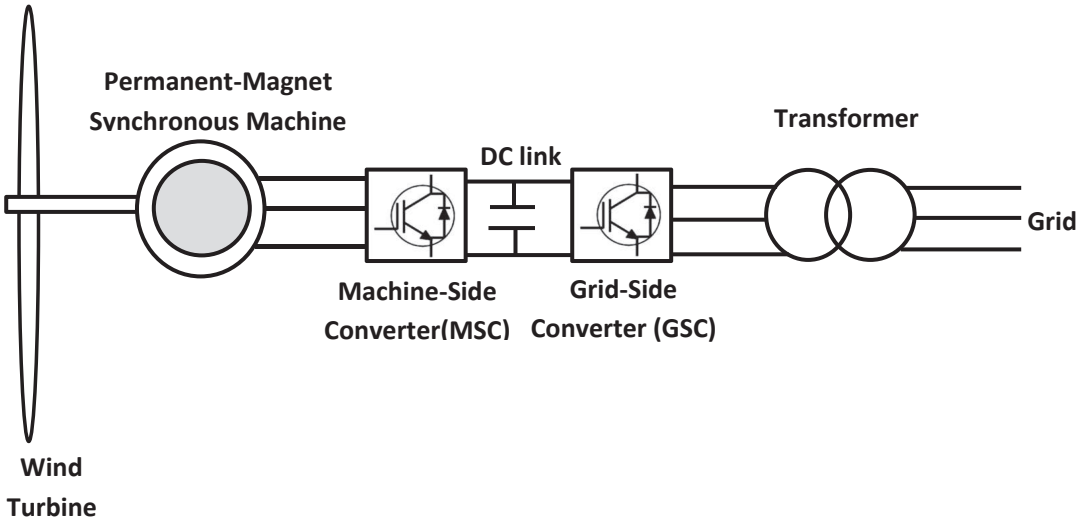

Figure 2.7: Schematic of type 4 wind generator

Fig. 2.7 shows a schematic of a type 4 wind generator. This variable-speed wind generator utilises either induction generator or synchronous generator and the stator is connected to the grid via full-scale power electronic converters. The utilisation of permanent-magnet synchronous generators facilitate gearless design of these type of wind generators.

2.3 Voltage Stability

According to [10], voltage stability is defined as "the ability of a power system to maintain steady voltages at all buses in the system after being subjected to a disturbance from a given initial operating condition". As per the theoretical aspects associated with voltage stability phenomenon, the main consequence of voltage instability is the inability of power systems to meet the reactive power demand [11].

The voltage instability can result sudden or progressive drop/rise in voltages of the busbars in a power system. The outcome of voltage stability can be loss of loads or tripping of transmission lines and/or generators or even a system-wide blackout.

The rotor angle instability, in which the rotor angles of the synchronous generators go out-of-step losing the synchronism, can also result in progressive drop of bus voltages. It should be noted that voltage instability refers to a situation when the rotor angle stability is not an issue [10].

The term voltage collapse is also used in conjunction with voltage instability and, according to [10], the voltage collapse is defined as "the process by which the sequence of events accompanying voltage instability leads to a blackout or abnormally low voltages in a significant part of the power system".

The voltage stability is classified into different categories based on different criteria as shown in Fig.2.8.

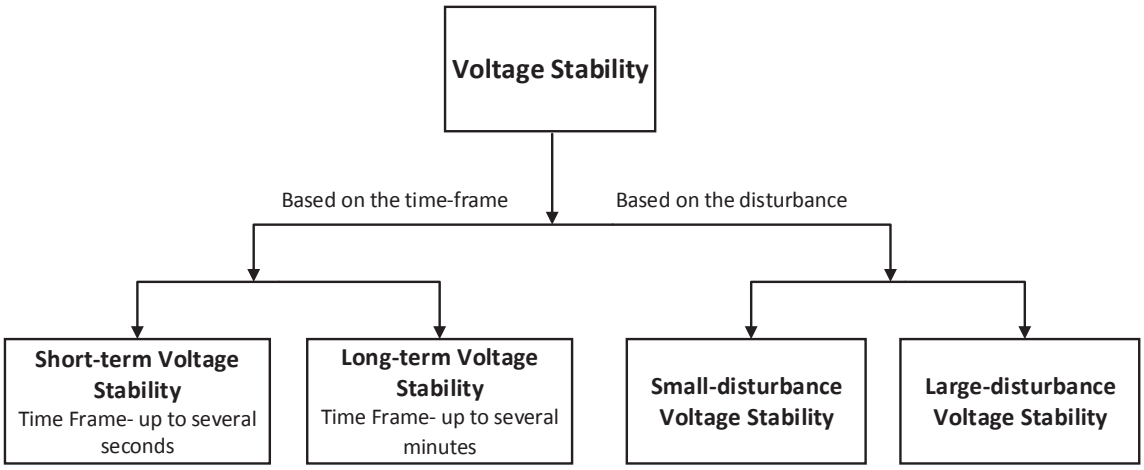

Figure 2.8: Classification of voltage stability

Voltage stability is generally a slow process and the system voltages may experience a large, progressive drop of voltage in few seconds or minutes after a disturbance [16]. Different authors have classified the dynamic phenomenon of voltage instability and collapse based on different time frames [17, 18]. Dynamic voltage instability phenomenon can be basically categorised into two categories:

- Short-term (transient) voltage instability - Typically, the major driving force of this type of instability is the behaviour of dynamic loads, such as induction motor loads after a disturbance. The time frame is up to several seconds.

- Long-term voltage instability - This type of instability usually involves a large disturbance and/or increase in load or increase in power transfer level [18]. It involves slow dynamic responses such as OLTC operation and OXL operation. Time frame is up to several minutes.

Furthermore, voltage stability phenomenon can be also categorised into two categories based on the type of disturbance involved as follows [10]:

- Large-disturbance voltage stability - Large-disturbance voltage stability is the ability to maintain steady voltages at the busbars, following large disturbances, such as system faults, loss of generation or system contingencies.

- Small-disturbance voltage stability - Small-disturbance voltage stability is the ability to maintain steady voltages at the busbars, following small perturbations, such as incremental change of the system load.

Moreover, voltage stability can be explained as either static or dynamic voltage stability, in general. Based on this voltage stability analysis methods are usually categorised into two categories:

- Steady-state (Static) Voltage Stability Analysis - Steady-state analysis is based on the power flow based techniques. In many cases, static analysis is used to assess voltage stability. The methods used for static analysis are explained in Section 2.4.

- Dynamic Voltage Stability Analysis - Steady-state methods do not consider system dynamics, such as generator dynamics, load dynamics and the time dependent control actions, such as the operation of OLTC and OXL. Therefore, steady-state analysis methods are not sufficient to accurately evaluate the voltage stability of a network [10,12]. Dynamic voltage stability analysis using dynamic simulations need to be conducted utilising dynamic models of power system components to derive more reliable results. All voltage stability types explained in Fig. 2.8 belong to dynamic voltage stability category, where

time-domain analysis is vital in analysing these types of voltage stabilities. The dynamic voltage stability analysis is explained in Section 2.6.

2.4 Methods for Steady-state Voltage Stability Assessment

Steady-state voltage stability is assessed using power flow based methods such as PV curves, VQ curves and QV modal analysis. In the following sections, those steady-state methods are discussed in detail.

2.4.1 PV Curves

A PV curve for a busbar is obtained by increasing the total active power of a load connected to a busbar or total load in an area, by conducting a series of power flow calculations at different snapshots. The voltage and the active power at each snapshot is recorded, and the power factor is maintained constant during the process.

Fig. 2.9 shows a typical PV curve. Up to the operating point O', voltage decreases, as the active power of the load demand increases. As the active power demand increases, the system generation has to be also increased to meet the demand. However, beyond the point O', as the demand increases, voltage decreases. The operating point O' is the critical operating point (nose point), and it corresponds to the maximum power transfer limit. Beyond this critical point, power flow will not converge, and techniques, such as continuation power flow can be used to obtain the operating points beyond the critical point [19].

If system operates at the operating point O, the active power distance between O and O' is known as the PV voltage stability margin. The PV voltage stability margin provides an indication on the proximity of a certain operating point to the voltage instability point.

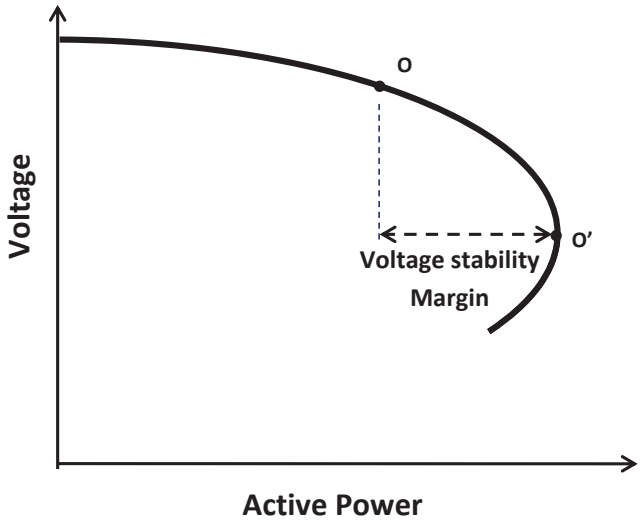

Figure 2.9: A typical PV curve

2.4.2 VQ Curves

The VQ curve can be obtained by connecting a fictitious synchronous condenser to the test bus and by varying reactive power over a range while recording the bus voltage [20]. A series of power flow simulations are conducted and the reactive power and voltage are recorded at different snapshots. Fig. 2.10 shows a typical VQ curve drawn for a busbar.

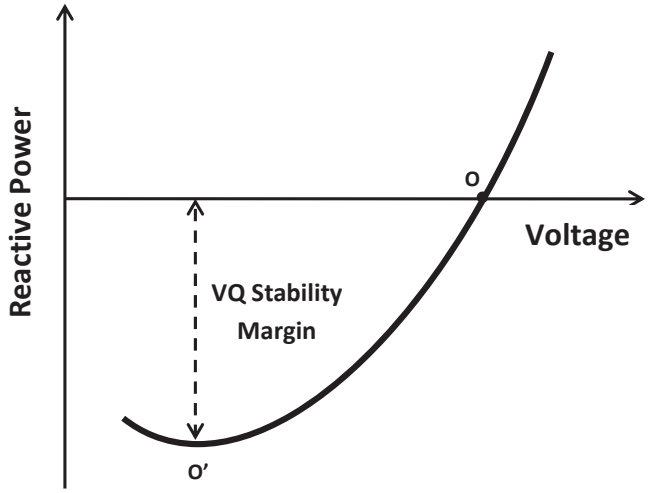

Figure 2.10: A typical VQ curve

The reactive power distance between the operating point (O) and the minimum point (O') of the VQ curve is known as the VQ voltage stability margin. It can give an indication on the proximity of a certain operating point to voltage instability.

2.4.3 QV Modal Analysis

The QV modal analysis method is described in [11,21]. This method can be used to investigate the system-wide voltage stability and to identify the areas with potential voltage stability problems.

As per Newton-Rapson method of power flow solution, the linearised power system model is given by,

$$\begin{bmatrix} \triangle P \\ \triangle Q \end{bmatrix} = \begin{bmatrix} J_{P\theta} & J_{PV} \\ J_{Q\theta} & J_{QV} \end{bmatrix} \begin{bmatrix} \triangle \theta \\ \triangle V \end{bmatrix} \tag{2.3}$$

where,

$\triangle P$- incremental change in active power

$\triangle Q$- incremental change in reactive power

$\triangle \theta$- incremental change in voltage angle

$\triangle V$- incremental change in voltage

If the active power is constant, $\triangle P$=0 and hence, (2.3) can be reduced to,

$$\triangle Q = J_R \triangle V \tag{2.4}$$

where,

$$J_R = J_{QV} - J_{Q\theta} {J_{P\theta}}^{-1} J_{PV} \tag{2.5}$$

According to the QV modal analysis, J_R which is known as the reduced Jacobian matrix can be used to analyse the voltage stability of the power system J_R.

Let,

$$J_R = \xi \Lambda \eta \tag{2.6}$$

where,

ξ- right eigen-vector matrix

Λ- left eigen-vector matrix

η- diagonal eigenvalue matrix

According to the matrix algebra,

$$I = \xi \Lambda \tag{2.7}$$

Using (2.6) and (2.7), (2.4) can be written as,

$$\triangle V = J_R^{-1} \triangle Q \tag{2.8}$$

$$\triangle V = \xi \Lambda^{-1} \eta \triangle Q \tag{2.9}$$

$$\triangle V = \sum_i \frac{\xi_i \eta_i}{\lambda_i} \tag{2.10}$$

where,

ξ_i- i $^{\text{th}}$ column right eigen-vector

η_i- i $^{\text{th}}$ row left eigen-vector

λ_i- i $^{\text{th}}$ eigenvalue

Each eigen value λ_i, corresponding right eigenvector and left eigen-vector define the i^{th} mode of stability.

(2.9) can be rearranged as,

$$\eta \triangle V = \eta \Lambda^{-1} \triangle Q \tag{2.11}$$

Let, $V{=}\eta\triangle V$ and $Q{=}\eta\triangle Q$. Then, (2.11) can be written as,

$$V = \Lambda^{-1} Q \tag{2.12}$$

Therefore, for the i$^{\text{th}}$ mode,

$$V_i = \frac{1}{\lambda_i} Q_i \tag{2.13}$$

The relationship between the eigenvalues and the voltage stability can be explained using (2.13). If $\lambda_i > 0$, V_i and Q_i vary in the same direction, which means the voltage and reactive power in the i^{th} mode vary in the same direction. Therefore, the network voltage is stable. If $\lambda_i < 0$, V_i and Q_i vary in opposite directions. Therefore, the network voltage is unstable. $\lambda_i = 0$ is the critical condition and voltage collapse could occur in the network.

The participation factor of bus k to mode i is given by,

$$P = \xi_{ki} \eta_{ki} \tag{2.14}$$

Bus participation factors indicate the information on the participation of bus k to the mode i. Participation factors can provide information on voltage stability of an area in a power system, associated with a certain mode. It can be used to identify whether a certain mode is localised or not localised, which can provide a better idea about the system condition.

When the eigenvalues are computed for a certain operating condition of a system, the mode with the lowest eigenvalue is considered to be the most critical mode. Bus participation factors provide an indication on the contribution of each busbar to this critical mode. The busbar with the highest participation factor contributes the

most towards the voltage collapse, and is considered as the weakest busbar in the system.

2.5 Steady-state Voltage Stability Analysis with Wind Power Generators

Due to the increasing wind power penetration levels in the power systems, it is important to evaluate its impact on power system voltage stability. Various studies have been conducted in [6, 22–28] to evaluate the steady-state voltage stability in power systems integrated with wind power generators.

The steady-state voltage stability of a wind rich network is evaluated utilising time series power flow techniques in [6]. It shows that the voltage stability margin of the power system can be increased through proper implementation of voltage control strategies in wind turbines. The study in [22], utilises an optimisation framework for proper coordination between VSWGs and other reactive power controllers in a network to enhance the steady-state voltage stability.

The Impact of DFIG based wind generation on voltage stability in transmission networks is studied in [23] considering the intermittency of wind generation and different penetration levels. A voltage collapse proximity indicator VCPI, based on network loadability is used. Although, the voltage stability has improved at low penetration levels, it was not found to provide better voltage stability at high penetration levels. The work in [23] also shows that connecting wind generation at multiple locations is better compared to a single location. However, less emphasis has been given to accurately represent the reactive power capability of the wind generators. In [24], it is shown that the adverse voltage stability effects can be mitigated by using reactive power regulation capability of DFIG based wind generation.

In [25], a voltage stability analysis has been conducted for a weak regional network with high wind power penetration levels. Simple induction generator based wind generation is considered and the possibility of operating an electric power sys-

tem beyond the traditional voltage stability limits by utilising a static VAr compensator (SVC) in the power system with the wind power generation is demonstrated. However, in this work, power electronic converter based VSWGs have not been considered.

The power system behaviour with large wind penetration is analysed for a 69 bus test system with fixed-speed and DFIG based wind power generation using modal analysis and dynamic simulations in [26] and [27]. It is demonstrated that, although flexible AC transmission system (FACTS) controllers are used with wind generation to improve the voltage control capabilities and to enhance power system stability, interactions among FACTS devices can reduce power system dynamic performance. The study also concludes that over compensation for reactive power can lead to dynamic instability. In [28], a new technique called Wind Integration Factor is introduced for evaluating the performance of wind farms with different capacities integrated at different locations. This method is developed using VQ voltage stability margin. It can be used to decide the suitable location and optimal penetration level of wind energy resources.

Some drawbacks of the studies in [6, 22–27] are; non use of the most widely used VSWGs in the studies and/or no accurate representation of the reactive power capabilities of the wind generators. Moreover, due to the increasing penetration levels of the renewable power generation in power systems, the existing conventional power generators are usually replaced by wind generators. Hence, it is imperative to compare the impact of wind generators and the conventional generators on steady-state voltage stability, which has not been examined in the existing literature.

Few studies in the literature [29–32] have considered the placement of wind generators in power networks considering the voltage stability. A wind farm placement method to improve static voltage stability margin is developed in [29] using continuation power flow method, which shows that voltage stability can be enhanced by maximizing the loading parameter. In [30], a procedure for efficient placement and operation of STATCOMs and storage systems, for improvement of static voltage

stability margin in power systems with embedded wind generation, is presented. A wind probability density function is used to derive the most probable level of the wind farm output power. The power injection share and the optimal power factors of each STATCOM and energy storage system are calculated at each wind power level to improve the voltage stability margin. The main focus of the study is on placement of STATCOMS and storage devices in networks with wind generation.

Few studies in the literature have utilised QV modal analysis and VQ curves to develop methodologies for optimal placement of wind generation considering voltage stability. In [28,29], a new method using QV modal analysis and VQ curves, has been developed to increase the level of wind penetration by integrating wind generators at strong busbars. It also shows that placing static var compensators in the weak busbars in the system can help to have higher the wind power penetration levels. A method to find the optimum level of wind penetration and the optimum point of wind energy integration using a technique called wind integration factor is introduced in [30]. It shows that higher wind penetration levels could be achieved by integrating wind through strong busbars.

However, these studies do not present any comprehensive methodology for placement of VSWGs Some of the drawbacks of these studies are: not considering the different types of VSWGs and their reactive power capabilities.

2.6 Dynamic Voltage Instability Phenomenon

2.6.1 Instability Mechanisms

As explained in Section 2.3, the dynamic voltage instability phenomenon is usually categorised into two types; short-term voltage stability and long-term voltage stability.

The main influencing factors of short-term voltage instability are the behavior of dynamic loads, such as induction motors. The behaviour of HVDC links is another example. In [16], three mechanisms, which can lead a power system to short-term

voltage instability are explained. These mechanisms are listed in Table 2.1.

Long-term voltage instability involves the responses of the components, such as OLTCs, OXLs and characteristics of loads, such as thermostatically controlled loads. The mechanisms, which can drive a system to long-term voltage instability have also been classified into three categories in [16], as illustrated by Table 2.2.

In addition to the mechanisms which drive power systems to short-term and long-term voltage instabilities, additional three mechanisms are listed in [16] under the category of short-term instability caused by long-term dynamics. This category illustrates the mechanisms which can lead a network to short-term instability, following a long-term voltage instability. The ultimate result is the short-term voltage instability, however, it is caused by long-term voltage instability. Due to the nature of this type of instability, it can be observed in long-term and hence often considered as long-term voltage instability, as described in [17]. Three different instability mechanisms as explained in [16], are summarised in Table 2.3 .

Table 2.1: Different mechanisms which can lead a power system to exhibit short-term voltage instability

Type	**Cause**	**Description**
Type ST-1	Loss of post-disturbance equilibrium of short-term dynamics	Typical case of this type of instability is the induction motor stalling after a disturbance, such as a loss of one transmission line in two parallel transmission lines, which increases the total transmission impedance. Due to the increase in the impedance, the motor mechanical and electrical torques may not be able to reach a stable post-disturbance equilibrium, which results in motor stalling, and the subsequent short-term voltage instability.
Type ST-2	Lack of attraction toward the stable post-disturbance equilibrium of short-term dynamics	A typical case of this type of instability is the stalling of induction motors after a short-circuit. Induction motors may not be able to re-accelerate after a network fault, if the motor is heavily loaded or in the cases of slow network fault clearing.
Type ST-3	Oscillatory instability of the post-disturbance equilibrium	This type of instability is rare. A typical example is generator-motor oscillations, due to interactions between them in short-term. This mainly arises due to the interactions caused by induction motor load restoration and the voltage regulation of the automatic voltage regulator (AVR) of synchronous machines [33].

Table 2.2: Different instability mechanisms which can lead a power system to long-term voltage instability

Type	**Cause**	**Description**
Type LT-1	Through loss of equilibrium of the long-term dynamics	This is the most typical instability mechanism. As a result of this type of voltage instability, the voltage will stabilise at a low voltage, due to the load-tap changer limitation [17].
Type LT-2	Through lack of attraction towards stable long-term equilibrium	This type of instability is caused by delayed corrective actions, such as switching of shunt compensation or load shedding.
Type LT-3	Through slowly growing voltage oscillations	According to [16], this type of instability has not been observed in real power systems. However, this type of voltage instability would cause long-term voltage oscillations which arises due to cascaded load restoration.

Table 2.3: Different instability mechanisms which can lead a power system to short-term voltage instability induced by long-term dynamics

Type	**Cause**	**Description**
Type S-LT-1	Loss of short-term equilibrium caused by long-term dynamics	Following the slow degradation of the voltage due to long-term voltage instability, a sudden transition caused by short-term dynamics can lead to voltage collapse. It can be caused by the loss of synchronism of synchronous generators or due to stalling of induction motors [17].
Type S-LT-2	Loss of attraction to the stable short-term equilibrium due to the shrinking region of attraction caused by long-term dynamics	A random parameter variation or a discrete transition can trigger short-term instability.
Type S-LT-3	Oscillatory instability of the short-term dynamics caused by long-term dynamics	This type of voltage instability occurs in systems with both voltage and electromechanical oscillation problems.

2.6.2 Dynamic Voltage Stability Asessement

In dynamic voltage stability assessment, the system dynamics have to be considered, accompanying the controllers of the generators (i.e. governors, excitation system) and the associated controls (such as OXL), the load dynamics and the time varying control actions (such as OLTC operations). The models of these controllers have to be considered in the dynamic analysis. The models of different power system components and the network dynamics can be modelled using a set of differential-algebraic equations (DAEs). However, there are many components in a power network and, hence the total number of DAEs will be very large in number. The system response can be derived by numerical integration. However, due to the large number of DAEs, it is computationally very difficult. Therefore, methods, such as quasi-dynamic simulation methods have been utilised for time domain simulation in the past [34, 35]. In quasi-dynamic simulation, a series of load-flow simulations are conducted along the trajectory of the voltage instability, considering different system components responding at different time scales. However, these simulations do not represent system dynamics as in dynamic simulation.

Quasi-steady-state simulation (QSS) is another method that is used to simplify time domain simulation. In QSS, it is assumed that a fast subsystem is infinitely fast and the short-term dynamics are at equilibrium when dealing with slow systems (long-term analysis). Furthermore, it is also assumed that the slow variables remain at constant during fast transients, when dealing with fast systems (short-term analysis) [15, 17, 36].

With the modern well-developed computer technology, it is feasible to run complete dynamic simulations, with a time step suitable for capturing both short-term and long-term dynamics.

2.7 Energy Function Analysis for Voltage Stability Studies

Energy function method has been historically used as a direct method to analyse the system transient stability without explicitly solving differential equations for the system dynamics. This method was developed based on Lyapunov's second method and has been used to determine the stability of non-linear systems with time-dependent controls.

Physical interpretation of the energy function method for transient stability evaluation can be explained as follows: A power system operates at a stable operating point before a fault occurs. During a power system fault, the equilibrium is disturbed and synchronous machines accelerate due to electrical and mechanical power imbalance. During the fault, the power system gains kinetic energy and potential energy. Following the fault clearance, the post-disturbance system should be capable of absorbing this energy to avoid instability. Ability to absorb this transient energy depends on the potential energy absorbing capability of the post-disturbance system. For a given post-disturbance network, there is a maximum or critical amount of energy that can be absorbed by the network in order to avoid instability. In order to evaluate system transient stability, the total system energy at the instant of fault clearing should be calculated which has to be compared with the critical energy of the post-disturbance system. If the total energy gained is larger than the critical energy, the system will be unstable, and vice versa [11].

Use of energy function based methods to determine voltage collapse in power systems is introduced in [37–40]. In [37], an energy based proximity measure to voltage collapse is developed. The energy distance between the high and low voltage power flow solutions is used as an proximity indicator to voltage collapse. After finding the high voltage (stable) and low voltage (unstable) power flow solutions for each operating point, the energy function can be calculated for each bus to determine the proximity to voltage collapse.

In the energy function based method applied to examine voltage stability, a stable operating point is considered as the minimum of the potential energy well.

However, system perturbations can push the system operating point away from the stable operating point. The minimum energy required for the system to become unstable (i.e., escape from energy well) is the potential energy of the closet unstable equilibrium point. The unstable equilibrium point corresponds to the low voltage power flow solution. Therefore, the energy difference between the current stable operating state and the corresponding low voltage power flow solution is used as a proximity indicator to voltage collapse [38]. In [38], a method has been developed to reduce the vulnerability to voltage collapse using the energy function and its sensitivity to control actions (such as generator and controls and transformer taps). In energy function method applied to voltage stability, determination of the low voltage power flow solution is crucial. In [39], an algorithm is developed for faster determination of the appropriate low voltage power flow solution. The work in [40], demonstrates the further extension of the of energy function method for online voltage security assessment and in contingency analysis. Subsequent work in [41,42] also explains the utilisation of this method.

In [41], a method is developed to determine energy function for a power system when HVDC links are involved. It also explains the use of energy function analysis for transient and voltage collapse analysis. In [42], the voltage collapse problem is addressed as a general transient stability problem, and a stability region that guarantees voltage stability is defined using an energy function approach. The IEEE PES technical report [43] provides a review of the energy function method for voltage stability assessment and a graphical illustration for the energy function analysis for voltage stability using a potential energy well is provided. An energy function based method is used in [44], in which generalised energy function has been used for voltage stability analysis of a multi-machine system and voltage stability is assessed using the energy margin between the high voltage and low voltage power flow solutions.

Some of the recent publications on the energy function method focus on the transient stability assessment using energy function method and the extension of the method to incorporate the dynamics of various power system components. Recently

published book [45] discusses the possibility of the application of structure preserving energy functions in wide-area monitoring systems using PMU data with the inclusion of renewable generation and FACTS devices, where the main focus is given to the transient stability.

As stated earlier, identifying the low voltage power flow solution is imperative in using the well-known energy function method for voltage stability analysis, which has been a major area of interest in some of the work published. A method to identify the critical low voltage solution using tangent vector method is discussed in the recent work [46]. Energy function based online coordinated voltage control scheme is introduced in [47].

The usual transient or voltage stability analysis using the time domain simulation demands extensive computational capability, time and effort due to the requirement to conduct numerical integration of nonlinear differential and algebraic equations, which define the system dynamics. The stability evaluation process is relatively intensive for large interconnected network studies, since a large number of scenarios have to be studied in order to evaluate the overall system stability. The main advantage of using energy function methods is that, it can be used as a direct stability assessment technique, which requires less computational capability, time and effort. However, one of the drawbacks in the approach for voltage stability assessment using energy function method is the accurate identification of the critical low voltage power flow solution for large interconnected networks. Furthermore, incorporating the characteristics of various power system components is also another constraint.

2.8 Dynamic Voltage Stability Analysis with Wind Power Generators

Limited number of studies exist, which analyse the dynamic voltage stability in the presence of wind power generators.

A structural voltage stability analysis of a power system with induction generator based wind generators is presented in [48]. A DAE model is developed for the system and the proximity to voltage collapse is monitored using a method based on singular-value decomposition, which is also used to determine the suitable locations for adding new equipment or load shedding. In [49], the large disturbance voltage stability is evaluated with geographically dispersed wind resources. A new voltage stability index is developed based on VQ stability margin and VQ trajectory. The study shows that the voltage stability in the areas with high penetration levels of either conventional generators or wind generators is improved. However, the areas with high penetration levels of both wind and conventional generators exhibits detrimental voltage stability behaviour. A case study of voltage stability of large-scale wind generation integrated into weak power network is presented in [50]. PV analysis is used to identify the requirement for some transmission line upgrades. Voltage instability and oscillations were observed in the dynamic voltage stability analysis. The study compares the capability of compensation devices, such as SVC, synchronous condenser and the variable frequency transformer to improve voltage stability issues.

There are few studies in the literature, which analyse the short-term voltage stability associated with wind power generation. The work in [51] shows that the voltage collapse can be delayed by proper control of VSWGs, and wind generators connected to distribution level along with loads can improve the short-term voltage stability. However the VSWGs are modelled as negative loads. In the study in [52], it is shown that the post-disturbance voltage profile can be improved by damping of oscillations and by reducing the overshoot, through proper utilisation of reactive power capability of DFIGs.

The work in [53] shows that the operating wind farms in voltage control mode is preferable, particularly for remote areas to mitigate voltage dips, using a case study of the Belgian power system. The work in [26] evaluates the dynamic behavior of power systems with high wind penetration levels containing FACTS devices. The

study reveals that increased compensation provided by FACTS devices can reduce the security limits, thus limiting the maximum level of wind generation that can be integrated.

The long-term voltage stability in networks with wind power generation is evaluated in [54–57]. The impact of DFIG and FCWG based wind generation on long-term voltage stability is evaluated using dynamic simulation in [54]. The study results demonstrate that the increased penetration levels of VSWG based wind generation is beneficial for long-term voltage stability. It is also revealed that the DFIGs can supply more reactive power to the system compared to FCWGs, when the GSC of the DFIG controls the reactive power. Impact of different DFIG control modes on the voltage stability is studied in [55] using dynamic simulations and it is shown that operating the DFIG in voltage control mode improves voltage stability.

In [56], a wind speed model is incorporated into to a dynamic model to examine long-term voltage stability using stochastic differential equations and a theoretical formulation is proposed to assess long-term voltage stability providing faster computational speed. In [57], a method for optimal capacity allocation of wind generators using voltage stability constrained optimal power flow is introduced. The method improves the loadability margin in the network by proper allocation of wind capacity.

Some of the drawbacks of the studies presented in the literature, which examine dynamic voltage stability in networks with wind power generation include; that proper dynamic models of the wind power generators are not utilised and disregard the impact of replacement of conventioanl generators with wind generators.

It is imperative to carry-out comprehensive studies on the impact of VSWGs on dynamic voltage instability, considering all relevant factors. The recent black system event in South Australia, which was primarily caused due to a dynamic voltage instability issue, occurred following several low voltage ride through events of a number of wind farms, further confirms the practical importance of such studies [58].

2.9 Power System Modelling for Voltage Stability Studies

2.9.1 Reactive Power Capabilities of Generators

The reactive power capability of generators is one of the crucial factors which affect the voltage stability of a power system. Essentially, the voltage stability of a power system is directly affected by the reactive power support available in the network, where generators act as main reactive power sources. Therefore, reactive power capability of generators is essential in maintaining the voltage stability of a network.

- Synchronous Generators -

  The generator reactive power capability is limited by the armature and field current limits, due to the maximum current that the armature and the field windings can carry continuously without overheating. In addition, the localised heating in the end region of the armature limits the synchronous generator capability in the under-excited operation. The capability chart of a typical synchronous machine (hydrogen-cooled steam turbine driven generator) is shown in Fig. 2.11 [11].

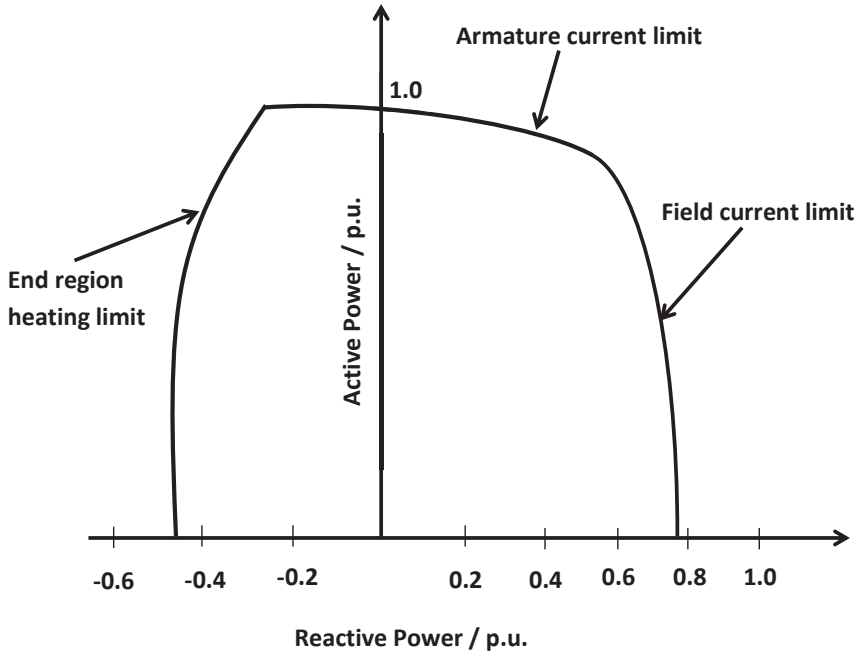

Figure 2.11: Capability chart of a typical synchronous generator

- Wind Generators -

  In a DFIG, the RSC of a DFIG directly controls the reactive power flow from the stator of the DFIG to the grid. The main parameters which define the reactive power capability of the DFIG are stator current, rotor current and rotor voltage [59]. The stator current limit is governed by the WRIG, and rotor voltage and rotor current are governed by both WRIG and the power-electronic converters. The GSC can also provide reactive power independently of the active power exchanged through the back-to-back converters. Hence, both RSC and GSC have to be considered in describing the reactive power capability of a DFIG.

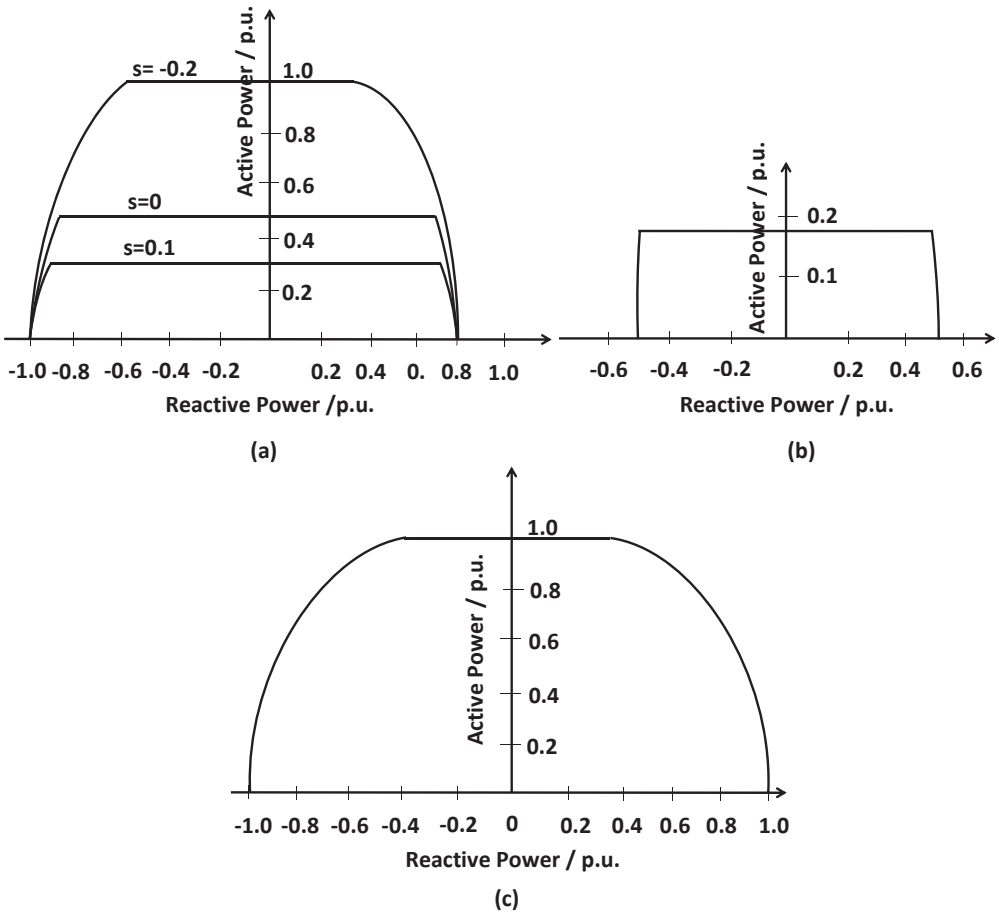

Figure 2.12: (a) Capability chart of a DFIG - stator with RSC control (b) Capability chart of a DFIG - GSC (c) Capability chart of a FCWG

Fig. 2.12 (a) and (b) show the two capability curves considering the RSC and GSC operations(base MVA- induction generator rating) [60]. As illustrated, the reactive power capability of the DFIG with RSC control depends on the active power output and the operating slip. Fig. 2.12 (c) shows a typical capability chart of a FCWG. When the full reactive power capability of a DFIG is considered by incorporating the reactive power support through both stator and the GSC, the DFIG has a relatively higher reactive power capability than the FCWG, as illustrated by the capability charts in Fig. 2.12(c).

It should be noted that the reactive power capability indicated by the capability chart is static (continuous) capability. It can be observed that a synchronous machine has a comparatively high reactive power capability at all active power levels (loading), whereas the DFIG (capability through stator) and the FCWG reactive power capabilities significantly vary with the generator loading levels. However, these VSWGs will not operate at maximum active power level most of the times due to the low wind speeds, and will have large capability to provide reactive power support.

2.9.2 Load Modelling

Load modelling is important in voltage stability studies [61,62]. Voltage dependency of the loads has to be modelled accurately.

Voltage dependent loads

- Exponential Load Model -

  The well known exponential load models are represented by (2.15) and (2.16);

$$P = P_0 \left(\frac{V}{V_0} \right)^{\alpha} \tag{2.15}$$

$$Q = Q_0 \left(\frac{V}{V_0} \right)^{\beta} \tag{2.16}$$

where P_0, Q_0 and V_0 are initial active power, reactive power and voltage respectively, and α and β are load exponents. Three most commonly used loads are,

- Constant power load : $\alpha = \beta = 0$
- Constant current load : $\alpha = \beta = 1$
- Constant impedance load : $\alpha = \beta = 2$

The load exponents for some widely used loads are listed in Table 2.4 [16, 20].

Table 2.4: Load exponents of some typical loads

Load type	α	β
Incandescent lamps	1.54	-
Room air conditioner	0.5	2.5
Furnace fan	0.08	1.6
Battery charger	2.59	4.06
Fluorescent lighting	1	3
Small industrial motors	0.1	0.6
Large industrial motors	0.05	0.5
Resistive space heater	2	0

- Polynomial Load Model -

  For more accurate representation of power system loads, the loads can be modelled as polynomial functions. A polynomial load model is composed of different types of loads with different voltage characteristics. A polynomial load can be represented in the form of (2.17) and (2.18)

$$P = P_0 \left[a1 \left(\frac{V}{V_0} \right)^{\alpha 1} + b1 \left(\frac{V}{V_0} \right)^{\beta 1} + c1 \left(\frac{V}{V_0} \right)^{\gamma 1} \right] \tag{2.17}$$

$$Q = Q_0 \left[a1 \left(\frac{V}{V_0} \right)^{\alpha 2} + b1 \left(\frac{V}{V_0} \right)^{\beta 2} + c1 \left(\frac{V}{V_0} \right)^{\gamma 2} \right] \tag{2.18}$$

where a1+b1+c1= 1.

The most common type of polynomial load is the ZIP load model, which composes of constant power, constant current and constant impedance loads.

- Induction motors -

  Induction motors are one of the most widely used power system load, particularly in industrial environments. The equivalent circuit of a simple induction motor is shown in Fig. 2.13, where R_s, X_s, R_r, X_r and X_m are stator resistance, stator reactance, rotor resistance, rotor reactance and magnetising reactance, respectively.

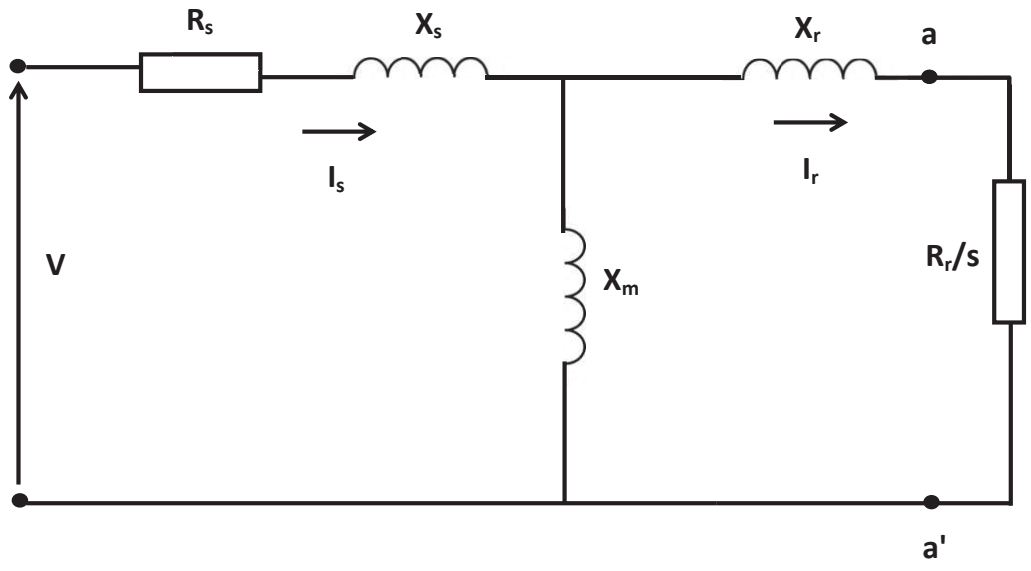

Figure 2.13: The equivalent circuit of an induction motor

Thevenin equivalent voltage and impedance across aa' looking towards the supply can be given by (2.19) and (2.20)

$$V_{TH} = \frac{VX_m}{\sqrt{R_s^2 + (X_s + X_m)^2}} \tag{2.19}$$

$$R_{TH} + jX_{TH} = \frac{(R_s + jX_s)jX_m}{R_s + jX_s + jX_m} + jX_r \tag{2.20}$$

The rotor current (I_R) and the electromagnetic torque (T_e) can be given by (2.21) and (2.22),

$$I_R = \frac{V_{TH}}{\sqrt{(R_{TH} + \frac{R_r}{s})^2 + (X_{TH})^2}} \tag{2.21}$$

$$T_e = \frac{{I_R}^2 R_r}{s} = \frac{{V_{TH}}^2 \frac{R_r}{s}}{\left(R_{TH} + \frac{R_r}{s}^2\right) + {X_{TH}}^2} \tag{2.22}$$

2.9.3 Dynamic Modelling of Variable-speed Wind Generators

This section explains the modelling of electrical components in VSWGs covering DFIGs and FCWGs. Vector control techniques are used in the control of the associated power electronic converters, which allows the decoupled active and reactive power control.

- Doubly-fed Induction Generators -

  In a DFIG, the RSC controls the active and reactive power flow from the stator to the grid by controlling the currents injected to the rotor. The GSC regulates the DC link voltage of the back-to-back converters by providing a path for the active power flow and it can also provide additional reactive power support to the grid.

  Dynamic modelling of DFIG wind generators is extensively explained in the literature [7, 63, 64]. A model of a DFIG represented in d-q reference frame is shown in Fig. 2.14, where v_{sd}, v_{sq} are stator voltages, v_{rd}, v_{rq} are rotor voltages referred to stator, λ_{sd}, λ_{sq} are stator fluxes, λ_{rd}, λ_{rq} are rotor fluxes referred to

stator, i_{sd}, i_{sq} are stator currents, i_{rd}, i_{rq} are rotor currents referred to stator, and R_s, R_r, L_{ls}, L_{lr}, L_m are stator resistance, rotor resistance, stator leakage inductance, rotor leakage inductance referred to stator and mutual inductance, respectively [7].

Using Fig. 2.14 [7], let, $L_s = L_{ls} + L_m$ and $L_r = L_{lr} + L_m$.

Hence, the stator and rotor flux equations can be given by,

$$\lambda_{sd} = L_s i_{sd} + L_m i_{rd} \tag{2.23}$$

$$\lambda_{sq} = L_s i_{sq} + L_m i_{rq} \tag{2.24}$$

$$\lambda_{rd} = L_r i_{rd} + L_m i_{sd} \tag{2.25}$$

$$\lambda_{rq} = L_r i_{rq} + L_m i_{sq} \tag{2.26}$$

d and q axis stator voltages can be given by,

$$v_{sd} = R_s i_{sd} - \omega \lambda_{sq} + \frac{d\left(\lambda_{sd}\right)}{dt} \tag{2.27}$$

$$v_{sq} = R_s i_{sq} + \omega \lambda_{sd} + \frac{d\left(\lambda_{sq}\right)}{dt} \tag{2.28}$$

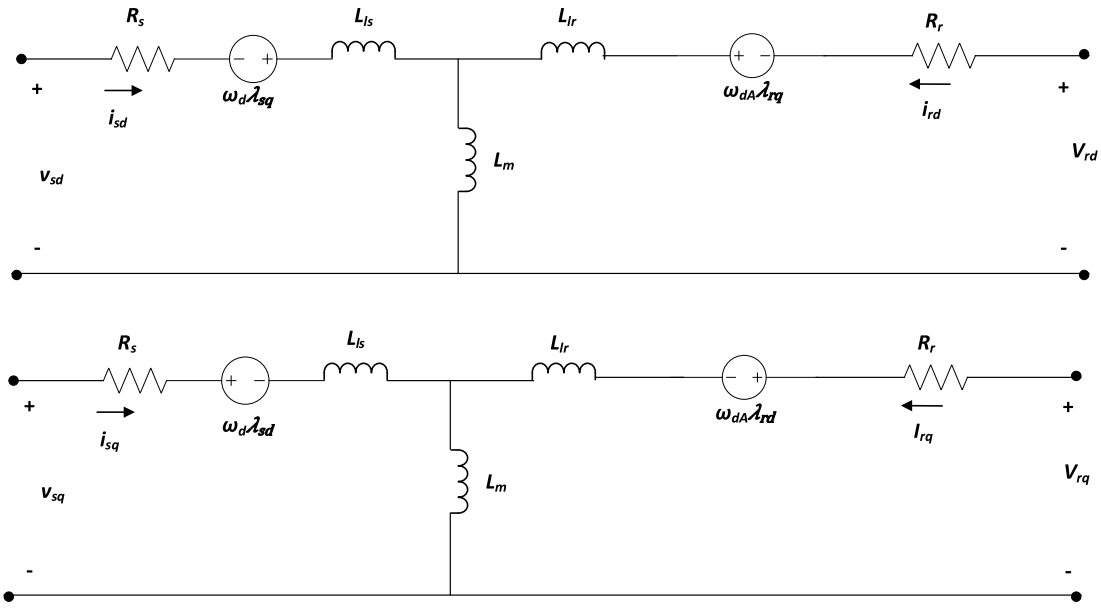

Figure 2.14: DFIG equivalent circuits (referred to stator)for d-axis and q-axis

d and q axis rotor voltages can be given by,

$$v_{rd} = R_r i_{rd} - \omega_{dA}\lambda_{rq} + \frac{d\left(\lambda_{rd}\right)}{dt} \tag{2.29}$$

$$v_{rq} = R_r i_{rq} + \omega_{dA}\lambda_{rd} + \frac{d\left(\lambda_{rq}\right)}{dt} \tag{2.30}$$

In designing the controllers for RSC, the voltage associated with transients in stator flux linkages are neglected, assuming that the variations in the grid voltage is small. Therefore, the rotor voltage equations (2.27) and (2.28) can be simplified as,

$$v_{sd} = R_s i_{sd} - \omega\lambda_{sq} \tag{2.31}$$

$$v_{sq} = R_s i_{sq} + \omega\lambda_{sd} \tag{2.32}$$

In the analysis in d-q reference frame, two control methods are widely used

based on the selection of the alignment of d and q axes;

- stator flux oriented control - d-axis is aligned with the stator flux vector. Therefore, λ_{sq}=0 and v_{sd}=0.
- stator voltage oriented control - d-axis is aligned with the stator voltage vector. Therefore, v_{sq}=0.

Using (2.23) and (2.24),

$$i_{sd} = \frac{\lambda_{sd}}{L_s} - \frac{L_m}{L_s} i_{rd} \tag{2.33}$$

$$i_{sq} = \frac{\lambda_{sq}}{L_s} - \frac{L_m}{L_s} i_{rq} \tag{2.34}$$

Active power from the stator P_s can be given by,

$$P_s = v_{sd} i_{sd} + v_{sq} i_{sq} \tag{2.35}$$

Considering the flux oriented control, λ_{sq}=0 and v_{sd}=0 hence,

$$P_s = -\frac{L_m}{L_s} v_{sq} i_{rq} \tag{2.36}$$

According to (2.36), the stator active power depends q-axis stator voltage and q-axis rotor current. It is independent of the d-axis rotor current.

Reactive power supplied by the stator, Q_s can be given by,

$$Q_s = v_{sq} i_{sd} - v_{sd} i_{sq} \tag{2.37}$$

Considering flux oriented control, λ_{sq}=0 and v_{sd}=0 hence,

$$Q_s = v_{sq} \left(\frac{\lambda_{sd}}{L_s} - \frac{L_m}{L_s} i_{rd} \right) \tag{2.38}$$

Substituting from (2.32) and assuming the voltage drop across the stator is negligible,

$$Q_s = \frac{{v_{sq}}^2}{\omega_s L_s} - \frac{L_m}{L_s} v_{sq} i_{rd} \tag{2.39}$$

According to (2.39), stator reactive power depends on q-axis stator voltage and d-axis rotor current. It is independent of the q-axis rotor current. As shown by (2.36) and (2.39), the active and reactive power from the stator can be independently controlled by the q-axis rotor current and the d-axis rotor current, respectively.

- Full-converter Wind Generators -

  Dynamic modelling of FCWG based wind generators is explained in the literature, such as [65, 66]. In FCWG, MSC controls the active power flow to the grid. It can also control the stator voltage. Instead of active power control, MSC can control the DC link voltage, as the active power can be transfered to the grid as long as the DC link voltage is constant. The GSC usullay controls the reactive power flow and the DC link voltage. Instead of controlling DC link voltage, it can control the active power flow as they are closely related.

  synchronous generator models for d-axis and q-axis are shown in Fig. 2.15 and 2.16, where, R_a, L_l, R_e,L_{lf}, L_{ld}, L_{md}, R_d, L_{lq} and L_{mq} are stator resistance, stator leakage inductance, field winding resistance, rotor leakage inductance, d-axis damper winding leakage inductance, d-axis mutual inductance, damper winding resistance q-axis damper winding inductance and q-axis mutual inductance. The model includes the stator winding, field winding (d-axis), and the damper windings (d-axis and q-axis).

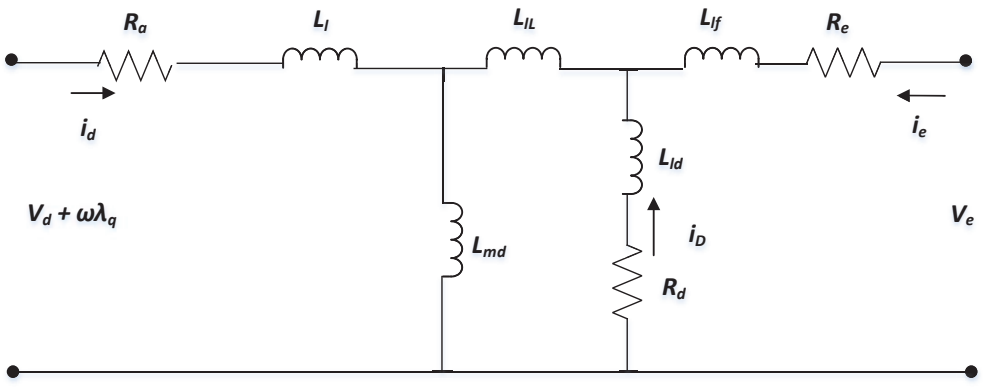

Figure 2.15: d-axis equivalent circuit of a synchronous machine

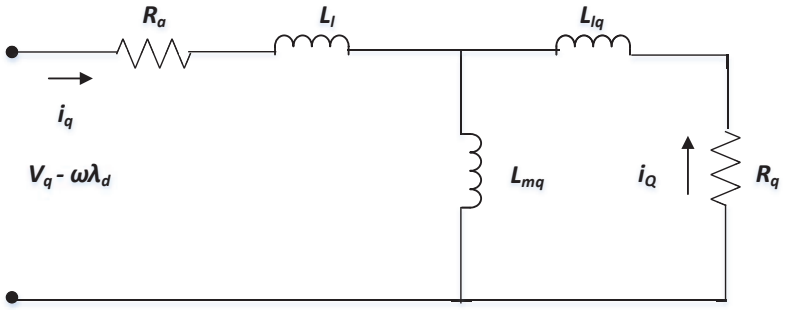

Figure 2.16: q-axis equivalent circuit of a synchronous machine

Equations for the stator winding are given by (2.40) and (2.41)

$$v_d = R_a i_d + \frac{d(\lambda_d)}{dt} - \omega\lambda_q \tag{2.40}$$

$$v_q = R_a i_q + \frac{d(\lambda_q)}{dt} + \omega\lambda_d \tag{2.41}$$

Equations for the field winding are given by (2.42) (2.43) and (2.44)

$$v_e = R_e i_e + \frac{d(\lambda_e)}{dt} \tag{2.42}$$

$$0 = R_d i_D + \frac{d\left(\lambda_D\right)}{dt} \tag{2.43}$$

$$0 = R_q i_Q + \frac{d\left(\lambda_Q\right)}{dt} \tag{2.44}$$

Torque equation for the synchronous machine is given by (2.45), where T_m, T_e and J are mechanical torque, electrical torque and the inertia constant.

$$T_m - T_e = J\dot{\omega} \tag{2.45}$$

Stator flux linkage equations are given by (2.46) and (2.47).

$$\lambda_d = \left(L_{md} + L_l\right) i_d + L_{md} i_e + L_{md} i_D \tag{2.46}$$

$$\lambda_q = \left(L_{mq} + L_l\right) i_q + L_{mq} i_Q \tag{2.47}$$

Rotor flux linkage equations are given by (2.48), (2.49) and (2.50).

$$\lambda_e = L_{md} i_d + \left(L_{md} + L_{lL} + L_{lf}\right) i_e + \left(L_{md} + L_{lL}\right) i_D \tag{2.48}$$

$$\lambda_D = L_{md} i_d + \left(L_{md} + L_{lL}\right) i_e + \left(L_{md} + L_{lL} + L_{ld}\right) i_D \tag{2.49}$$

$$\lambda_Q = L_{mq} i_q + \left(L_{mq} + L_{lq}\right) i_Q \tag{2.50}$$

By neglecting the stator transients (2.40) and (2.41) can be reduced to (2.51) and (2.52).

$$v_d = R_a i_d - \omega \lambda_q \tag{2.51}$$

$$v_q = R_a i_q + \omega \lambda_d \tag{2.52}$$

The active and reactive power can be given by (2.53) and (2.54),

$$P = \frac{3}{2}\left(v_d i_d + v_q i_q\right) \tag{2.53}$$

$$Q_s = \frac{3}{2}\left(v_d i_q - v_q i_d\right) \tag{2.54}$$

When the AC voltage oriented control is utilised, v_q=0. Hence, the active power and reactive power can be controlled by d and q axis current.

2.10 Summary

This chapter summarised the existing literature in the areas of wind power generation, voltage stability, methods for static and dynamic voltage stability evaluation and voltage stability analysis of power systems integrated with wind power generation.

The basics of wind power generation and prevalent generation technologies utilised to harness wind power were summarised. A review of basic theories of voltage stability and various different methods available in the literature for steady-state voltage stability evaluation such as, PV curves, VQ curves and QV modal analysis were also included. The importance of evaluating the impact of the increased penetration levels of wind power generation on power system voltage stability was identified. Even though most of the existing work on this topic considered steady-state voltage stability, it was identified that there are gaps in existing work which have to be filled through further research.

The literature on the basics of the dynamic voltage instability phenomenon were summarised with a comparative discussion of various different instability mechanisms which can lead a network to dynamic voltage instability. The distinct meth-

ods available for dynamic voltage stability assessment were reviewed. The existing literature in energy function analysis for voltage stability analysis as direct methods for voltage stability analysis were reviewed.

The importance of evaluating the dynamic voltage instability of wind rich networks was identified. The published literature on dynamic voltage stability analysis of wind rich networks were critically reviewed to identify the gaps in the existing work. In voltage stability studies utilising the suitable models of various power system components is crucial. Hence, the existing literature on developing suitable models of power system components for voltage stability studies were reviewed.

Chapter 3

Investigation of Steady-state Voltage Stability of Power Systems with Variable-speed Wind Generators

3.1 Introduction

Steady-state voltage stability analysis is the most convenient and the simplest method to evaluate the voltage stability of a power system. Different techniques can be used to evaluate the steady-state voltage stability, which were explained in Chapter 2. In this chapter, the results of preliminary investigations on the impact of increased penetration levels of VSWGs on voltage stability are presented.

The reactive power in a power network directly affects the voltage stability. Therefore, VQ curves and the QV modal analysis methods can be used to obtain accurate results in steady-state voltage stability studies. In this chapter, these two methods are used for voltage stability evaluation. In Section 3.2, the concept of VQ instability is explained in-detail with the impact of different parameters on the VQ instability.

As explained in Chapter 2, the importance of evaluating the voltage stability of power systems with large penetration levels of wind power generation has been identified in the literature, and the steady-state voltage stability of wind rich networks has been evaluated in [6, 22–27]. However, some of these studies have not accurately represented the reactive power capabilities of the wind generators, which is imperative in voltage stability studies. Moreover, some of the studies have not considered the VSWGs, which are the most commonly used wind generators presently. Furthermore, with the increasing penetration levels of the renewable generators in power systems, some of the conventional generators are being retired/decommissioned from some power systems. Due to this reason, it is imperative to compare the capability of different types of wind generators and the synchronous generators to maintain the voltage stability in power systems. However, this factor has also not been comprehensively considered in the literature. Due to these reasons, existing literature still lacks a complete steady-state voltage stability study considering the aforementioned factors.

Section 3.3 illustrates the IEEE 14 bus test system developed in DIgSILENT Power Factory, which is used in the studies in this chapter.

Section 3.4 evaluates the steady-state voltage stability of a wind rich network considering DFIG based wind generators. The important factors such as, the suitable voltage control strategy and the impact of reactive power capability of the DFIGs are considered in the study. Moreover, the reactive power capability of the DFIG and the FCWG are accurately represented and the impact of different VSWGs and the conventional generators on the voltage stability are compared.

Typically, the placement of VSWGs in power systems depends on the availability of wind resource. However, there may be few possible connection points for a wind farm in a network, and it is important to have a method to decide the optimum location for the wind farm. In Section 3.5, a method for placement of VSWGs in power systems to improve the voltage stability utilising the reactive power capability available from a VSWGs is introduced using the QV modal analysis technique and

VQ curves.

3.2 Voltage Stability Evaluation using VQ Curves - VQ Instability Margin

Section 2.4.2 explained how VQ curves could be used for voltage stability evaluation. This section includes a detailed explanation on voltage stability evaluation using VQ curves.

3.2.1 VQ Voltage Instability Margin Index (VQVIMI)

As stated in Section 2.4.2, VQ voltage stability margin can provide an indication on the proximity of a certain operating point to voltage instability, and it is usually measured in MVArs. In this section, a new voltage stability index, VQ Voltage Instability Margin Index (VQVIMI) is introduced as a more convenient indicator to estimate the reactive power distance of a certain operating point to voltage instability. VQVIMI is defined by (3.1) and it corresponds to the distance (L_1L_2) between the operating point and the critical point, as shown in Fig. 3.1. In (3.1), voltage is given in per unit and the reactive power is normalised with respect to the largest reactive power margin ($Q_{VQ'}$) observed for a particular bus. VQVIMI approaches zero as the system gets closer to to VQ instability.

$$VQVIMI = L_1L_2 = \sqrt{\left(\left(\frac{Q_{SS}}{|Q_{VQ'}|}\right) - \left(\frac{Q_{VQ}}{|Q_{VQ'}|}\right)\right)^2 + (V_{SS} - V_{VQ})^2} \qquad (3.1)$$

VQVIMI can vary between 0 to 1.414 for different operating points. In the vicinity the critical point of voltage instability, VQVIMI approaches 0.

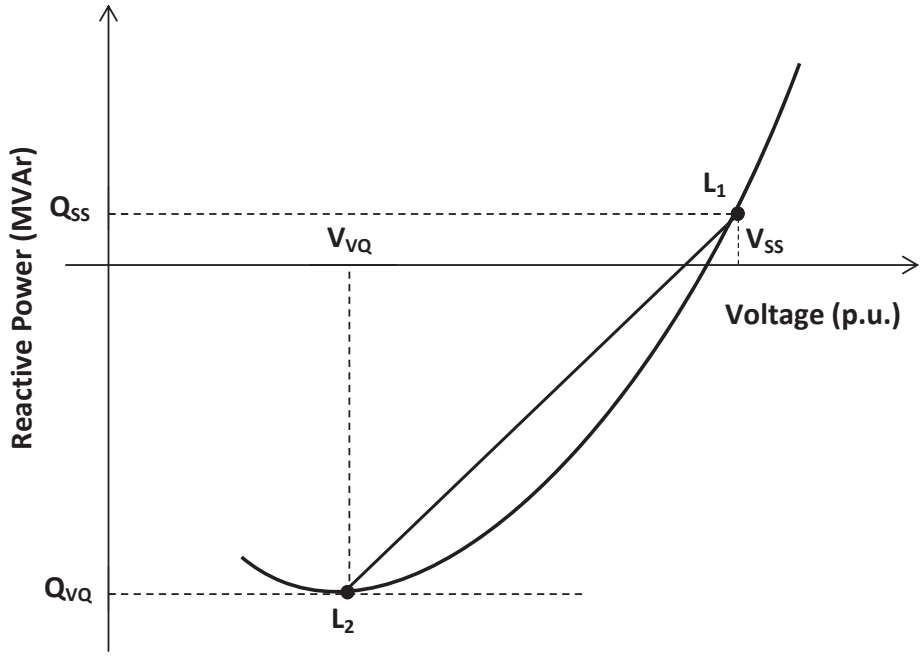

Figure 3.1: Illustration of VQVIMI

3.2.2 VQ instability

To illustrate the VQ voltage instability, the test system shown in Fig. 3.2 was used, of which the details are listed in Appendix A.

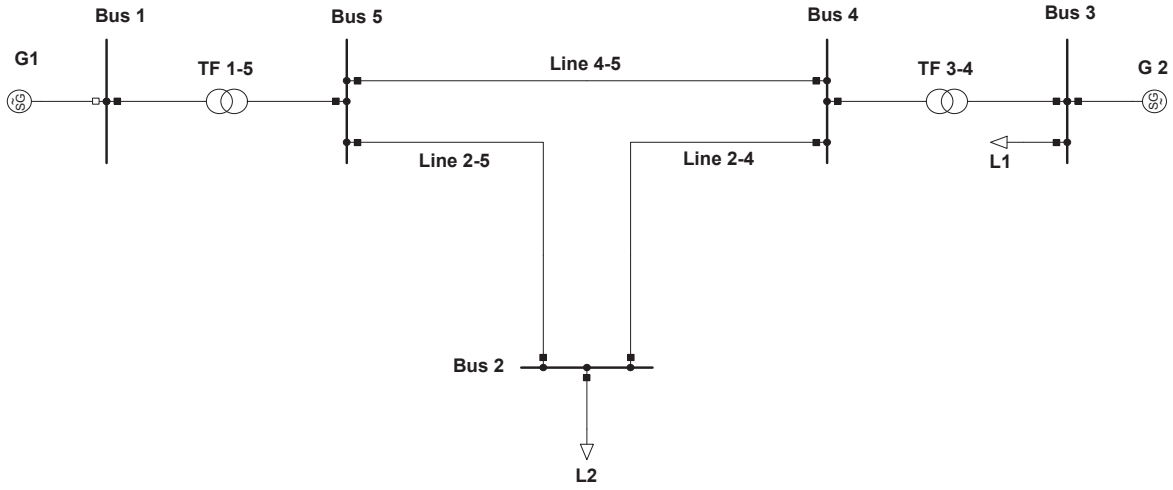

Figure 3.2: Single line diagram of the five bus test system

In order to illustrate the VQ instability, active power of load L2 at Bus 2 is varied in the range of 800 MW- 900 MW, while keeping its reactive power constant and the VQ curves are drawn for each case (Case I). Fig. 3.3 shows the corresponding VQ curves. Furthermore, the reactive power of the load L2 is varied from 280 MVAr-400 MVAr while keeping the active power constant and the VQ curves are drawn for each case, respectively (Case II). Table 3.1 lists the VQ instability margins for the two cases.

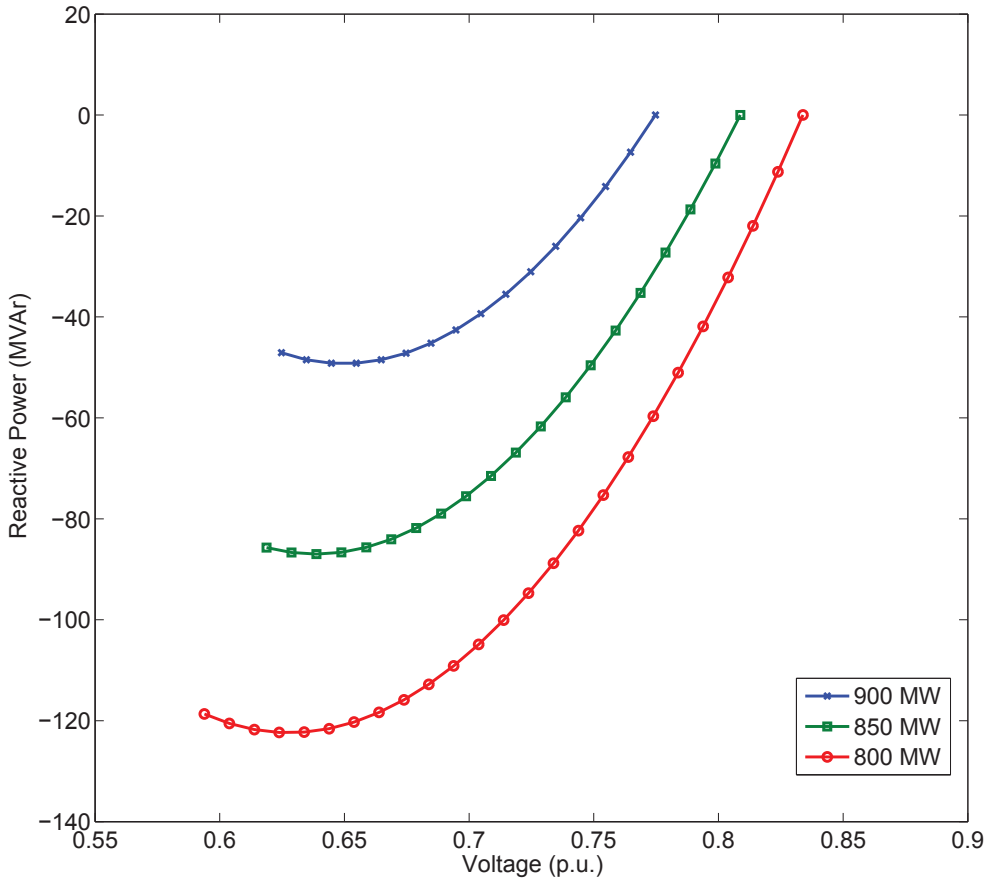

Figure 3.3: VQ curves for different active power levels of L2

As explained in Sections 2.4.1 and 2.4.2, the load flow calculation will not converge beyond the critical point of the PV curve or VQ curve. The critical point of the PV curve corresponds to the maximum active power that can be transferred (or maximum active power load) and the critical point of the VQ curve corresponds to the maximum reactive power that can be transferred (or maximum reactive power

load) under system steady-state conditions. As the load active or reactive power is increased, the system gets closer to voltage instability, and hence, the active or reactive power stability margin approach zero. In this section, its impact on VQ stability margin is studied. Fig. 3.3 and Table 3.1 confirm that the VQ stability margin reduces as the load active power or reactive power is increased. A larger VQ stability margin can be achieved by using additional reactive power support at the bus under consideration, using reactive power compensation devices.

Table 3.1: VQ stability margin for load variations

Case I		**Case II**	
L2 Active power (MW)	VQ instability Margin (MVAr)	L2 Reactive power (MVAr)	VQ instability Margin (MVAr)
800	122.2	280	122.3
850	86.9	320	82.4
900	49.2	360	42.4
–	–	400	2.4

In the next scenario, the impact of different load charatersistics on the VQ instability is studied. In order to study this, exponential load model, as explained in Section 2.9.2 is considered and the load characteristics of L2 is adjusted to represent constant power, constant current and constant impedance. Fig. 3.4 shows VQ curves corresponding to the three different load characteristics, and Table 3.2 lists the corresponding VQVIMI. The behaviour of the constant impedance load is highly voltage dependent compared to other two load types. Hence, at lower voltage levels, it draws lower power compared to the other two loads. Therefore, with constant impedance load, higher VQ stability margin and hence higher VQVIMI can be observed. This observation confirms that the load characteristics is an important factor which affects the VQ instability.

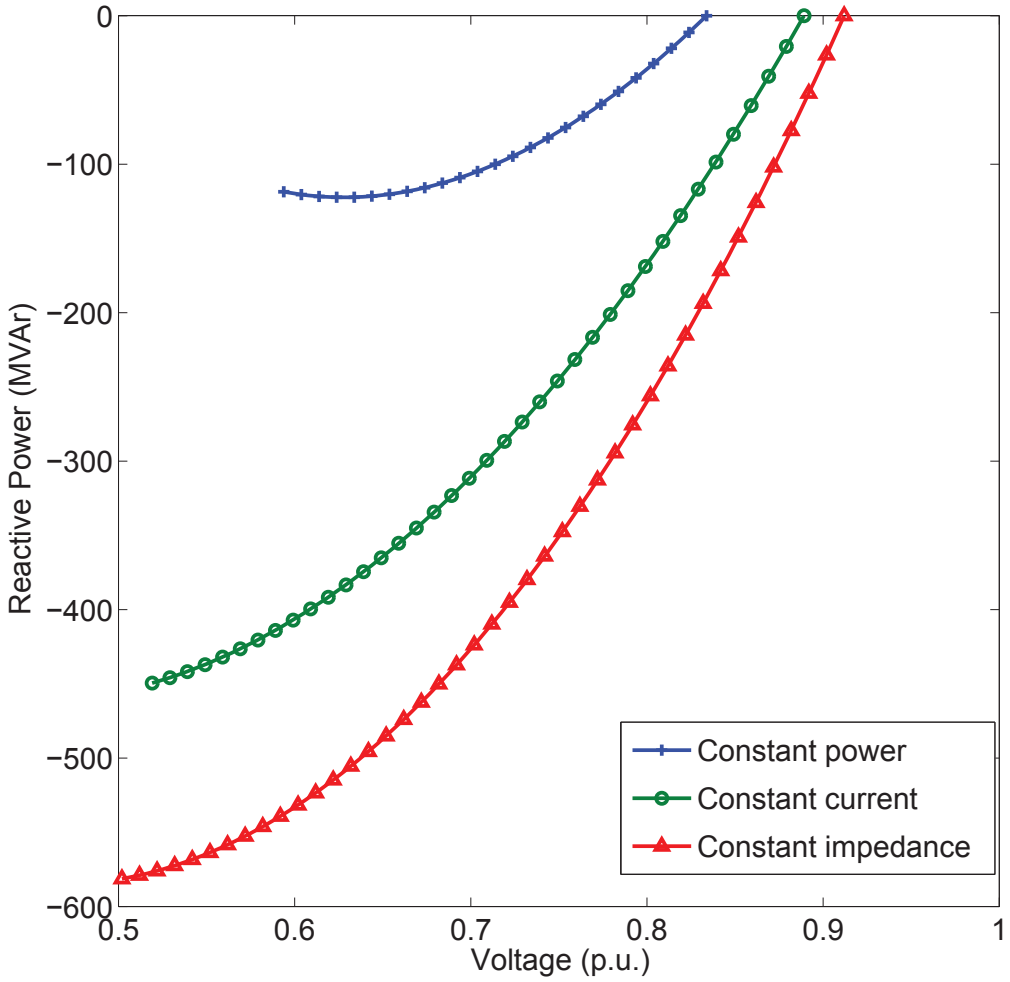

Figure 3.4: VQ curves for different load characteristics of L2

Table 3.2: VQVIMI for different load characteristics

Load type	**VQVIMI**
Constant power	0.297
Constant current	0.857
Constant impedance	1.081

3.3 Test System

IEEE 14 bus test system as shown in Fig. 3.5 modelled in DIgSILENT Power Factory was used for the subsequent studies in this chapter, of which the parameters

are listed in Appendix A.

For the studies in Section 3.4, all loads connected at high voltage (110 kV) busbars were modelled as industrial loads and all loads connected to medium voltage (33 kV and 11 kV) busbars were modelled with a composition of 40% commercial loads and 60% residential loads. The load compositions considered in the study are shown in Table 3.3 [67]. Loads were modelled as polynomial loads as explained in Section 2.9.2. Model of loads connected to medium voltage busbars are given in (3.2) and (3.3). Model of loads connected to high voltage busbars are given in (3.4) and (3.5). The exponents were selected based on the correponding load exponents for the four different types of loads, considered in the models, as illusrated in Section 2.9.2. DFIG and FCWG based VSWGs modelled in DIgSILENT Power Factory were considered in the study. The rective power capabilities of the generators discussed in Section 2.9.1 were considered. The GSC of the DFIG wind generator was operated at unity power factor.

Table 3.3: Load composition for polynomial load models

Load type	**Load composition**		
	Residential	**Commercial**	**Industrial**
Resistive	25	14	0
Small motor	75	51	20
Large motor	0	0	59
Discharge Lighting	0	35	21

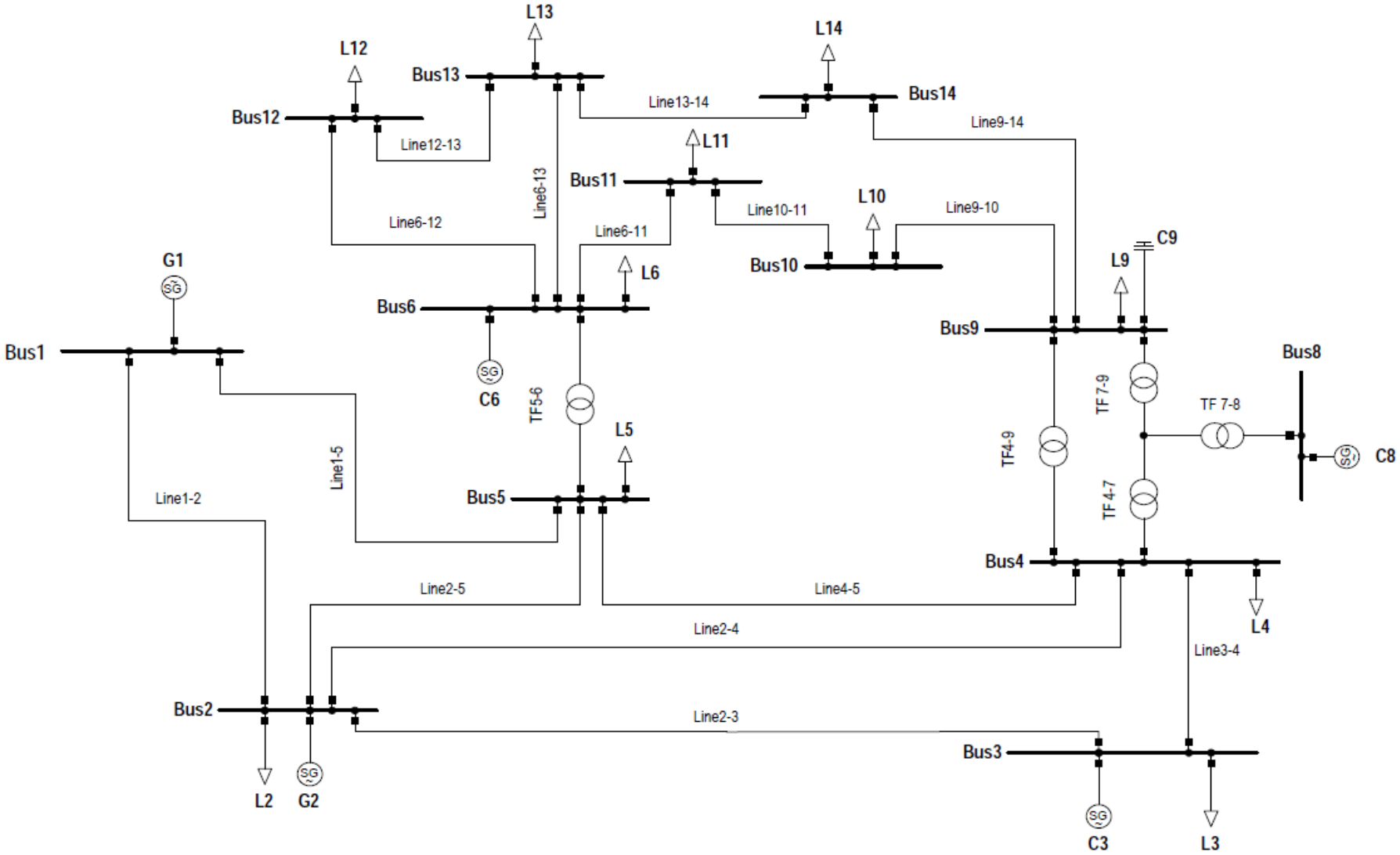

Figure 3.5: Single line diagram of the IEEE-14 bus test system

$$P = P_0 \left[0.206 \left(\frac{V}{V_0} \right)^2 + 0.654 \left(\frac{V}{V_0} \right)^{0.1} + 0.14 \left(\frac{V}{V_0} \right)^1 \right] \tag{3.2}$$

$$Q = Q_0 \left[0.206 \left(\frac{V}{V_0} \right)^0 + 0.654 \left(\frac{V}{V_0} \right)^{0.6} + 0.14 \left(\frac{V}{V_0} \right)^3 \right] \tag{3.3}$$

$$P = P_0 \left[0.2 \left(\frac{V}{V_0} \right)^{0.1} + 0.59 \left(\frac{V}{V_0} \right)^{0.05} + 0.21 \left(\frac{V}{V_0} \right)^1 \right] \tag{3.4}$$

$$Q = Q_0 \left[0.2 \left(\frac{V}{V_0} \right)^{0.6} + 0.59 \left(\frac{V}{V_0} \right)^{0.5} + 0.21 \left(\frac{V}{V_0} \right)^3 \right] \tag{3.5}$$

3.4 Steady-state Voltage Stability Analysis with VSWGs

3.4.1 Impact of Wind Generator Voltage Control Strategy on Voltage Stability

The voltage control strategy utilised for a wind generator affects the voltage stability of the network. Usually, conventional power generators are operated in either voltage control mode or power factor control mode. In this section, the impact of wind generator control strategy on voltage stability is studied using the test system (Fig. 3.5) explained in Section 3.3. The synchronous generator connected to Bus 2 was replaced with a DFIG wind generator with an equivalent capacity (total capacity - 2 MW×50 generators , total active power output- 40 MW) and the control strategy of the DFIG was altered to power factor control and voltage control modes, respectively. The VQ stability margin of Bus 5 was computed using DIgSILENT Power Factory.

Fig. 3.6 shows the variation of the VQ stability margin for various operating power factors (lagging/supplying), when the DFIG is operated at power factor control mode. The corresponding VQVIMI values are shown in Table 3.4. When the DFIG is operated at a low power factor, it supplies more reactive power to the network and hence, the VQ stability margin of the nearby busbars under consideration

is higher (hence, the VQVIMI) as illustrated by Fig. 3.6.

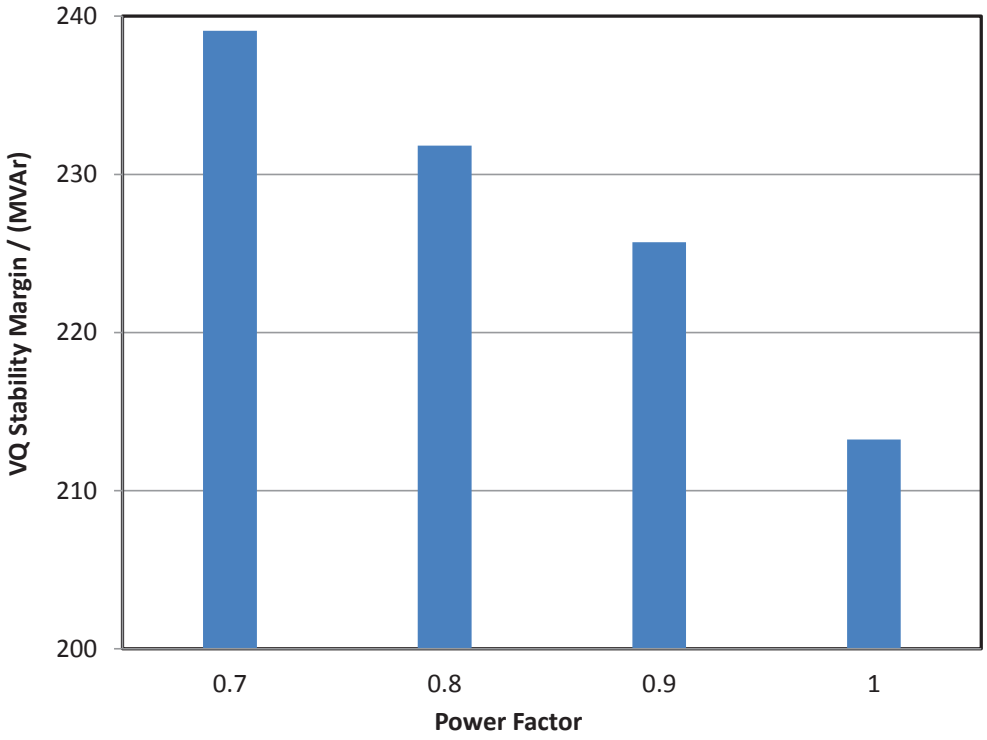

Figure 3.6: VQ stability margin of Bus 5 for power factor control mode of operation of DFIG at Bus 2

Table 3.4: VQVIMI for different control modes

Power Factor Control		**Voltage Control**	
Power Factor	VQVIMI	Control Voltage (p.u.)	VQVIMI
0.7	1.036	0.96	1.041
0.8	1.004	0.98	1.041
0.9	0.979	1.00	1.041
1	0.926	1.02	1.041
–	–	1.04	1.041

However, when a generator is operated in power factor control mode, it supplies constant reactive power for a particular active power output, regardless of the network conditions. Due to this reason, a wind generator operated at power fac-

tor control mode would not utilise its full reactive power capability to support the network during a voltage instability.

To investigate the effect of voltage control mode of the DFIG wind generator, the DFIG wind generator is operated in voltage control mode at various control voltages from 0.96 p.u. to 1.04 p.u. and the VQ stabilility margin is computed. Regardless of the control voltage, the VQ stability margin is almost constant at about 255 MVArs (VQVIMI is constant at 1.041), as shown in Fig. 3.7, which is larger compared to the power factor control mode of operation. Once the generator is operated at voltage control mode, the generator will maintain the terminal voltage at a defined value at all times by varying the reactive power output within the reactive power capability, defined by the capability chart. Therefore, operating wind generators at voltage control mode is favourable for network voltage stability and to utilise the full reactive power capability of a wind generator.

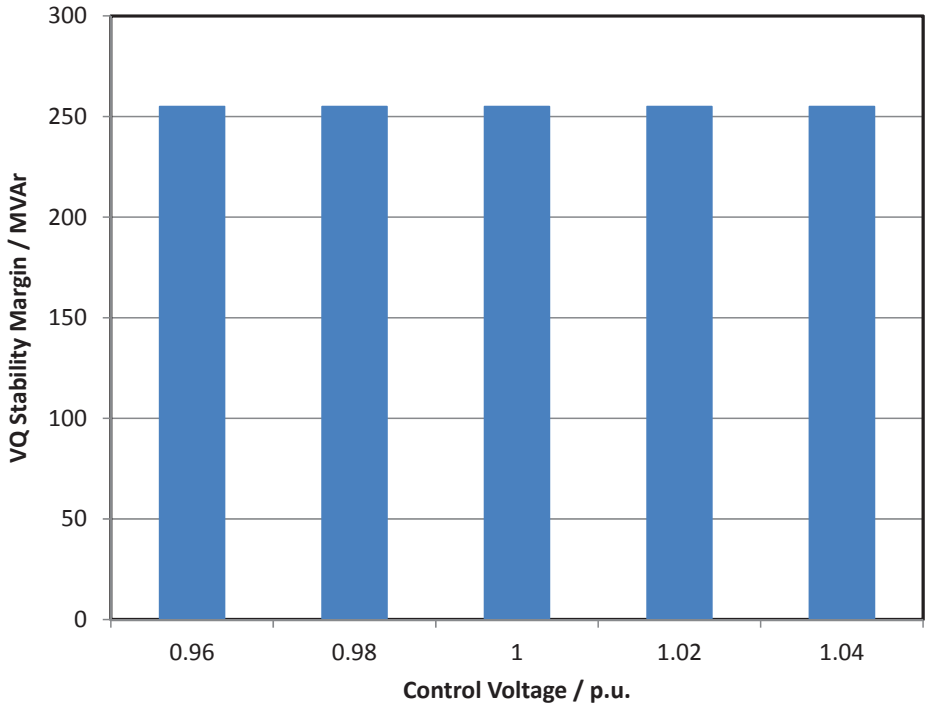

Figure 3.7: VQ stability margin of Bus 5 for voltage control mode of operation of DFIG at Bus 2

3.4.2 Impact of Reactive Power Capability of Wind Generators on Voltage Stability

In voltage stability studies, consideration of accurate reactive power capability limits of wind generators is imperative. To demonstrate the importance of utilisation of accurate reactive power limits, the synchronous generator in Bus 2 is replaced by an equivalent DFIG wind generator and the VQ stability margin is computed for different reactive power capability limits of the DFIG wind generator. Fig. 3.8 shows the three different reactive power capability limits considered for the DFIG wind generator; original (100%) reactive power capability, 75% and 50% of the original reactive power capability.

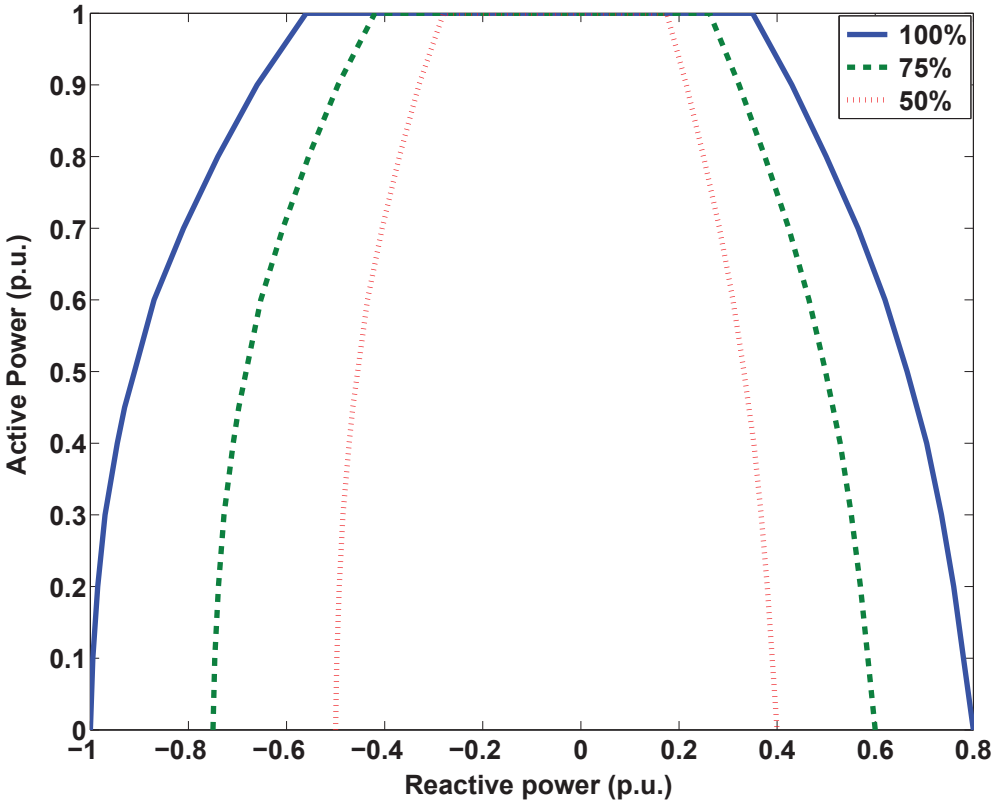

Figure 3.8: Different capability characteristics for DFIG wind generator

Fig. 3.9 shows the VQ stability margins for Bus 5 for the three different reactive power capabilities considered. It illustrates higher VQ stability margins for higher reactive power capability limits. This demonstrates the importance of accu-

rate representation of reactive power capabilities of the wind generators in voltage stability studies. It also demonstrates that wind generators with high reactive power capability is favorable for steady-state voltage stability of a power network.

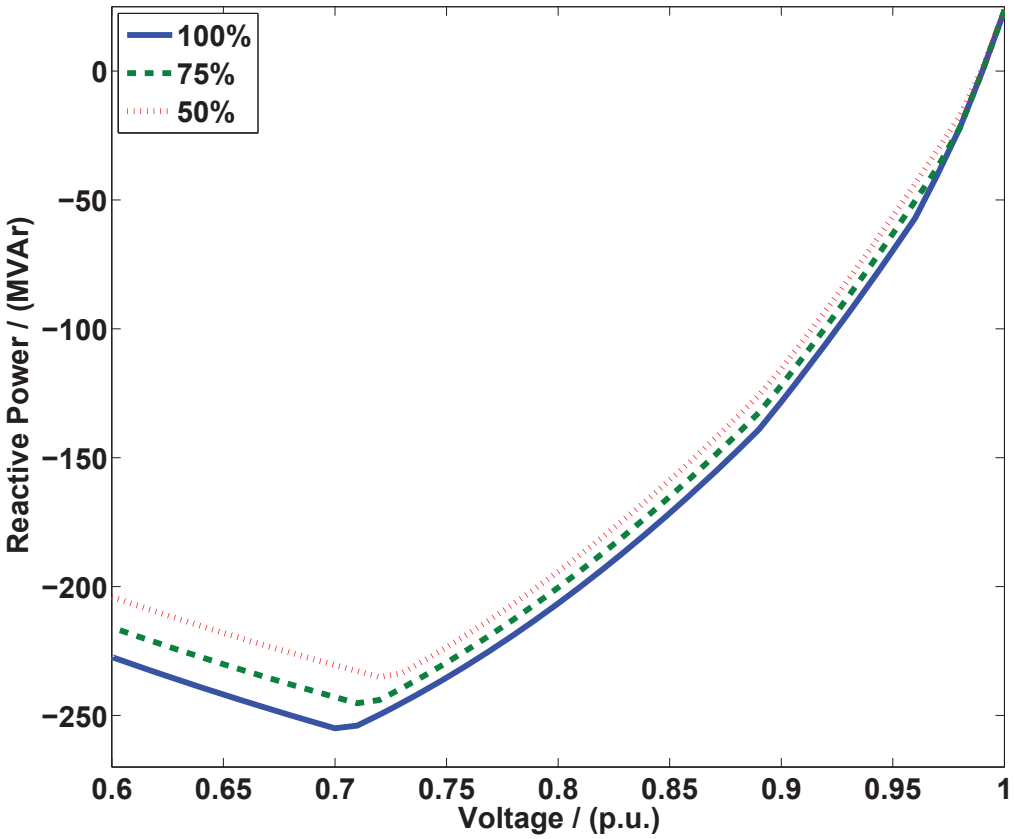

Figure 3.9: VQ curves for different capability characteristics of DFIG wind generator

3.4.3 Comparison of the Impact of Different Generators on Voltage Stability

In this section, the impact of synchronous generators and VSWGs on steady-state voltage stability is compared considering VQ instability margin. The synchronous generator connected to Bus 2 was replaced with an equivalent DFIG and FCWG wind generators and the VQ stability margin of Bus 5 was computed. The reactive power capability charts for synchronous generator, DFIG and FCWG wind generators described in Section 2.9.1 were considered. However, the GSC of the DFIG was operated at unity power factor. As explained in Section 2.9.1, the reactive power

capability of the generators, particularly wind generators significantly vary with the loading of the generator. Therefore, two loading levels (40% and 80%) of each generator were considered. Fig. 3.10 shows the VQ curves for two loading levels of the different generators.

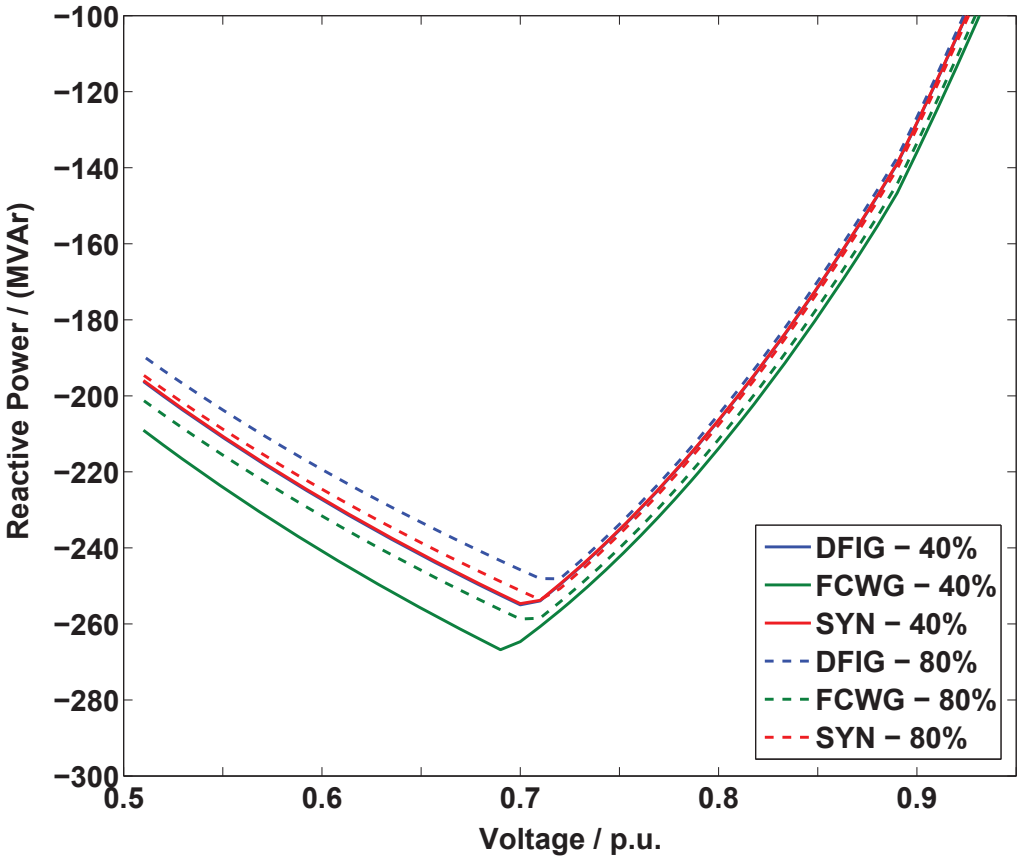

Figure 3.10: VQ curves for different generators operated at different loading levels

Fig. 3.10 confirms that the reactive power margin of DFIG and FCWG vary significantly with the loading level. They have high reactive power capability at low loading conditions, as expected. However, the reactive power capability of the synchronous generator does not vary much with the loading level, as expected according to the capability chart shown in Fig. 2.11. For both loading levels considered, the highest VQ stability margin can be observed with the FCWG. At 40% loading, the VQ stability margin with the DFIG and the synchronous generator are almost the same. However, when the loading of the generator is increased to 80%, the VQ stability margin with the DFIG is sigificantly reduced compared to the synchronous

generator. It should be noted that the additional reactive power capability available for a DFIG from the GSC is not considered in this study, and the DFIG will have a slightly higher reactive power capability than what was predicted above.

This study reveals that, if a synchronous generator in a network is replaced with an equivalent FCWG wind generator, it would improve the voltage stability. If the synchronous generator is replaced with a DFIG wind generator, it can improve the voltage stability depending on the loading level. However, if the additional reactive power capability from the GSC is also considered, DFIG would also improve the voltage stability at any loading condition. This study illustrates that the DFIG and FCWG based VSWGs have the capability to improve the steady-state voltage stability of a power system.

3.5 Placement of VSWGs in Power Networks Considering Steady-state Voltage Stability

In this section, the most suitable location to place VSWGs in a network is investigated considering the steady-state voltage stability. QV modal analysis and the VQ curves explained in Section 2.4.3 are used in the methodology. The wind generators were operated in voltage control mode to eshtablish maximum reactive power support for the network.

3.5.1 Modal Analysis Results for the Test System

The QV modal analysis was conducted for the IEEE 14 bus test system. Table 3.5 lists the corresponding eigen values for the test system. According to the results, $\lambda_7 = 2.6555$ is the lowest eigen value, hence the mode associated with it is the most critical mode for the voltage stability. Fig. 3.11 shows the bus participation factor for this mode.

According to Fig. 3.11, Bus 14 has the highest participation factor, hence Bus 14 contributes the most to the critical mode indicating that it is the weakest busbar

in the network. Similarly, bus 5 has the lowest participation factor and hence, it is the strongest busbar in the network.

Table 3.5: Eigenvalues for IEEE 14 bus test system

λ_1	63.3637
λ_2	38.2816
λ_3	20.9850
λ_4	18.3096
λ_5	15.8665
λ_6	10.8986
λ_7	2.6555
λ_8	5.3747

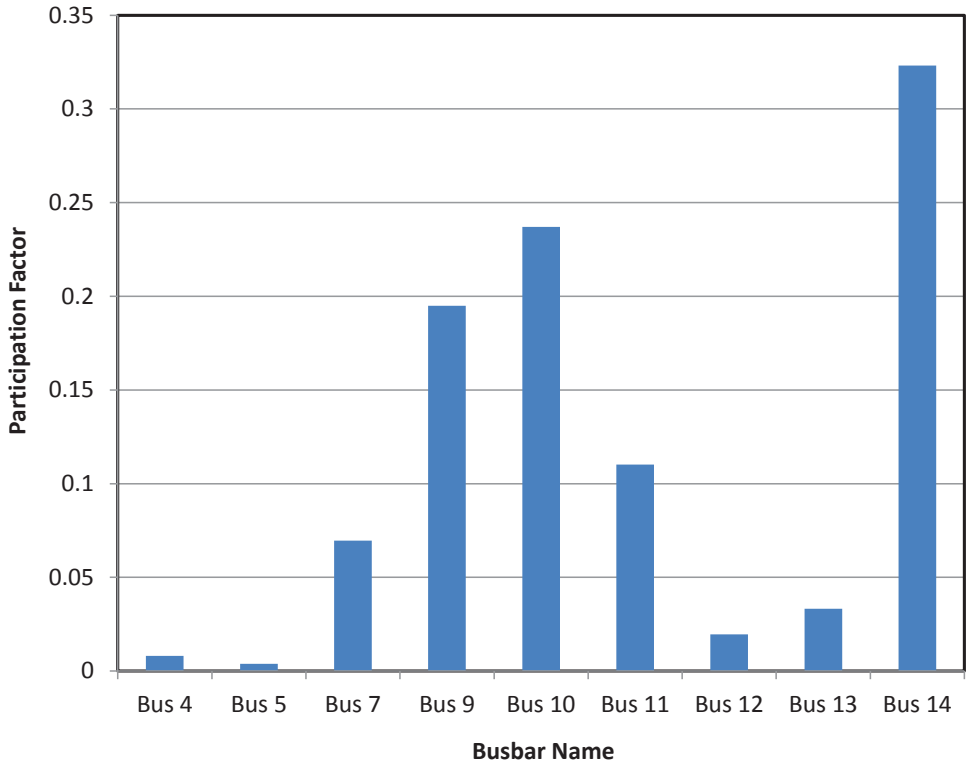

Figure 3.11: Bus participation factors for (λ_7= 2.6555) of IEEE 14 bus test system

These results were further confirmed by computing the VQ stability margins of each busbar, and Fig. 3.12 shows the VQ stability margins of the busbars. According to Fig. 3.12, Bus 14 resulted the the lowest VQ stability margin and Bus 5 resulted the highest VQ stability margin. Therefore, according to both QV modal analysis and VQ curves, Bus 14 is the weakest busbar and Bus 5 is the strongest busbar in the network.

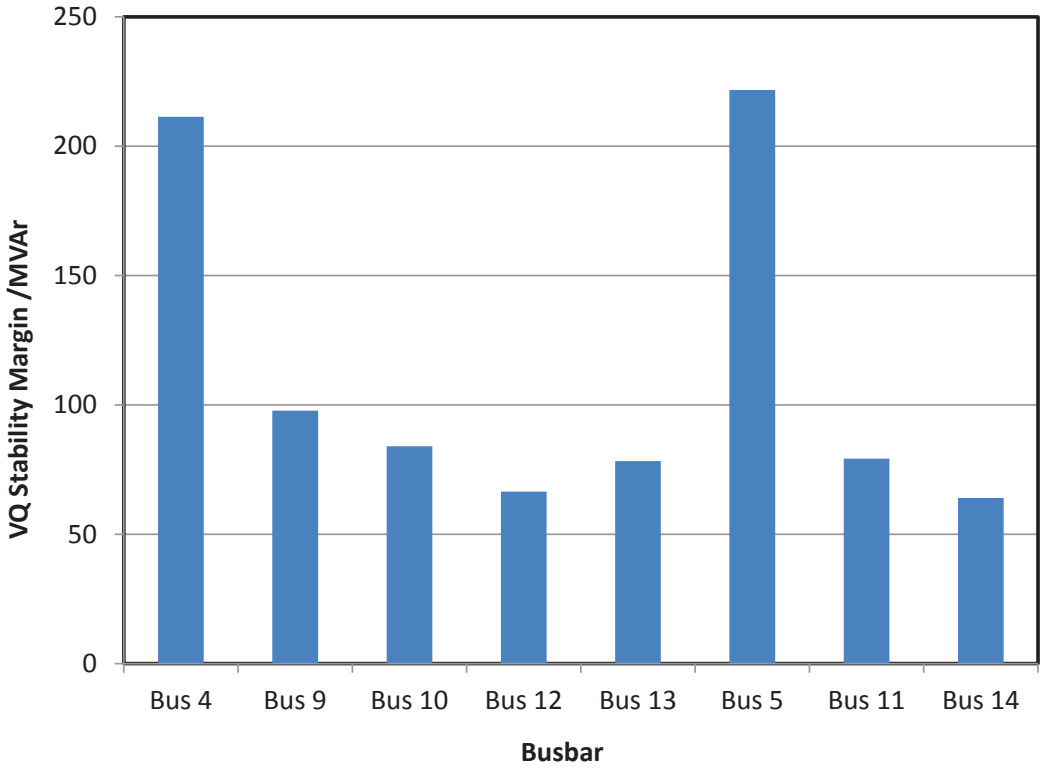

Figure 3.12: VQ stability margins of the busbars

3.5.2 Integration of DFIG Wind Generators at the Weak Busbars

In this section, the impact of integration of the DFIG wind generators at the weakest busbar on steady-state voltage stability is studied. A DFIG wind farm with different capacities was connected to Bus 14 and the VQ stability margin of the different busbars were computed. Fig. 3.13 shows the VQ curves for Bus 14 at different wind power outputs at Bus 14. Fig. 3.13 demonstrates that the VQ stability margin has increased with the increased wind generator output. With the added wind

generation capacities of 20 MW, 40 MW and 80 MW, the VQ stability margin has increased by 17.2%, 32.5% and 53.9%, respectively.

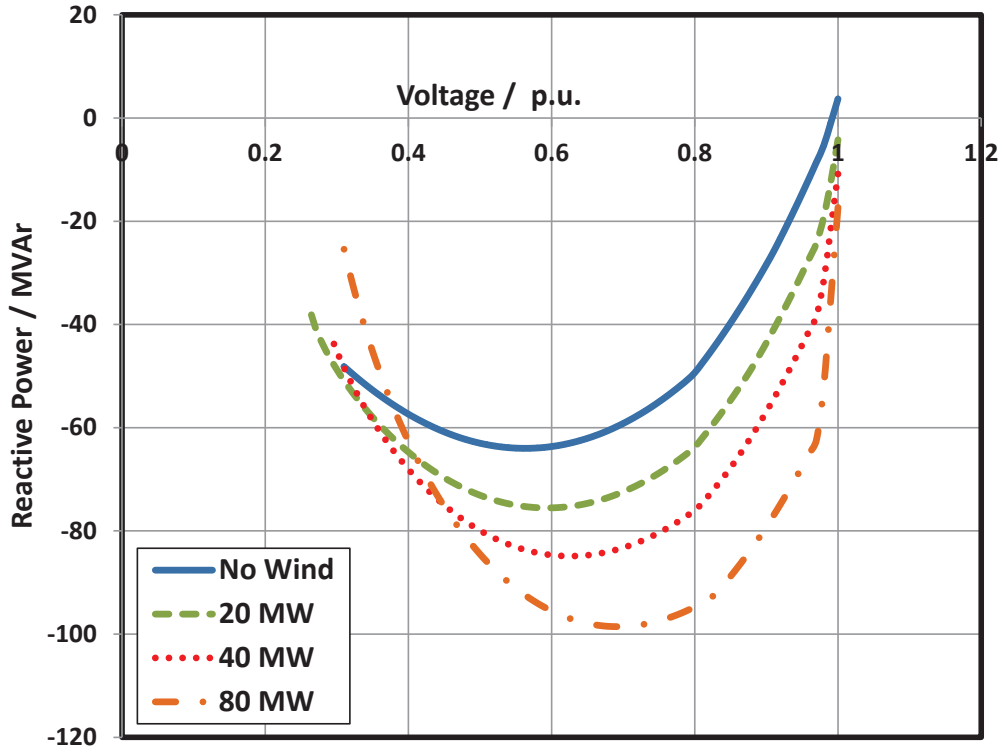

Figure 3.13: VQ curves for Bus 14 with added DFIG wind generation to Bus 14

In voltage stability studies, usually, it is important to maintain the total system generation capacity constant although renewable power generation is added. This is because, when a new generator is added to a load busbar, it would naturally improve the voltage stability. For accurate estimation of the capability of the added generation, it is appropriate to reduce some existing generation capacity by an equivalent amount to the added generation and study the impact of the added new generation. Therefore, as the next step, the MVA capacity of existing synchronous generator at Bus 2 was reduced by an equivalent amount to the added wind generation at Bus 14, and the effect of VQ stability margin of Bus 14 was studied.

Fig. 3.14 shows the comparison of the results with and without maintaining the system generation capacity constant. However, for this system, there is only a slight difference in the results. The reason for this observation is that all generators and

the major load centres of this test system are concentrated in two separate ends. Usually, reactive power support to the loads is provided by the nearby generators. Therefore, integrating a new generator at the close proximity to the load centre and reducing the generation located far way does not have a major impact on the voltage stability at the load busbars. However, this is an important factor to be considered in voltage stability studies to derive valid conclusions, as this can severely affect the conclusions drawn for certain power systems. This factor is important for some renewable rich networks, where the existing conventional generators are being decommissioned due to higher renewable power penetration levels.

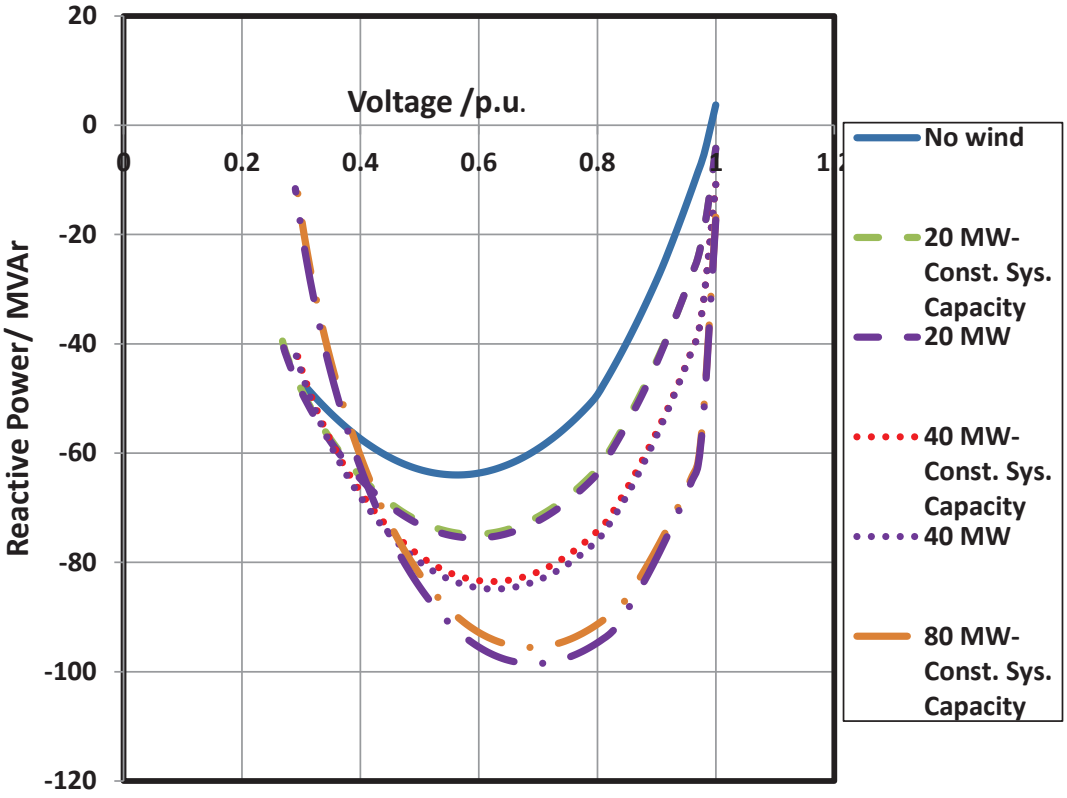

Figure 3.14: VQ curves for Bus 14 with added DFIG wind generation to Bus 14

3.5.3 Integration of DFIG Wind Generators at the Strong Busbars

In this section, the impact of integration of the DFIG wind generators at strong busbars on the steady-state voltage stability is studied. A DFIG wind farm with different capacities was connected to Bus 5, and the VQ stability margin of the

different busbars were computed. Similar to Section 3.5.2, the added wind generation increases the VQ stability margin of Bus 5, as shown in Fig. 3.15. With the added wind generation with capacities of 20 MW, 40 MW and 80 MW, the VQ stability margin is increased by 6.3%, 12.2% and 23.5%, respectively.

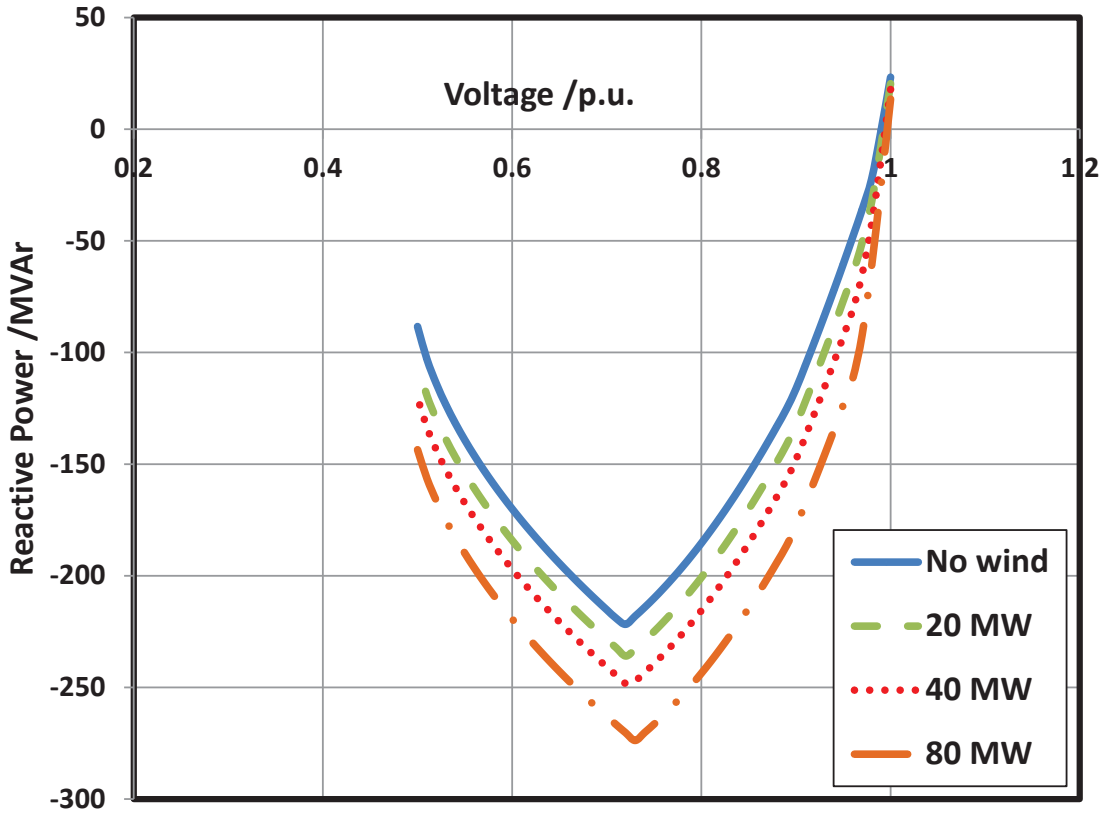

Figure 3.15: VQ curves for Bus 5 with added DFIG wind generation to Bus 5

As weak busbars in the system are crucial for the overall voltage stability of the network, it is important to assess the impact of added generation on the weak busbars. In this scenario, the wind generation is integrated to the network at the Bus 5. To assess the impact of the added generation on the weak busbars, the VQ stability margins of the Bus 14 was computed. Fig. 3.16 shows the VQ curves generated for Bus 14 (the weakest busbar) for different wind generation levels at bus 5. When the wind generation with capacities of 20 MW, 40 MW and 80 MW is added to Bus 5, the VQ stability margin has increased by 3.9%, 7.6% and 14.6%, respectively. Therefore, the added wind generation has slightly increased the QV

stability margin of Bus 14.

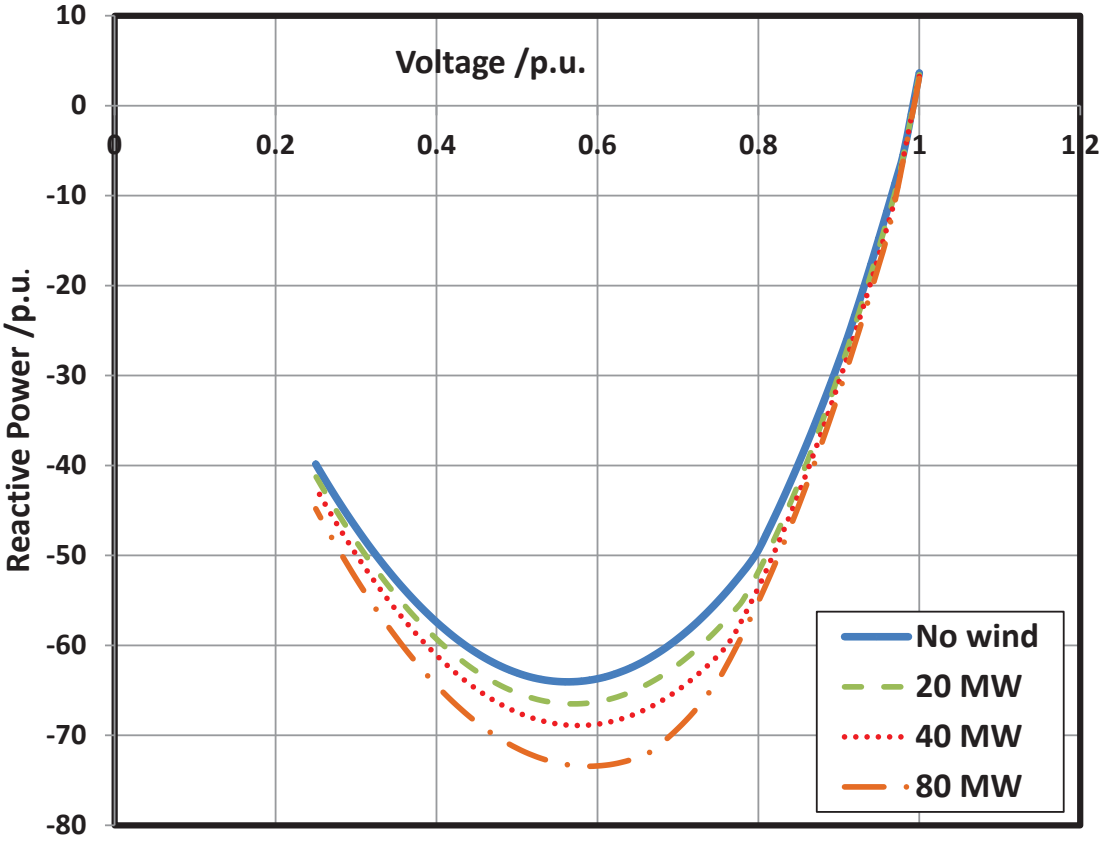

Figure 3.16: VQ curves for Bus 14 with added DFIG wind generation to Bus 5

3.5.4 Comparison of results

In this section, the results described in Section 3.5.2 and 3.5.3 are compared. According to the results, the added DFIG wind generation to either weak or strong busbars improves the VQ stability margin of the busbar itself, hence, improves the steady-state voltage stability in general. The percentage increase in VQ stability margin of the two busbars , with various wind generation levels connected to the busbars are compared in Table 3.6. According to the results, added 20 MW of wind generation to Bus 14 increases the voltage stability margin of Bus 14 by 17.2%, whereas the same amount of wind generation added to bus 5 improves the VQ stability margin of the Bus 5 by only 6.3%. It is also noted that the same level of DFIG wind generation added to Bus 5 increases the voltage stability margin of Bus

14 by only 3.9%. However, the weak busbars are crucial for overall voltage stability of a power system and the addition of wind generation to the strong busbar does not significantly improve the voltage stability of the weak busbars. From these observations, it can be concluded that integration of DFIG based wind generation at weak busbars of a network is better for steady-state voltage stability of the network. It can significantly improve the voltage stability of the weak areas and hence, the overall voltage stability of the network.

Table 3.6: Comparison of Results

Wind Generator Location	**Test bus**	**% Increase in VQ Stability Margin**		
		20 MW	**40 MW**	**80 MW**
14	14	17.2	32.5	53.9
5	5	6.3	12.2	23.5
5	14	3.9	7.6	14.6

3.5.5 Integration of FCWG based Wind Generators

In this section, the impact of added FCWG based wind generation at the weak busbar (Bus 14) is compared with the equivalent integration of DFIG based wind generation. A FCWG based wind farm with different capacities is added to Bus 14, and the VQ stability margins of the Bus 14 was computed as shown in Fig. 3.17. The percentage increase in the VQ stability margin with the two types of generation is listed in Table 3.7. According to the results, with the added wind generation of 80 MW, the DFIG increases the VQ stability margin of Bus 14 by 53.9%, whereas the FCWG increases the VQ stability margin by 73.4%. As illustrated by these results, a FCWG can improve the voltage stability margin of a weak busbar more than a DFIG with similar capacity. This is due to the higher reactive power capability of FCWG, as explained with the capability charts in Section 2.9.1. However, it should be noted that the reactive power capability through DFIG GSC was not considered here.

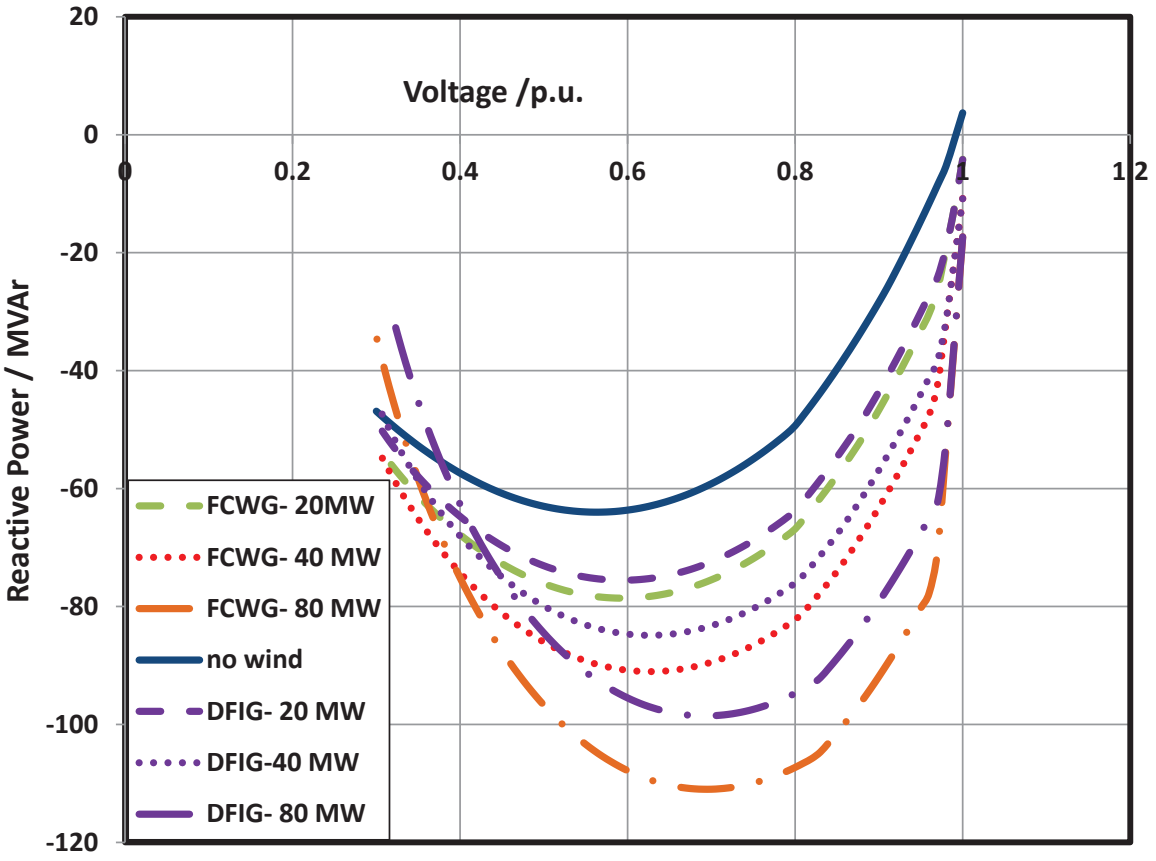

Figure 3.17: Comparison of VQ curves for Bus 14 with added DFIG and FCWG wind generation to Bus 14

Table 3.7: Comparison of results: DFIG and FCWG

Wind Generator	**% Increase in VQ Stability Margin**		
	20 MW	**40 MW**	**80 MW**
DFIG	17.2	32.5	53.9
FCWG	22.7	42.2	73.4

3.6 Summary

In this chapter, the preliminary investigations of the impact of VSWGs on voltage stability were conducted, considering steady-state voltage stability. The VQ curves and the QV modal analysis tools were used in the voltage stability analysis. The

detailed explanation of VQ instability using a five bus test system illustrated the impact of the load active and reactive power, and the voltage-dependent load characteristics on the VQ stability margin and hence, the steady-state voltage stability.

The investigation of the impact of VSWGs on steady-state voltage stability was carried out using the IEEE 14 bus test system developed in DIgSILENT Power Factory. The DFIG and FCWG based VSWGs were considered in the study and the reactive power capability of these generators were accurately represented. The investigations with the DFIG based wind generation demonstrated that operation of the VSWGs in voltage control strategy is better for the steady-state voltage stability compared to power factor control strategy, due to the fact that the reactive power capability of the VSWGs can be properly utilised to support the network voltage stability. The study also emphasised the importance of the accurate representation of the reactive power capability of wind generators in voltage stability studies. The study has shown that the wind generators with higher reactive power capability can support to maintain a larger VQ stability margins and hence, better voltage stability.

Moreover, the impact of conventional synchronous generators and, DFIG and FCWG based VSWGs on the steady-state voltage stability was compared and it was illustrated that these VSWGs have the capability to improve the steady-state voltage stability. Although, the synchronous generators have a better reactive power capability at all loading conditions of the generator, the reactive power capability of the VSWGs significantly vary with the generator loading level.

If a synchronous generator in a network is replaced with an equivalent FCWG, latter can improve the voltage stability even at higher loading levels. If a synchronous generator is replaced with an equivalent DFIG, latter cannot significantly improve the voltage stability, if the GSC is operated at unity power factor. However, if the GSC reactive power capability is also utilised, DFIG can also improve the voltage stability depending on the loading level.

In this chapter, QV modal analysis was used to identify the strong and weak

areas of a power system in terms of voltage stability. It was found that integration of VSWGs in the weak areas in a network (as identified by the QV modal analysis) can support the voltage stability. Due to the reactive power capability of the power electronic converter based VSWGs, they can support to maintain a larger reactive power margins at weak parts of the network and hence it is beneficial for the overall voltage stability of the network.

The final conclusions of this chapter are drawn by considering the full inherent reactive power capability available from the VSWGs. However, there are other site-specific factors that can affect reactive power capability available at the grid connection point of large wind farms, which will be explained in Chapter 4. Therefore, it is important to estimate the reactive power capability available at the connection point of a wind farm, considering the specific site conditions.

Chapter 4

Long-term Voltage Stability Analysis of Power Systems in the Presence of Variable-speed Wind Generators

4.1 Introduction

Voltage stability is affected by the generator and load dynamics, and time dependent control actions of power system components, such as OLTCs, AVRs, OXLs and UELs. Therefore, steady-state analysis methods are not sufficient to accurately evaluate voltage stability of a network, hence dynamic simulations incorporating accurate dynamic models of power networks have to be conducted to derive realistic conclusions [12]. As explained in Chapter 2, dynamic voltage stability phenomenon is usually categorised into two categories; short-term voltage stability and long-term voltage stability. In this chapter, the impact of VSWGs on long-term voltage stability is investigated.

In dynamic analysis of voltage stability in the presence of VSWGs, it is imperative to utilise accurate dynamic models of VSWGs along with dynamic models of

power systems. In Chapter 2, the basic concepts of dynamic modelling of DFIG wind generators were explained. In Section 4.2 of this chapter, dynamic models of the VSWGs utilised in this thesis are explained, using the analytical techniques presented in Chapter 2. The test system used for studies presented in this Chapter is explained in Section 4.3.

As explained in Chapter 2, limited studies exist in the literature which investigate the long-term voltage stability of power systems in the presence of VSWGs. Therefore, a detailed long-term voltage stability analysis in the presence of DFIG and FCWG based VSWGs is conducted in the present study, utilising complete dynamic model of a test system and dynamic simulations.

Chapter 2 lists different mechanisms, which can lead a power system to long-term voltage instability. In this chapter, two of those mechanisms are considered:

- LT-1 type instability - This is the most common mechanism which lead a power system to long-term voltage instability
- S-LT1 type instability - Short-term voltage instability induced by long-term dynamics in power systems having large induction motor loads

The impact of DFIG and FCWG based wind generation on LT-1 type long-term voltage instability is analysed in Sections 4.4 and 4.5.

With the increasing penetration levels of renewable power generators in power systems, tendency is that the existing synchronous generators are decommissioned. The impact of replacement of synchronous generators with VSWGs is considered in the voltage stability analysis presented in this chapter, which has not been evaluated previously. Moreover, the behaviour of DFIG and FCWG based VSWGs on long-term voltage stability is compared in Section 4.5. It also evaluates the impact of different wind generator loading levels on long-term voltage stability.

The impact of DFIG wind generation on long-term voltage stability in power systems with large induction motor loads is evaluated in Section 4.6 and the results demonstrate the behaviour of VSWGs during S-LT1 type long -term voltage

instability.

4.2 Variable-speed Wind Generator Models

4.2.1 Doubly-fed Induction Generator Simulation Model

The DFIG simulation model is developed in DIgSILENT Power Factory [68], of which an overview is shown in Fig. 4.1. The model consists of an aerodynamic model, a WRIG and the converters. A simplified overview of the DFIG control strategy adopted is shown in Fig. 4.2. The prime mover consists of the wind turbine, drive shaft and pitch controller. The pitch control limits the turbine power output to the rated power output at high wind speeds.

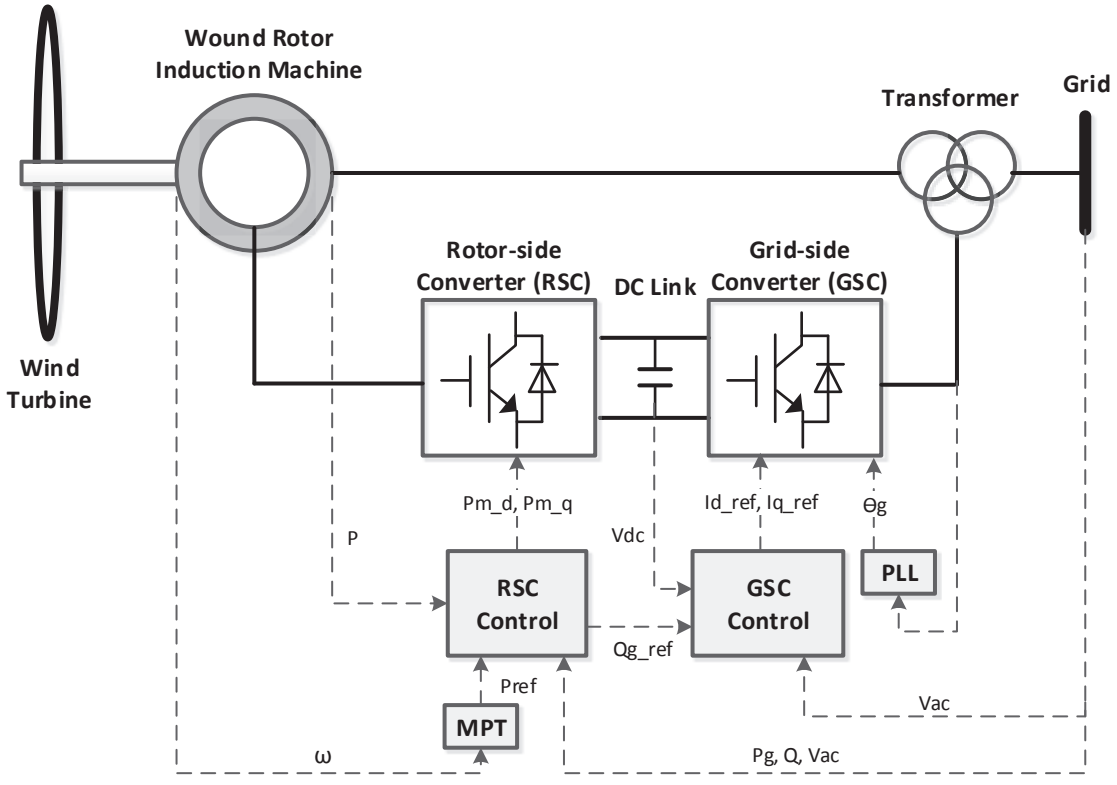

Figure 4.1: An overview of the DFIG model

In a DFIG, the RSC controls the active and reactive power flow from the stator to the grid by controlling the currents injected to the rotor. The GSC regulates

the DC link voltage by providing a path for the active power flow and it can also provide additional reactive power support to the grid.

As illustrated in Section 2.9.3, the dynamic model of the DFIG is represented in d-q reference frame which facilitates the decoupled active and reactive power control. As shown in Fig. 4.2, the RSC control consists of a two stage controller: PQ control and current control. PQ control is a slower power controller which calculates the q and d axis current references based on the active and reactive power measurements, and the active and reactive power references generated by maximum power tracking control and the reactive power controller. The current control block is a faster current controller to regulate the rotor currents to the rotor current references specified by the PQ control block. The stator flux oriented control is used for the RSC control. Below the rated power output of the turbine, the wind turbine generates the maximum possible active power based on the wind speed. This operation is controlled by maximum power tracking (MPT) block which calculates the optimum active power reference for PQ control.

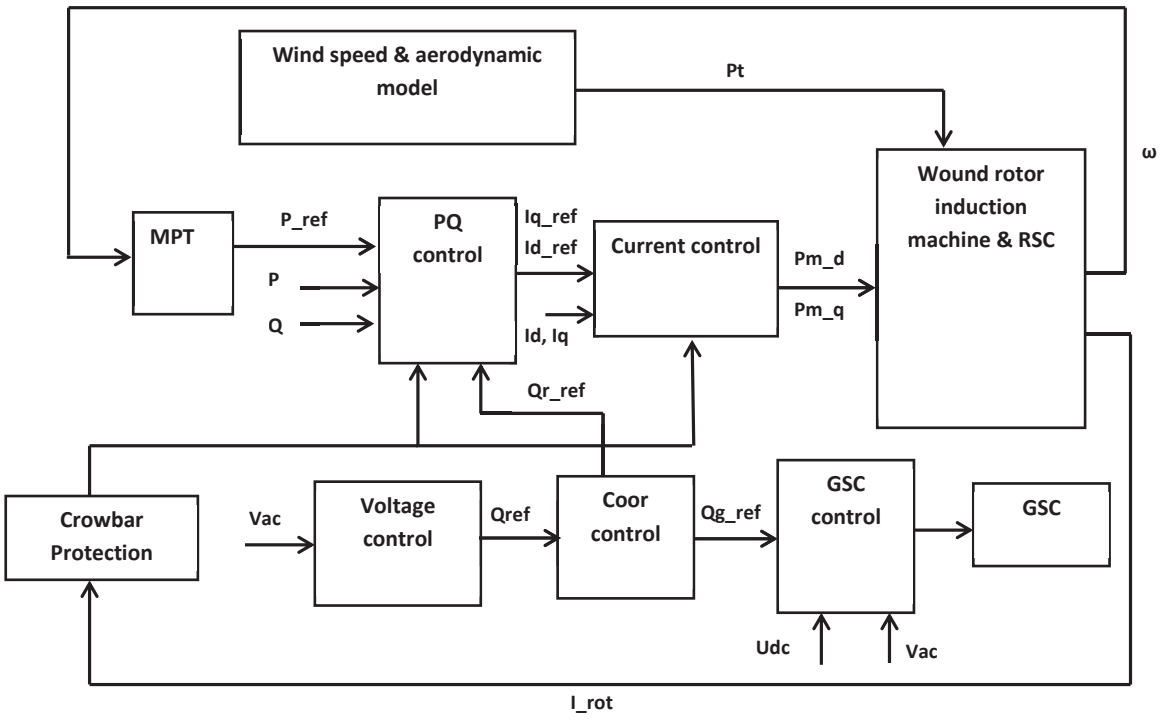

Figure 4.2: A simplified overview of DFIG control strategy

The reactive power references for RSC and GSC are calculated by the reactive power controller. In voltage stability studies, it is important to represent the reactive power controller of the generator very accurately as it has a strong influence on network voltage control. The reactive power controller of the DFIG is developed to utilise the full reactive power capability of the DFIG, where it can exchange reactive power in two ways: through the stator by RSC control and through the GSC. Fig. 4.3 illustrates the reactive power controller utilised in the DFIG. The reactive power controller is developed based on a voltage control strategy. If the PCC voltage (V_{ac}) varies beyond a pre-defined dead-band (0.98 p.u. - 1.1 p.u.), the DFIG starts to regulate the voltage. The reactive power references for the RSC control (for the reactive power exchange through stator) and GSC (Qg_ref) are calculated based on the corresponding reactive power capability diagrams illustrated in Chapter 2.9.1. The reactive power capability from the RSC depends on the level of active power exchange. The RSC reactive power reference (Qr_ref) is selected considering the active power operating level (P) and using the corresponding reactive power capability chart. If the reactive power supplied through the stator is not sufficient to regulate the voltage, the GSC starts to supply additional reactive power. This is usually known as the STATCOM operation of GSC.

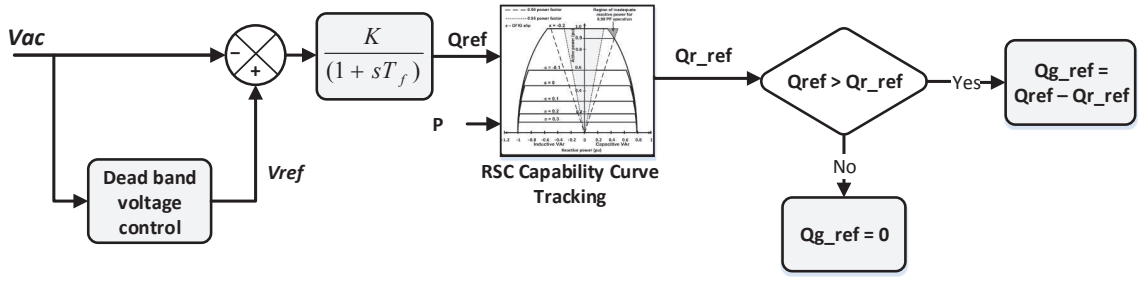

Figure 4.3: The reactive power controller of the DFIG

The GSC control of the DFIG is developed using a similar approach to the RSC control. However, it operates in AC voltage oriented reference frame. The crowbar protection is implemented in the protection block as shown in Fig. 4.2 for rotor over-current protection.

The data of an aggregated wind farm model comprising of 13 wind turbines, each rated at 1.5 MW is utilised in the simulations [69]. The RSC and the GSC are rated at 50% of the machine rating. The wind farm underground cable impedances are lumped with the transformer impedance [60].

4.2.2 Full-converter Wind Generator Simulation Model

The simulation model of the FCWG was developed in DIgSILENT Power Factory [65]. An overview of the FCWG simulation model is shown in Fig. 4.4. The model consists of an aerodynamic model, a multi-pole synchronous generator and the full scale power converters. The main difference between DFIG and the FCWG is the utilisation of full-scale power converters.

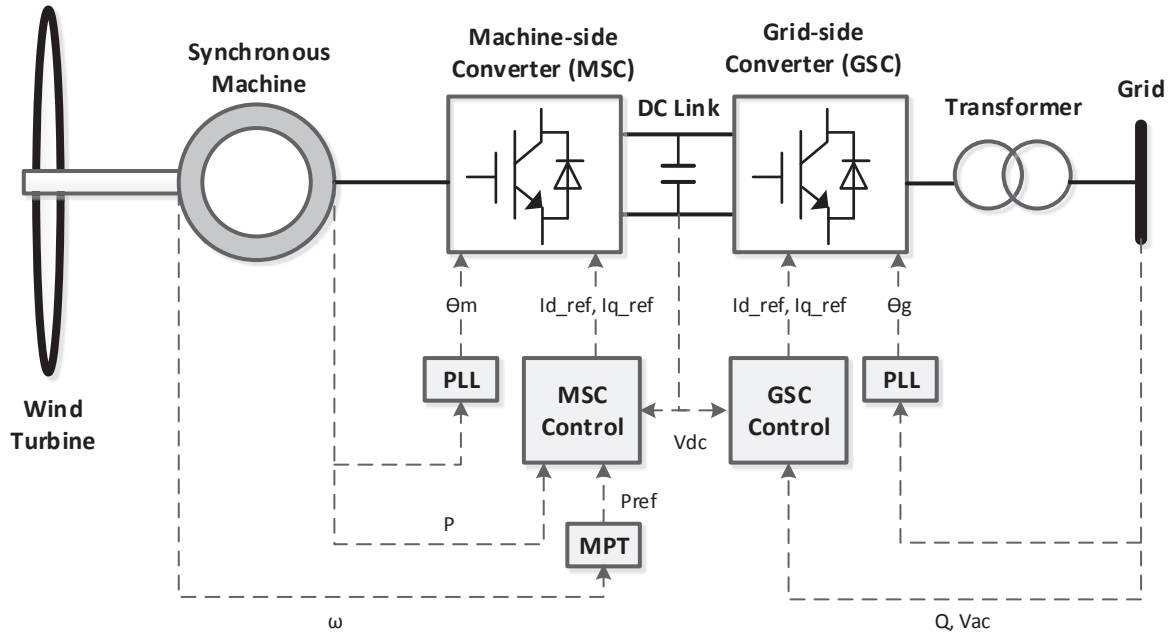

Figure 4.4: An overview of the FCWG model

As shown in Fig. 4.5(a), the prime mover consists of wind turbine, shaft and pitch control. Below the rated power output level of the generator active power is regulated using maximum power point tracking (MPT) characteristics which calculates the optimum active power reference to the power controller considering the wind speed. When the shaft speed exceeds the rated speed, active power set point remains the

same and the pitch controller controls the turbine speed to the allowable value.

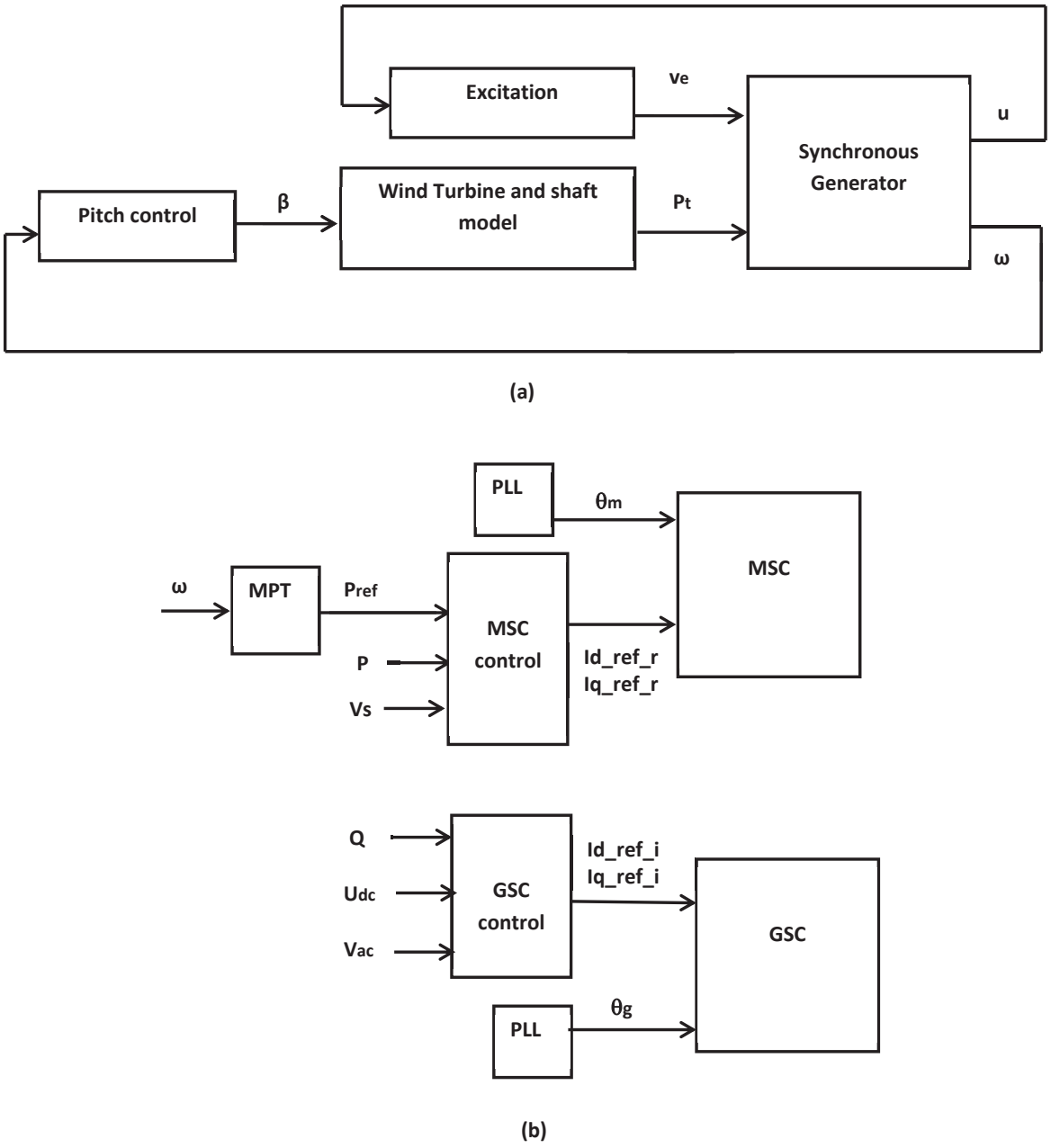

Figure 4.5: (a) Overview of the generator and aerodynamic model (b)Overview of the control strategies of the MSC and GSC of the FCWG

The stator of the FCWG is connected to the MSC, which controls the active power flow to the grid and controls the stator voltage. GSC facilitates the power transfer through MSC to the grid. It regulates the DC link voltage and provides reactive power support. The simplified overview of MSC and GSC control is shown in

Fig. 4.5(b). The model of the FCWG is also represented in d-q reference frame and stator voltage oriented control is utilised. Reactive power controller is implemented with the GSC control, and is based on the same voltage control strategy as in the case with DFIG. In this study, an aggregated wind farm model comprising 13 wind turbines, each rated at 1.5 MW is used in the simulations.

4.3 Test Network Development

The test network shown in Fig. 4.6 is used in the long-term voltage stability analysis [16]. G1 and G2 are synchronous generators and dynamic model of each generator is equipped with a Type DC1A excitation system, and an MAXEX2 type OXL model (DIgSILENT Power Factory library model) having short-term inverse-time characteristics [70].

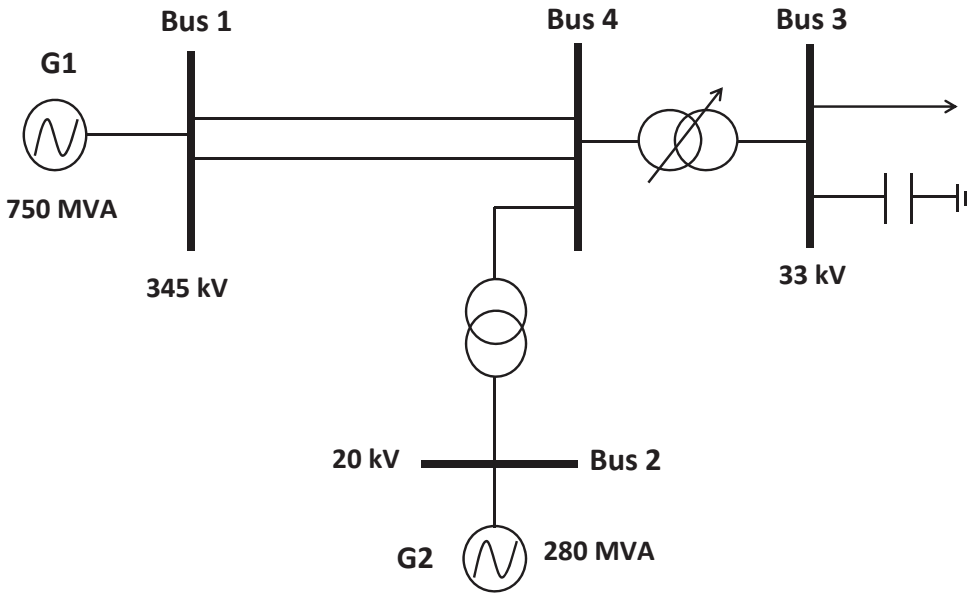

Figure 4.6: Test network

The step-down transformer between bus 3 and 4 is equipped with an OLTC. The load connected at bus 3 is modelled using an exponential load model as explained in Section 2.9.2 with load exponents α =1.5 and β =2.5. The load exponents are selected to represent a typical load model considering the load exponents of typical

loads (i.e 2.4).All other system parameters are listed in Appendix B.

4.4 Long-term Voltage Instability in the presense of DFIG Wind Generation

4.4.1 Scenario Description

In the long-term voltage stability analysis in the presence of DFIG wind generators, four case studies are considered, under two distinct scenarios, as shown in Table 4.1.

Considering the test system arrangement and the system parameters explained in the Section 4.3, bus 4 in the test system is located electrically closer to the load at bus 3. Similarly, bus 1 is located electrically far away from the load in bus 3. In the study presented in this chapter, two scenarios are considered to study the impact of integration of DFIG wind generation at bus 1 and 4.

Table 4.1: Scenario description for long-term voltage stability analysis in the presence of DFIG wind generation

Scenario-1		**Scenario-2**	
DFIG based wind generation at Bus 1		DFIG wind generation at Bus 4	
Case A	**Case B**	**Case C**	**Case D**
With unaltered synchronous generation capacity in the system	With reduced synchronous generation capacity	With unaltered synchronous generation capacity in the system	With reduced synchronous generation capacity

Moreover, with the increasing penetration levels of renewable generators in power systems, the renewable power generators are expected to replace the existing conventional synchronous generators in the system. To investigate the impact of displacement of existing synchronous generation, two cases are considered under each scenario, as shown in Table 4.1. In Case A and Case C, the existing synchronous

generation capacity in the system is maintained without alteration, while wind generation is added. However, in Case B and D, the synchronous generation capacity in the test system is reduced by an equivalent amount to the added wind generation, to investigate the impact of displacement of synchronous generator based generation by wind generation.

In the four cases (Case A-D) presented in Table 4.1, the DFIG based wind generation is added to the designated busbar via a line with a reactance of 0.0084 p.u. Each DFIG is operated at 70% of its active power rating. A system load ramping event is simulated to investigate the long-term voltage stability of the system, where the active power demand is increased by 0.3% per second with respect to initial load starting from t = 10 s to 110 s.

4.4.2 Case A - DFIG Wind Generation at Bus 1 with Unaltered Synchronous Generation Capacity

In Case A, the DFIG based wind generation is added to bus 1 without decommissioning any existing synchronous generators in the test system.

Fig. 4.7 shows the voltage profile at bus 3 following a load disturbance event. It is seen that, when the load is gradually increased, voltage starts to decrease. In the case without any wind generation, when the load is gradually increased, the voltage gradually starts to decrease. At t = 64 s, the OXL of G2 operates and the voltage reduces to 0.95 p.u., and subsequently the tap changer begins restoring the voltage after a delay. Although the load voltage attempts to recover with each tap operation, it further increases the reactive power demand at the high voltage terminal of the transformer, which further increases the reactive power demand of the system. At about t = 93 s, the OXL of the G1 operates resulting a larger reduction in the voltage (voltage decreases to 0.72 p.u). However, during low voltage periods, wind generators are allowed to trip after a prescribed time according to the low voltage ride-through requirements. Therefore, the instance at which the voltage instability is initiated and the voltage profile up to about 0.9 p.u. is considered for comparisons.

Once the wind generation is added to the network, voltage instability initiates after t = 64 s. This is due to the fact that the OXLs operates later than in the case with no wind generation and hence the voltage reduction initiates later. According to this observation, added wind generation helps the system to operate within acceptable voltage levels for an extended period of time in comparison to the base case. This is favourable for voltage stability of the system. However, it should be noted that, the system total generation capacity is increased with the added wind generation in this case. Therefore, Case B corresponds to a more realistic scenario, which can be used to compare the actual capability of wind generation to support long-term voltage stability.

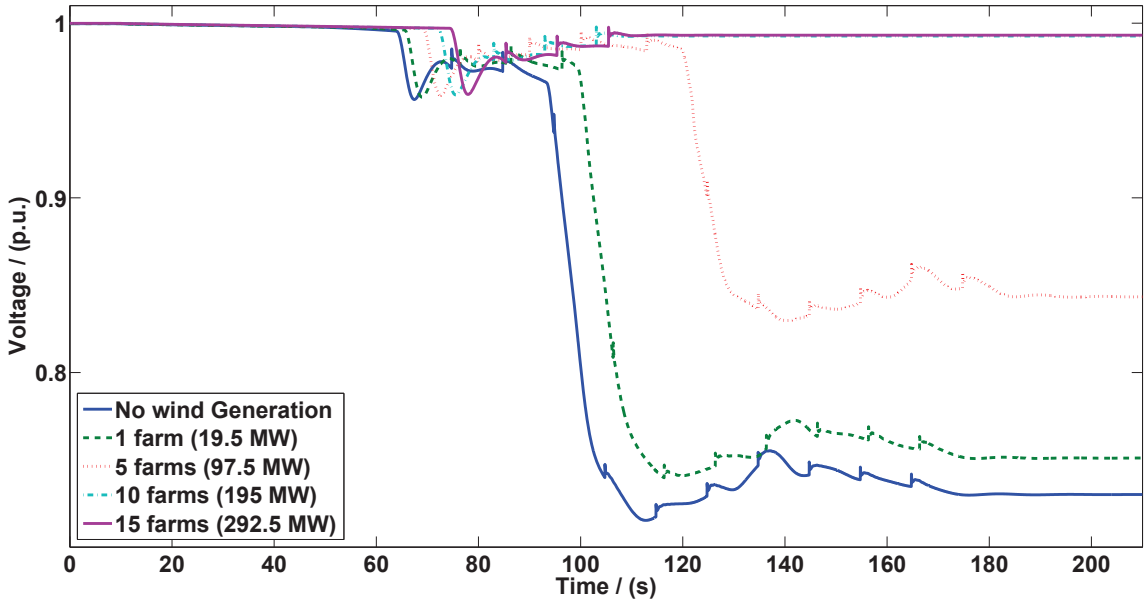

Figure 4.7: Voltage profile of bus 3 for Case A

4.4.3 Case B - DFIG Wind Generation at Bus 1 with Reduced Synchronous Generation Capacity

In this case, the total generation capacity in the system is maintained constant as wind generation is added to bus 1. This is achieved by reducing the MVA capacity of the existing synchronous generation at bus 1 by an equivalent amount to the added DFIG wind generation capacity to bus 1. Fig. 4.8 (a) illustrates the system dynamic

performance for the same load recovery event with and without wind generation (wind penetration level is varied from 2.6% to 40%). Fig 4.8 (b) and (c) show the reactive power output through stator and GSC of the DFIG at various wind penetration levels.

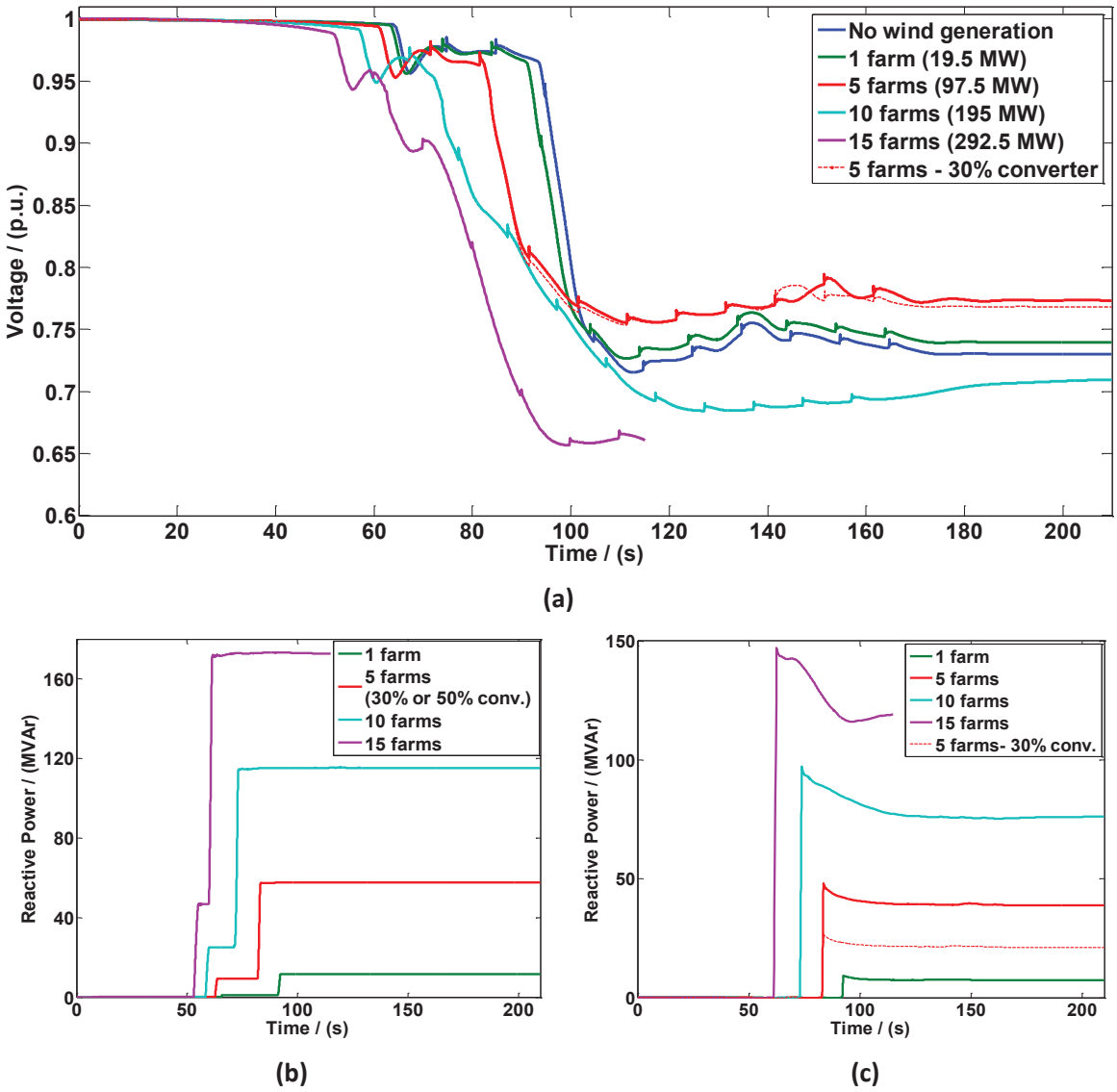

Figure 4.8: (a) Voltage profile of bus 3 for Case B (b) Reactive power output through stator by RSC control (c) Reactive power output from GSC

Fig. 4.8 also illustrates the behaviour with 30% rating of GSC for the case with 5 wind farms. Although, the reactive power support available from GSC with 30% converter rating is less than for the case with 50% rated converter, the GSC reactive

power support is provided when the reactive power support through the stator is not sufficient to support the voltage reduction. The system voltages have alraedy reduced to a low value by then, and hence the increased reactive power could not facilitate an effective improvement to the network voltages.

It is seen that as the wind generation capacity in the system increases, voltage starts to decrease rapidly. Therefore, OXLs of the generators operate quickly, initiating voltage instability. Therefore, if the added wind generation has to replace an equivalent capacity of synchronous generation in the system, it cannot support the system as much as the synchronous generation with an equivalent capacity. The main reason for this observation is the difference in the dynamic reactive power capability of DFIG wind generation and the synchronous generators. The overload capability of synchronous generators allow the system to be stable for a longer period, whereas wind generators cannot provide such reactive power requirement.

Moreover, the actual reactive power capability available at the wind farm PCC is less than the aggregated reactive power from all wind generators in the wind farm. A wind farm is composed of a large number of small wind turbine generators distributed in a large geographical area. Therefore, significant amount of underground cables and low-voltage transformers are used within the farm itself. Due to the losses associated with these internal impedances, the actual reactive power support available at the wind farm collector point (PCC) is less than the expected reactive power though the machine/converter capability. In this case, it is noted that the reactive power available at the PCC is about 15 MVArs less than the total reactive power output at the generator terminal for the case with 5 wind farms during the voltage instability as shown in Fig. 4.9, an aspect which can be considered as another factor which affects the reactive power support from a wind farm.

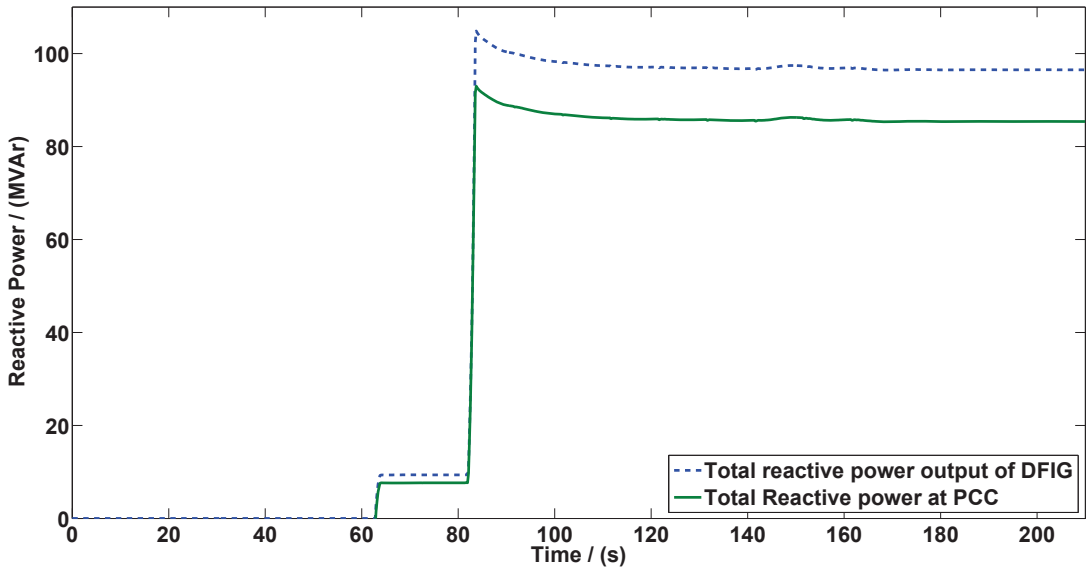

Figure 4.9: Total reactive power output of DFIG and the reactive power available at wind farm collector point

According to the voltage control strategy utilised for the DFIG, it provides the maximum possible reactive power support during the voltage instability. However, the response of the DFIG to long-term voltage stability is not favourable in this case.

4.4.4 Case C - DFIG Wind Generation at Bus 4 with Unaltered Synchronous Generation Capacity

This case is similar to Case A except for the difference, where wind generation is added to bus 4 which is near to the load at bus 3. Fig. 4.10 shows the results for this case where the initiation of voltage instability is delayed in the presence of DFIG wind generation compared to the case without any wind generation. This is favourable for system voltage stability. However, Case D presented next is relatively more realistic, in which existing synchronous generation is replaced with an equivalent capacity of wind generation.

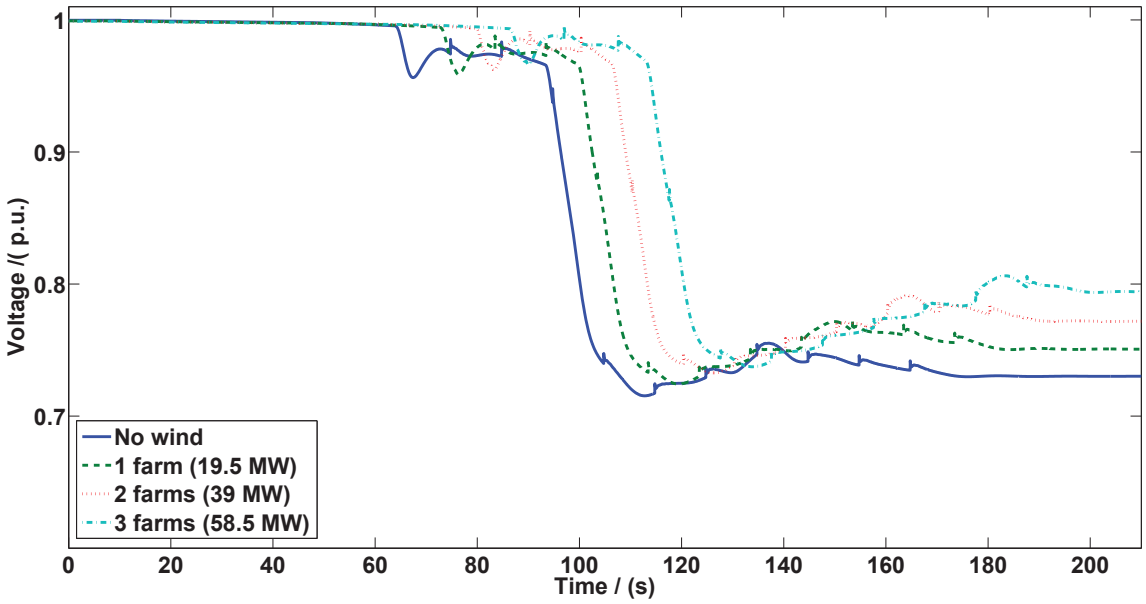

Figure 4.10: Voltage profile of bus 3 for Case C

4.4.5 Case D - DFIG Wind Generation at Bus 4 with Reduced Synchronous Generation Capacity

In this case, the total system generation capacity is maintained constant, as the DFIG based wind generation is integrated at bus 4 to the system. This is achieved by reducing the MVA capacity and the active power set point of the existing synchronous generation at bus 2 (G2) by an amount equal to the added wind generation. Fig. 4.11 shows the relevant results for Case D.

Reactive power support is usually provided by the generators near to the network disturbance. Therefore, G2 is crucial in responding to the load ramp event, which will be heavily loaded compared G1. This can be further explained as follows:

Let,

Q_1 - reactive power output of G1

Q_2 - reactive power output of G2

V_3 - bus 3 voltage

δ_2 - voltage angle of bus 2

δ_3 - voltage angle of bus 3

X_{14} - line reactance of line 1-4

X_{24} - transformer reactance of transformer 2-4.

Let the turns ratio of transformer 3-4 be 1:t. As bus 1 is the slack bus and bus 2 is a PV bus, the voltages at the two buses are maintained at 1 p.u. at steady-state. Hence, the reactive power output of G1 and G2 can be given as in (4.1) and (4.3),

$$Q_1 = \frac{1}{X_{14}} - \frac{V_3.cos\delta_3}{t.X_{14}} \tag{4.1}$$

$$Q_2 = \frac{{V_2}^2}{X_{24}} - \frac{V_2.V_3.cos\left(\delta_2 - \delta_3\right)}{t.X_{24}} \tag{4.2}$$

$$Q_2 = \frac{1}{X_{24}} - \frac{V_3.cos\left(\delta_2 - \delta_3\right)}{t.X_{24}} \tag{4.3}$$

The reactive power sensitivities with respect to bus 3 voltage can be expressed in (4.4) and (4.5),

$$\frac{\partial Q_1}{\partial V_3} = \frac{-cos\delta_3}{t.X_{14}} \tag{4.4}$$

$$\frac{\partial Q_2}{\partial V_3} = \frac{-cos\left(\delta_2 - \delta_3\right)}{t.X_{24}} \tag{4.5}$$

In steady state $\delta_2 \approx \delta_3 \approx 0$, $X_{14} > X_{24}$ and t is constant. Hence,

$$\frac{\partial Q_2}{\partial V_3} > \frac{\partial Q_1}{\partial V_3} \tag{4.6}$$

Therefore, reactive power output of G2 is more sensitive to the voltage variations in bus 3 than that of G1. Hence, G2 is loaded more than G1, although G1 is a generator with a larger capacity and hence a larger reactive power capability. This

is further confirmed by Fig. 4.12(a). Due to this reason, usually, G2 will operate closer to its reactive power limit at the steady-state and its capability to provide increased reactive power during a disturbance is significantly reduced, whereas G1 can increase its reactive power output during a disturbance to a large extent.

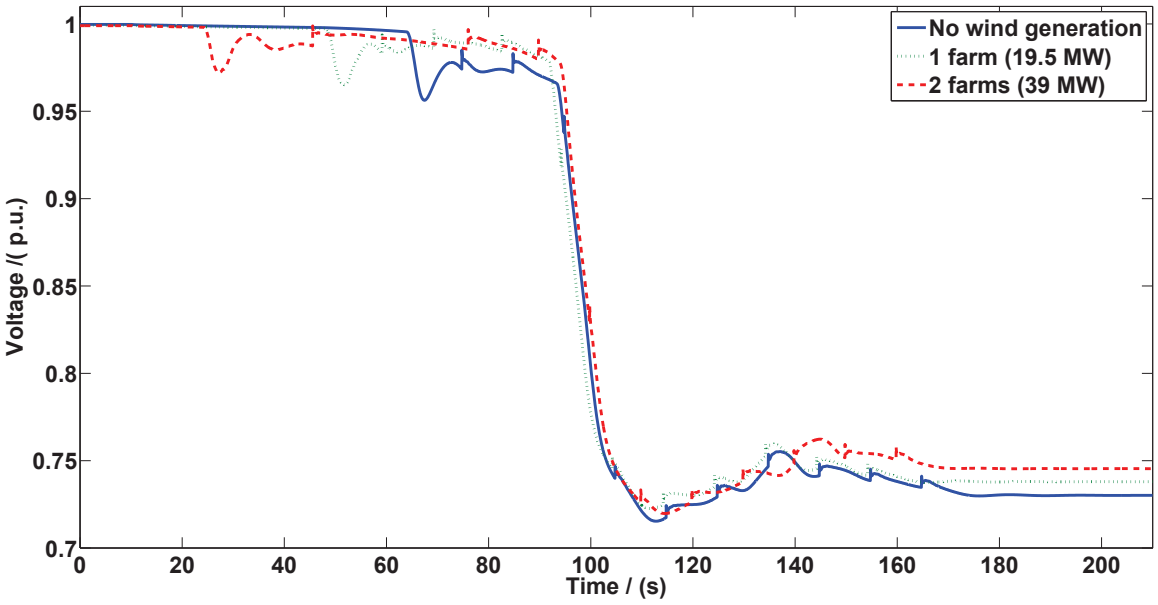

Figure 4.11: Voltage profile of bus 3 for Case D

According to the results shown in Fig. 4.11, voltage instability initiates at an instant earlier compared to the case with no wind generation in the system. The operation of OXL of G2 advances, as added wind generation is increased. Due to the fact that G2 is operating closer to the limits, the OXL of the G2 operates quickly following the disturbance. Subsequent tap changer operations makes the system conditions worse from a voltage stability perspective. With two wind farms added to bus 4, the OXL of G2 operates 15 s after the load disturbance. However, high wind penetration levels at bus 1 could be achieved while maintaining the voltage stability for a longer period after the disturbance. In Case B, voltage instability initiates after 50 s from the load event, with 15 wind farms (40% wind penetration) connected to bus 1. This is due to the fact that the local generation is replaced in Case D, which is imperative for system stability during disturbances.

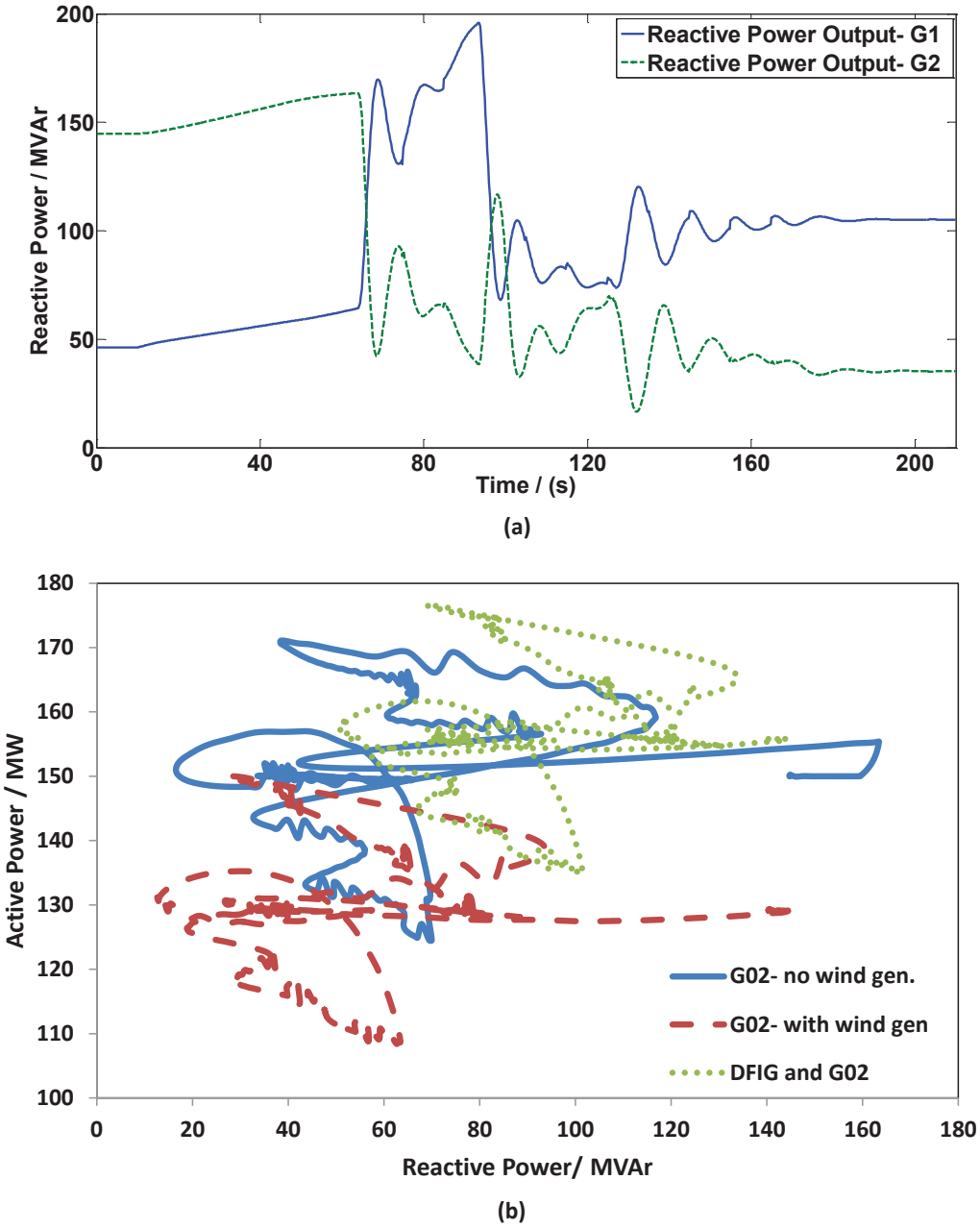

Figure 4.12: (a) Reactive power output of G1 and G2 (b) Active Power and reactive power operating range

Furthermore, as local synchronous generation capacity is reduced, the overload capability of the local generation is also reduced in the same proportion. This can be confirmed using Fig. 4.12 (b), which shows the P-Q operating range of G2 for the case with no wind generation and for the case with 2 wind farms at bus 4. It also shows the variation of total reactive power support provided by G2 and the

DFIG with the total active power for the same case. It shows that the reactive power output of G2 varies over a larger range when there is no wind generation. However, when the existing synchronous generation is displaced by wind generation, the reactive power versus active power trajectory has become narrower due to the reduced overload capability. Apart from these factors, other factors such as reactive power losses within the wind farm also leads the system to voltage instability much faster, when the synchronous generation is replaced with an equivalent amount of wind generation.

4.5 Long-term Voltage Instability with FCWG Wind Generation

4.5.1 Scenario 1- Comparison of DFIG and FCWG

In this scenario, the FCWG based wind generation with different capacities is added to bus 1 and the existing synchronous generation at bus 1 is reduced accordingly to maintain total system capacity constant similar to the Case B in Section 4.4. Each FCWG is loaded to 70% of the full individual capacity.

According to Fig. 4.13 (a), voltage instability initiates quicker in this case in comparison to the case with no wind generation in the system. As the wind generation output is increased the instability initiates earlier due to the operation of the OXL of G2. When the operation of DFIG and FCWG is considered, it can be observed that the voltage instability initiates quickly with FCWG based generation compared to a case with approximately similar capacity DFIG wind generation. This is due to the reduced reactive power support available from the FCWG compared to DFIG based generation, which can be confirmed using Fig. 4.13 (b). This phenomenon can be further understood by considering the capability charts of the VSWGs explained in Section 2.9.1.

Four separate cases were considered in analysing the long-term voltage instability associated with DFIG wind generation in Section 4.4. However, with regard to

FCWG, only one case is considered to avoid repetition. The results for other cases will have a similar pattern, where they demonstrate the reduced voltage support available from FCWG compared to DFIG.

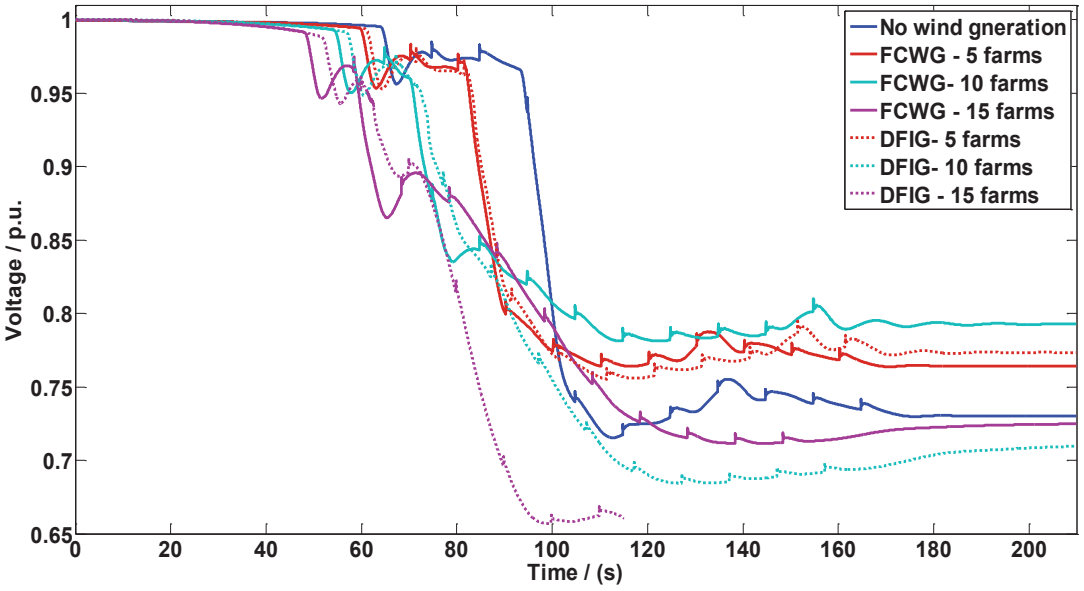

(a)

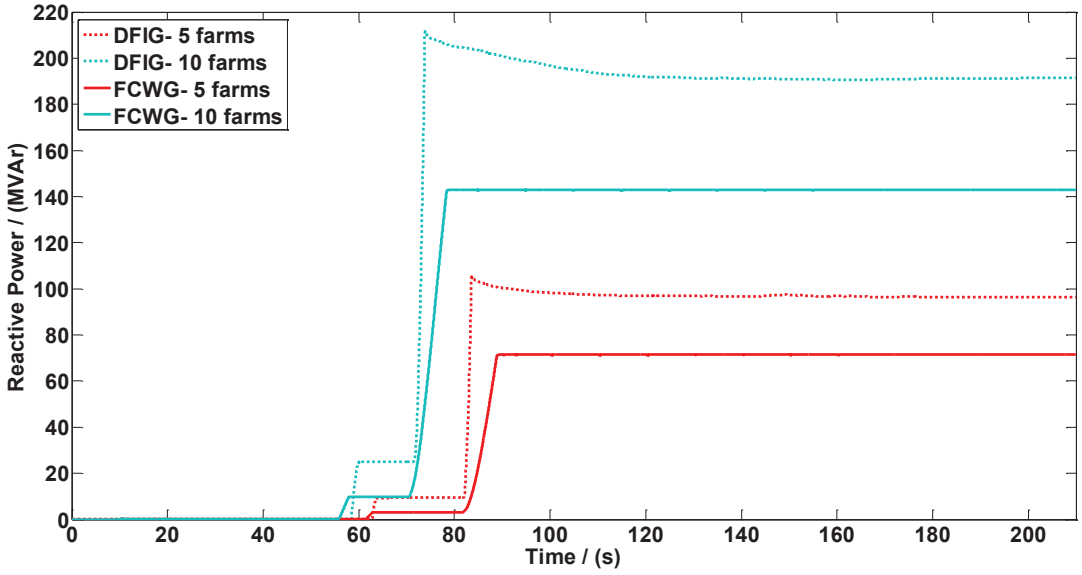

(b)

Figure 4.13: (a) DFIG and FCWG Comparison (b) Comparison of reactive power outputs

4.5.2 Scenario 2- Influence of Wind Generator Loading

In this scenario, the FCWG is operated at different loading conditions to study the effect of differences in the reactive power capabilities at different loading conditions of the wind generators on long-term voltage instability.

According to the capability charts, reactive power capability of FCWG and the DFIG (through stator) depend on the active power output. At lower active power output levels, they have a higher reactive power capability. In this scenario, two FCWG wind farms connected to bus 1 are operated under three different loading conditions while maintaining the system capacity constant. Fig. 4.14 (a) shows the variation of bus 3 voltage and the reactive power output of FCWG at 50%-90% loading conditions. It should be noted that having FCWG at bus 4 shows a similar trend in the results, when it is operated at different loading conditions.

When the FCWG is operated at low loading level, the FCWG has more reactive power capability as evident from Fig. 4.14 (b). However, the burden on synchronous generators in the system to provide active power is higher, as wind generators supply less active power in this case compared to the cases with higher loading level. Therefore, the capability of the synchronous generators in the network to provide reactive power is reduced when the wind generators are operated at low loading level. Therefore, the OXL of G2 operates quickly initiating voltage instability, when the FCWG operates at low loading level. However, if the same wind power output can be obtained by a large number of less loaded wind generators, the above would not happen, as there is no change in the reactive power demand from the synchronous machines in the system, which is favourable for voltage stability of the network.

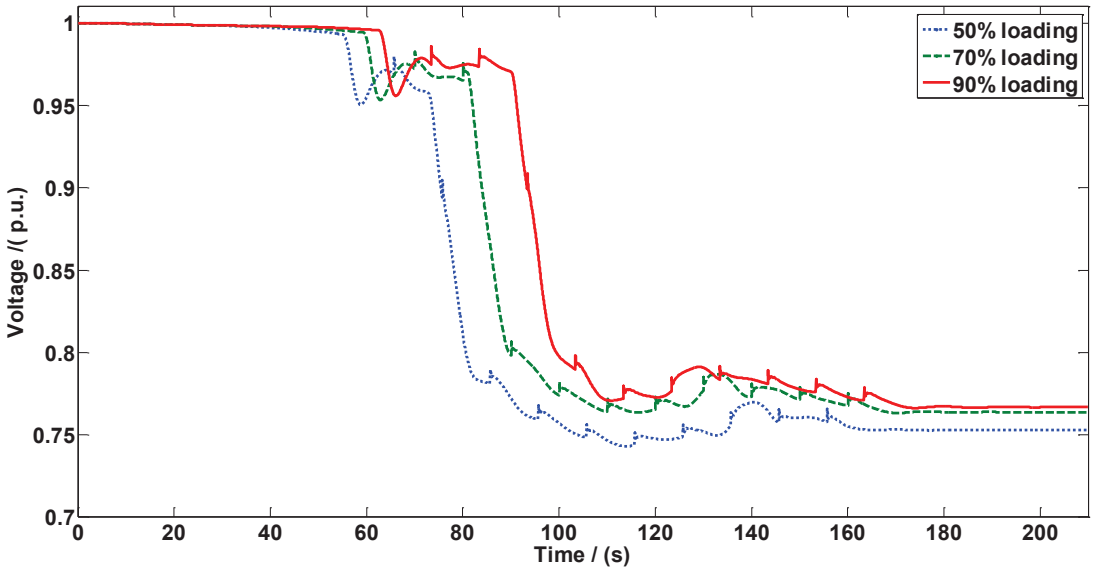

(a)

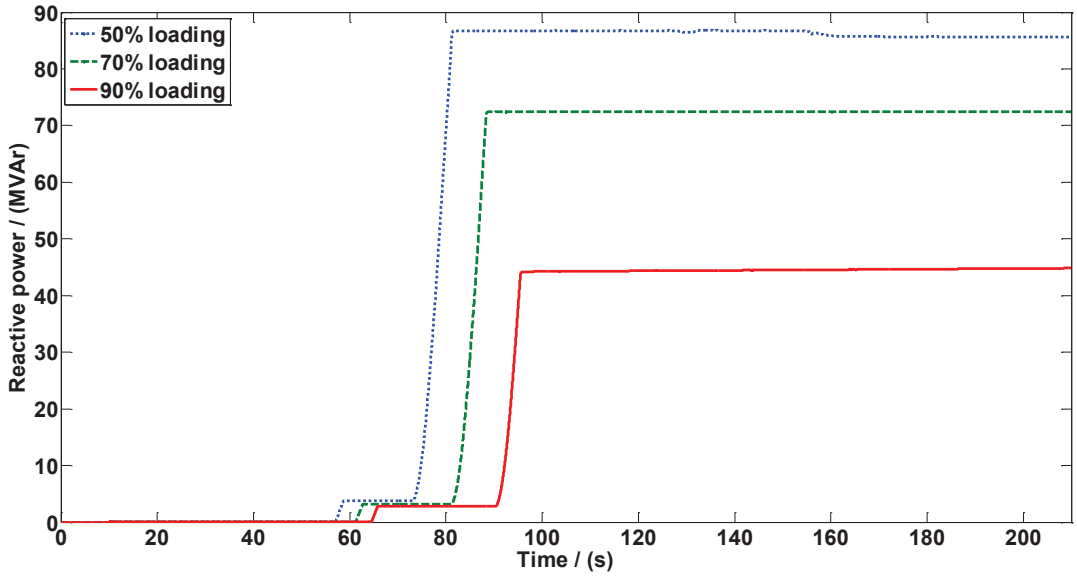

(b)

Figure 4.14: (a) Voltage variation at different loading levels (b) Reactive power output of FCWG at different loading levels

4.6 Long-term Voltage Instability in Power Networks with Induction Motor Loads

In this section, the impact of VSWGs on the long-term voltage instability of power systems containing significant induction motor loads is studied. In this study, 30% of the load connected to bus 3 of the test system explained in Section 4.3 is composed of induction motors. The induction motor parameters are listed in Appendix B. The total induction motor load compises 27 parallel conncected induction motors, and it is integrated to bus 3 via a transformer. The same load disturbance considered in the previous section is considered. The DFIG based wind generation is integrated at bus 1 while maintaining the total generation capacity of the test system constant, and the impact of the long-term voltage stability is assessed.

Fig. 4.15 shows the voltage profile at bus 3 without any wind generation and with different levels of DFIG wind generation connected to bus 1. The induction motor load draws constant reactive power from the network when the voltage is within the acceptable levels, compared to the exponential voltage dependent load used in the previous section. However, when the voltage drops to low values, the induction motors stall, drawing a large amount of reactive power as shown in Fig 4.16 (a). Although the OXL of G2 operates after initiating the load disturbance at about t= 25 s in the case without any wind generation, the voltage recovers to acceptable levels mainly by the OLTC operation. The major voltage instability is initiated after the OXL limitation of G1 at about t =122 s. Then, the voltage reduces to a lower value and the system leads to voltage collapse due to the induction motor stalling, which can be confirmed from the variation of the induction motor slip as shown in Fig. 4.16 (a).

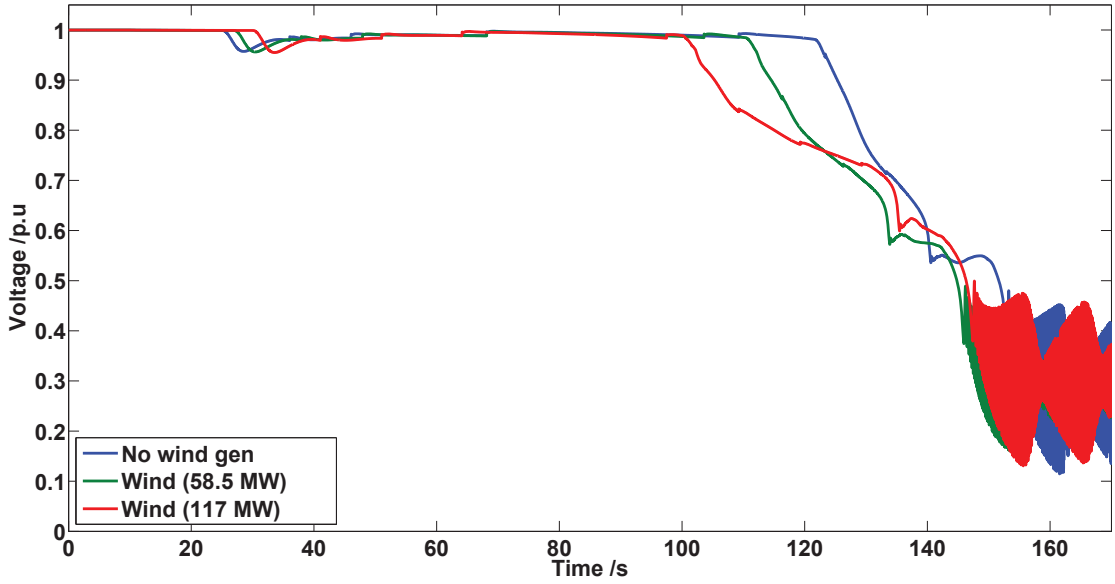

Figure 4.15: Voltage Profile of Bus 3

According to the results shown in Fig 4.15, the voltage instability is initiated quickly when the DFIG based wind generation is added to bus 1 and with the increased DFIG based wind power penetration. Fig. 4.16 also illustrate the reactive power output of G1 and the DFIG during the event. Similar to the previous cases, DFIG based VSWGs cannot improve long-term voltage stability of the power systems which contain significant induction motor loads.

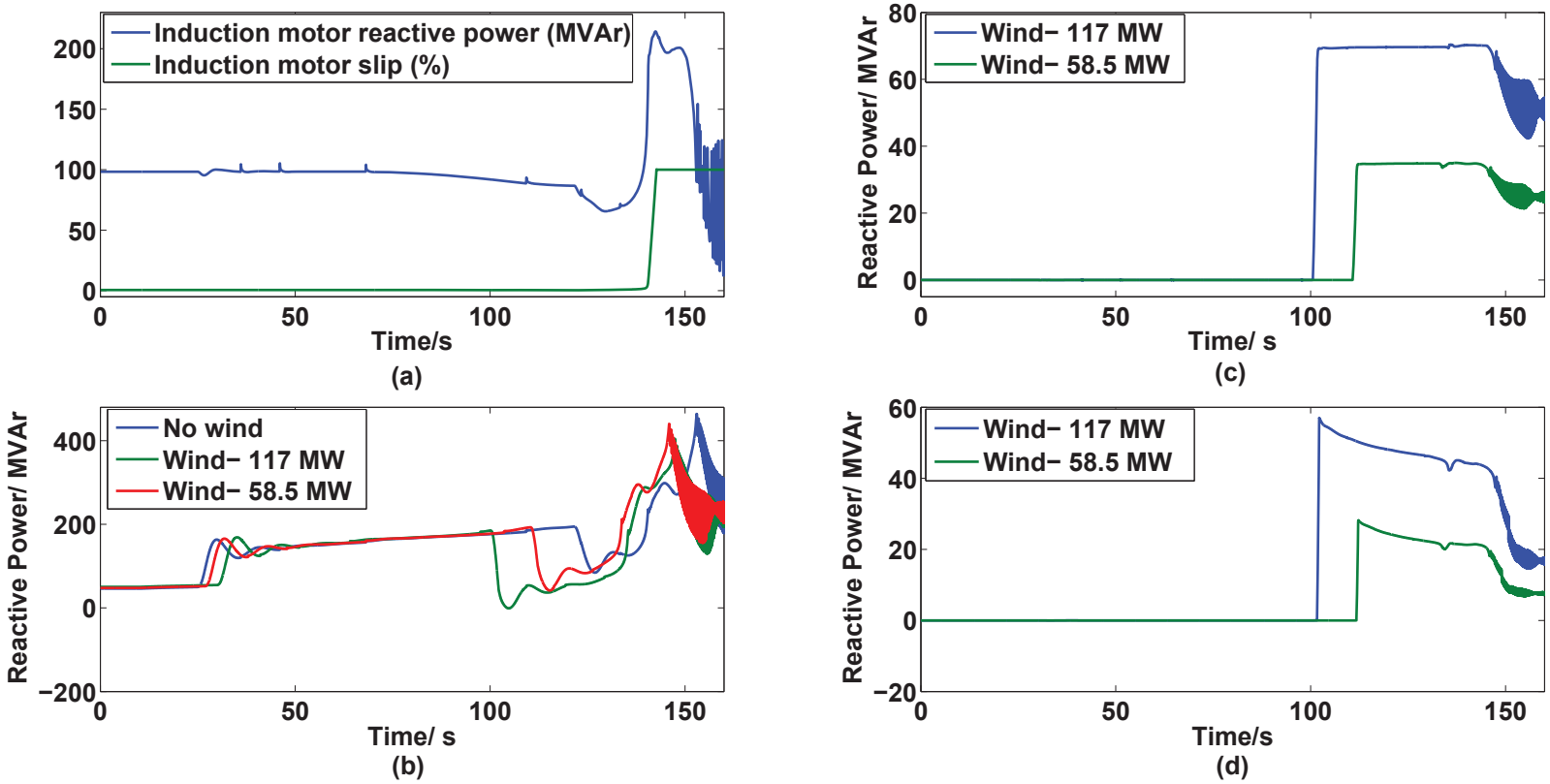

Figure 4.16: (a) Reactive power consumption and the slip of the induction motor (b) Reactive power output of G1 (c) Reactive power output of the DFIG- through stator (d) Reactive power output of the DFIG - through GSC

4.7 Summary

In this chapter, the results of long-term voltage stability analysis of power systems integrated with VSWGs were presented. The dynamic models of the DFIG and the FCWG based wind generators used in the studies were explained. The voltage stability analysis was conducted using a five bus test system modeled in DIgSILENT Power Factory. Two common mechanisms which lead power networks to exhibit long-term voltage instability were considered.

Results demonstrated that the VSWGs added to a power system without making any changes to the total system generation capacity, improves the long-term voltage stability of the network. The DFIG and FCWG based VSWGs have the capability to provide reactive power, in addition to the active power. However, with the increasing penetration levels of the renewable power generators in networks, some of the existing synchronous generators are usually retired or decommissioned. Therefore, VSWGs have to replace the capabilities of some of the existing synchronous generators in power systems. This factor has been extensively considered in the work presented in this Chapter. The results demonstrated that the capability of the VSWGs to support the power system, under such conditions is less compared to the synchronous generators in general. Although VSWGs have significant reactive power capabilities, the major difference between the response of the synchronous generators and VSWGs is the dynamic overload capability of the synchronous generators. Moreover, the reactive power support available from a wind farm is limited by the internal losses within the wind farm. It is recommended to use additional reactive power support along with the wind farms to prevent the long-term voltage instability under such unfavorable system conditions. Although some of the existing work claim improved reactive power support provided by VSWGs, this work suggests that these wind generators still needs additional reactive power support in cases, where they have to replace exiting synchronous generators.

The results of the work presented in this chapter also demonstrated that the connection point of a wind farm is an important factor which affects the long-term

voltage stability. Usually, the reactive power support to the loads are provided by the nearby generators. Therefore, the local generation is crucial for load centers. The replacement of a synchronous generation local to a load centre, with wind generators can have detrimental effects on the long-term voltage stability. However, if the wind generation is added without making any changes to the existing generation, it is favorable for the long-term voltage stability.

When the reactive power capability characteristics of the DFIG and FCWG based VSWGs explained in Chapter 2 are compared, DFIG has a higher reactive power capability compared to a FCWG, when the reactive power support from the GSC of the DFIG is also considered. Furthermore, in the comparison of the response of these two types of generators during a long-term voltage instability event, it was shown that the DFIG has a relatively higher capability to support the system compared to a FCWG.

According to the capability charts of the VSWGs explained in the Chapter 2, their reactive power capability also depend on the operating active power level or the loading level of the generators. Under low loading conditions, during low wind speed conditions, these generators have higher reactive power capabilities. This factor had also been considered in the studies presented in this Chapter. According to the results, in the cases where the VSWGs have to replace existing synchronous generators, although the VSWGs have higher reactive power capability during low loading conditions, detrimental effects on the long-term voltage stability can be observed, due to the low active power output of the VSWGs.

The long-term voltage instability in networks with significant levels of induction motor loads was also illustrated in this chapter. In the scenario with significant induction motor loads, the unfavorable response of the DFIG compared to synchronous generators during a long-term voltage instability event was noted.

It should be noted that the best possible voltage control strategy is used in the studies in this chapter utilising the maximum possible reactive power support of the DFIG and the FCWG based generation. However, the response of the VSWGs to the

long-term voltage stability is not favorable in some conditions. Therefore, additional reactive power support devices, such as static compensators (STATCOMs) have to used along with the VSWGs, particularly in networks with very high wind power penetration levels, where the existing number of synchronous generators are not significant.

Chapter 5

Development of an Energy Function Based Method for Long-term Dynamic Voltage Stability Assessment

5.1 Introduction

This chapter presents an alternative methodology for the verification of long-term dynamic voltage stability in power systems using an energy function based approach. The potential of extending the proposed energy function methodology to evaluate the voltage stability of wind rich power networks is also discussed in this chapter.

Voltage stability is a dynamic phenomenon, where dynamic simulations can be used for precise evaluation of voltage stability. However, conducting complete dynamic simulations for large interconnected networks is time-consuming and demands significant computational capability, due to the requirement for incorporation of all dynamic models and the numerical integration associated with the calculation process.

In the past, researches have introduced direct methods for stability analysis of

power systems [71, 72]. Direct methods are alternative methods which can be used for power system stability analysis which were generally developed using energy function based techniques. The main advantage of using direct methods is the ability to evaluate the system stability without explicitly solving the differential equations for the system. Furthermore, these methods are capable providing information on the degree of stability of a power network. However, practical application of most of the direct methods developed in the past is limited mainly due to the limitations in application of the methodologies to large interconnected networks which are represented using detailed models.

The direct methods available in the existing literature are generally used for transient stability evaluation. The energy function based method for power system stability analysis has also initially been introduced as a method for transient stability evaluation. However, it has been later extended for voltage stability evaluation [37–40].

In the energy function based method for voltage stability analysis, the energy distance between the stable equilibrium point and, the closet unstable equilibrium point of a system operating condition is used as a proximity indicator to voltage collapse (critical point of voltage instability). The energy margin between the high and low voltage power flow solutions is computed to calculate this energy measure [37]. However, there are practical limitations in using this method, mainly due to the limitations in establishing the critical low voltage power flow solution for large power networks. Thus, application of the energy function method for voltage stability analysis is limited to planning level studies. In this chapter, a novel energy function method for voltage stability evaluation is introduced for long-term dynamic voltage stability evaluation. The method is developed based on the conventional energy function approach, and it can be used for voltage stability evaluation without the aforementioned practical limitations. In this method, the energy margin between a pre-determined stable operating point and any subsequent operating point of a network is evaluated. This 'energy margin' directly reflects the voltage instability

in the network.

In Section 5.2, basic theoretical derivations of the proposed energy function approach is explained using a simple two bus network. It demonstrates the capability of the proposed energy margin and the rate of change of energy margin to identify dynamic voltage instabilities in a network through sensitivity analysis. It also compares the conventional energy function based method for voltage stability assessment and the proposed method.

In section 5.3, the extension of the proposed method to a large power network is illustrated using the Reliability and Voltage Stability (RVS) test system. Due to the direct correlation between the proposed energy margin and the voltage instability, one of the main applications of this method can be in online voltage security assessment, which is explained in Section 5.4. Due to the increasing renewable power penetration levels in electricity networks around the world, power systems are becoming more dynamic and, less predictable and reliable. Hence, the usage of real-time security measures in current and future power systems is vital more than ever before. With the development of phasor measurement technologies and the related communication infrastructure, the implementation of the methods become easier.

Section 5.5 of this Chapter demonstrates the application of the proposed method to evaluate the long-term dynamic voltage instability of a network with wind generation using some case studies presented in Chapter 4. It also provides additional verification for the results presented in Chapter 4.

5.2 Energy Function Explanation of Long-term Dynamic Voltage Instability

5.2.1 Theoretical Derivations

The preliminary concepts of the energy function method for voltage stability analysis is explained using the simple two bus system shown in Fig. 5.1, where V_1, δ_1, V,

δ_2, B, P, Q and I are Bus 1 voltage magnitude, Bus 1 voltage angle, Bus 2 voltage magnitude, Bus 2 voltage angle, line susceptance, load active power, reactive power and current, respectively [37].

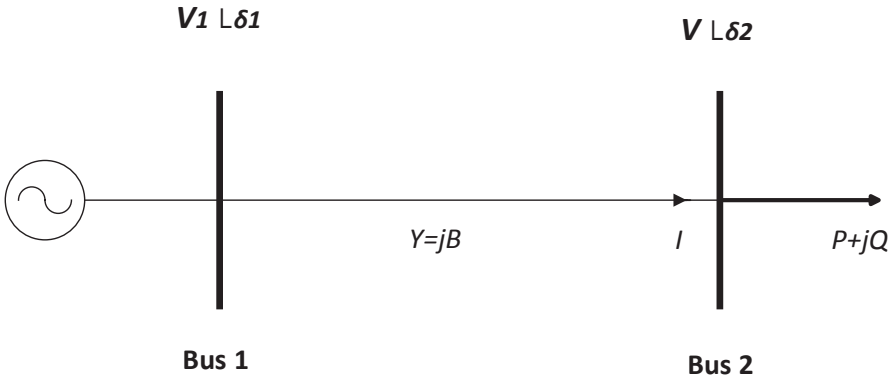

Figure 5.1: Two bus system

For Bus 2 in Fig. 5.1,

$$P + jQ = VI^* \tag{5.1}$$

$$P + jQ = V\angle\delta_2\left(\frac{(V_1\angle\delta_1 - V\angle\delta_2)}{X\angle 90^0}\right)^* \tag{5.2}$$

$$P + jQ = VB\angle\delta_2\left(V_1\angle\left(90^0 - \delta_1\right) - V\angle\left(90^0 - \delta_2\right)\right) \tag{5.3}$$

Let, $\alpha = \delta_1$ - δ_2. Equating the real and imaginary parts of (5.3),

$$P = VV_1Bsin\alpha \tag{5.4}$$

$$Q = VV_1Bcos\alpha - V^2B \tag{5.5}$$

Therefore, power balance equation for Bus 2 is given by,

$$P - VV_1 Bsin\alpha = 0 \tag{5.6}$$

$$Q - VV_1 Bcos\alpha + V^2 B = 0 \tag{5.7}$$

Considering the classical generator model [73],

$$\frac{2H}{\omega_0}\ddot{\delta} + \frac{D}{\omega_0}\dot{\delta} = P_m - P_e \tag{5.8}$$

where, *H*, *D*, *Pm*, *Pe* and δ are inertia constant, damping coefficient, mechanical power, electrical power and rotor angle.

Using (5.8),

$$M\dot{\omega} + D\omega = P_m - P_e \tag{5.9}$$

$$M\dot{\omega} - P_m + D\omega + VV_1 Bsin\alpha = 0 \tag{5.10}$$

where,

$$\omega = \dot{\delta} \tag{5.11}$$

$$M = 2H \tag{5.12}$$

Let, $f(\alpha, V) = VV_1 Bsin\alpha - P$. Hence, (5.10) can be expressed as,

$$\dot{\omega} = -M^{-1}D\omega - M^{-1}f(\alpha, V) \tag{5.13}$$

Assuming that the real power demand is modelled as a constant and a linear term dependent on the bus frequency, using (5.6),

$$P + D_l\dot{\delta_2} - VV_1Bsin\alpha = 0 \tag{5.14}$$

$$D_l\dot{\delta_2} = f(\alpha, V) \tag{5.15}$$

$$\dot{\alpha} = -D_l f(\alpha, V) + \omega \tag{5.16}$$

Using reactive power balance given by (5.7),

$$V^{-1}\left(Q - VV_1Bcos\alpha + V^2B\right) = 0 \tag{5.17}$$

Let,

$$g(\alpha, V) = V^{-1}\left(Q - VV_1Bcos\alpha + V^2B\right) \tag{5.18}$$

Hence,

$$g(\alpha, V) = 0 \tag{5.19}$$

Converting the algebraic equation (5.19) to a differential equation,

$$\varepsilon\dot{V} = -g(\alpha, V) \tag{5.20}$$

Note that ε is a very small time constant, and the equilibrium of the differential equation (5.20) and the solution of the algebraic equation (5.19) are the same. Hence, the conversion of (5.19) to a differential equation is valid [37].

Therefore, the set of differential equations (5.13),(5.16) and (5.20) define the power system dynamics of the two bus network shown in Fig. 5.1. For an equilibrium point (0, α_0, V_0), energy function E can be derived as [37],

$$E = \int_0^{\omega} M\omega \ \mathrm{d}\omega + \int_{\alpha_0,V_0}^{\alpha,V} f\left(\alpha, V\right) \ \mathrm{d}\alpha + \int_{\alpha_0,V_0}^{\alpha,V} g\left(\alpha, V\right) \ \mathrm{d}V \tag{5.21}$$

Using the concepts of path independent integrals [74], the solution for (5.21) can be given by,

$$E = \frac{M\omega^2}{2} - BVV_1 cos\alpha + BV_0V_1 cos\alpha_0 + \frac{B}{2}\left(V^2 - {V_0}^2\right) - P\left(\alpha - \alpha_0\right) + Qln\frac{V}{V_0} \quad (5.22)$$

Assuming the frequency remains constant, energy function in (5.22) becomes,

$$E = -BVV_1 cos\alpha + BV_0V_1 cos\alpha_0 + \frac{B}{2}\left(V^2 - {V_0}^2\right) - P\left(\alpha - \alpha_0\right) + Qln\frac{V}{V_0} \quad (5.23)$$

In the conventioanl energy function method for voltage stability assessment, which was explained in Chapter 2, (0, α_0, V_0) is a stable equilibrium point of the system and (ω, α, V) is the closet unstable equilibrium point. Stable and unstable equilibrium points can be given by the stable and unstable power flow solutions of network. As the stable and unstable power flow solutions coalesce at the onset of voltage collapse, the value of the energy function becomes zero at the critical point of voltage collapse. If the load demand in a network is slowly increased, and the energy function is calculated at each snapshot of the system, the energy function will start from a finite value and approaches zero at the point of voltage collapse. Hence, the energy distance between the high and low voltage power flow solutions at a particular operating condition of a power network is used in the literature, as an proximity indicator to the voltage collapse.

However, as explained in Chapter 2, finding the appropriate low voltage power flow solution of a large network is a difficult task. Therefore, the practical usage of the method is restricted. In this chapter, a new method is developed to use the energy function method for voltage stability assessment of networks using a hassle-free approach.

For a two bus network, the energy function is given by (5.23). However, in this approach, (0, α_0, V_0) is a pre-determined stable equilibrium point of the system and (ω, α, V) is any subsequent operating point of the network. Therefore, in this method, energy margin between a pre-determined stable operating point of the

network and any subsequent operating point is calculated. Hence, it is more sensible to call "E" as the "Energy Margin".

Therefore, for a particular network, all variables are known constants, except V, V_1, α, P and Q in (5.23). With the recent developments in PMU based measurement technology, the variables V, V_1, α, P and Q for a particular network can be measured in a synchronous manner. Therefore, the energy margin can be calculated for a particular network using (5.23) with respect to a pre-determined stable operating point. In the subsequent sections of this chapter, the methodology of utilising this energy margin for voltage stability assessment is described in detail.

5.2.2 Verification of the Methodology using a Two Bus Network

A test system similar to Fig. 5.1 is modelled in DIgSILENT Power Factory with a line admittance of 8.88 p.u. Load is modelled as a constant power load with a value of 30 MW and 30 MVAr. A complete dynamic simulation is conducted to simulate a voltage collapse scenario. The synchronous generator at Bus 1 is modelled with a Type DC1A excitation system, a governor and OXL with inverse-time characteristics [70]. To simulate a voltage collapse scenario, the load active power demand was progressively increased by 2% per second with respect to initial load level starting from t =15 s to 115 s. Fig. 5.2 shows the voltage variation of Bus 2 with time. According to Fig. 5.2, voltage collapse is initiated at about t = 118 s.

To apply the methodology suggested in this chapter, the power flow solution of the base case system (pre-disturbance system) is considered as the stable equilibrium point. Hence, V_0= 1.01 p.u. and α_0= -2.3^0 (-0.04 rad).

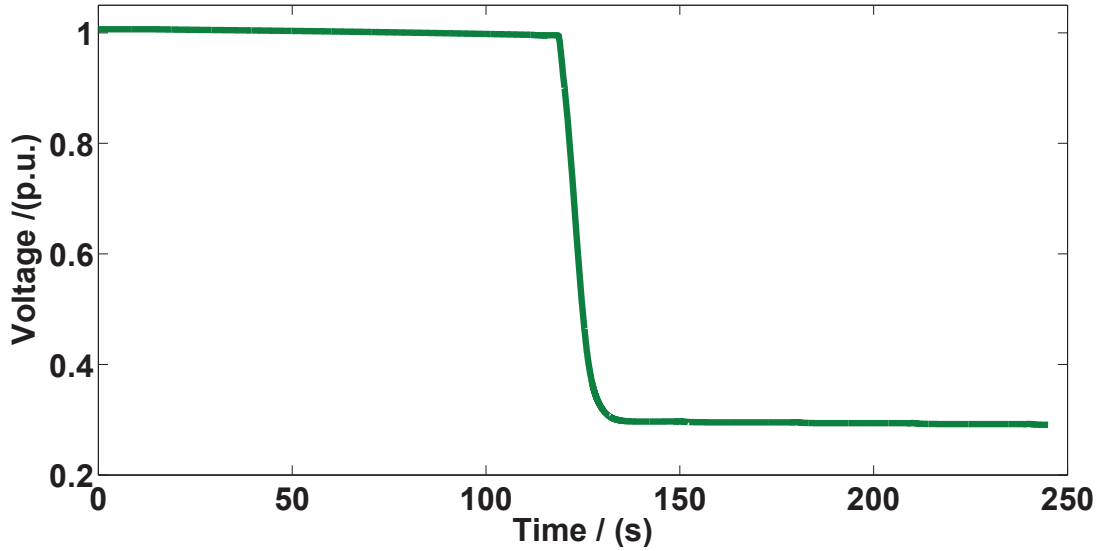

Figure 5.2: Variation of Bus 2 Voltage with time

The energy margin for this system is given by,

$$E = -8.88VV_1cos\alpha + 8.9688V_1cos\left(2.3^0\right) + 4.44\left(V^2 - 1.01^2\right) - P\left(\alpha + 0.04\right) + Qln\frac{V}{1.01} \tag{5.24}$$

At each snapshot of time along the voltage trajectory shown in Fig. 5.2, the energy margin is calculated using (5.24). Fig. 5.3 shows the variation of energy margin. As shown in Fig. 5.3, the energy margin value during the stable pre-disturbance operation is almost zero. As the voltage decreases with the increasing load demand, the energy margin decreases slowly and at the onset of voltage collapse at about t = 118 s, energy margin also reduces rapidly.

Considering the variation of energy margin with time, rate of change of energy margin (dE/dt) is selected as a a good indicator to identify voltage collapse. Fig. 5.4 shows the variation of rate of change of energy margin (dE/dt). As shown in Fig. 5.4, the rate of change of energy margin is zero at the stable operation and during the voltage collapse, it shows a large negative value at t= 118 s.

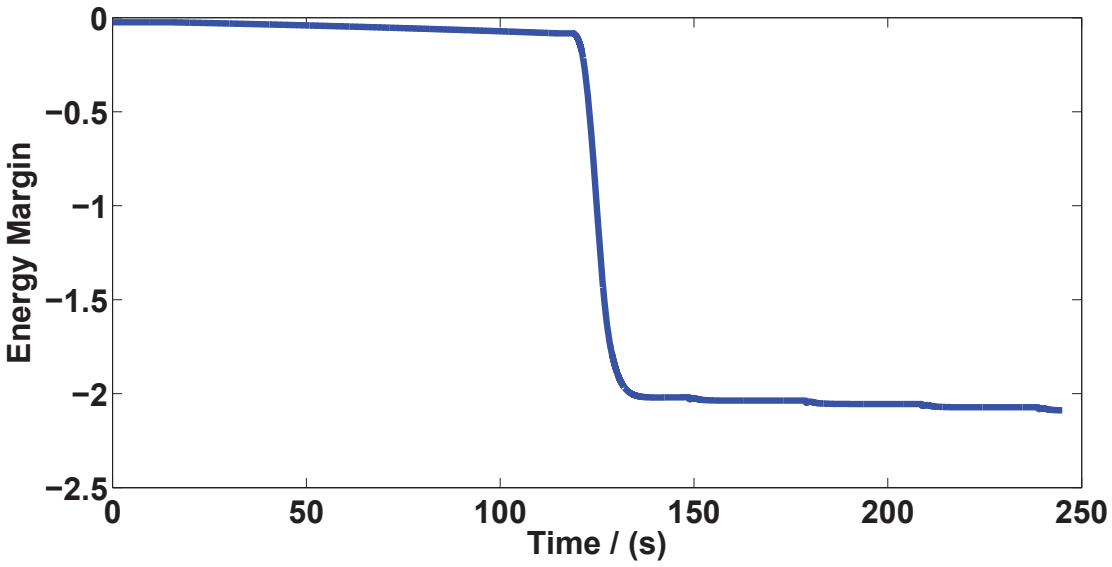

Figure 5.3: Variation of energy margin with time

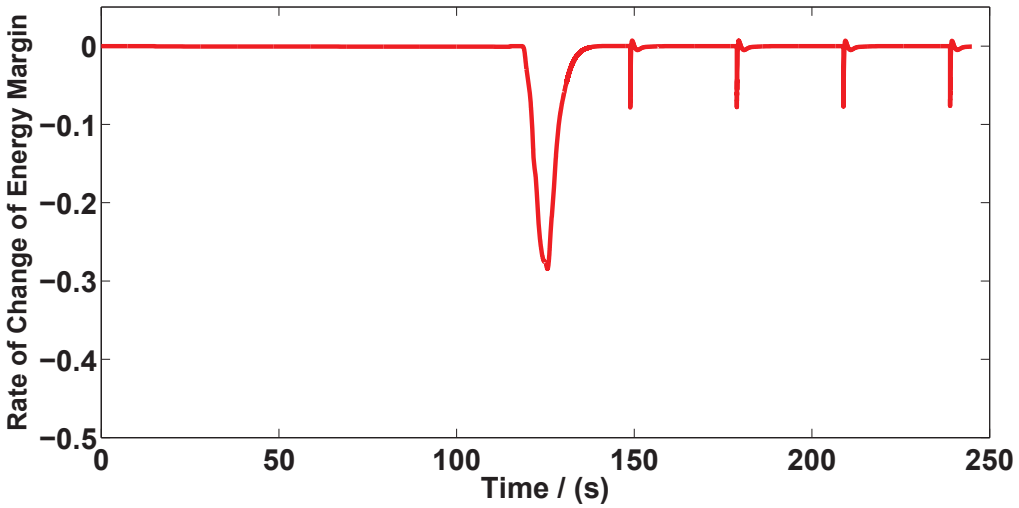

Figure 5.4: Variation of rate of change of energy margin with time

- **Sensitivity Analysis**

  A sensitivity analysis can be carried out to investigate the sensitivity of different variable in (5.23) to energy margin.

  Fig. 5.5 shows the variation of the magnitudes of different variables of the energy margin equation with time during the voltage collapse scenario presented in Fig. 5.2.

Fig. 5.6 and Fig. 5.7 show the sensitivity of energy margin to different variables which show that the sensitivity of energy margin to all other parameters except V (load bus voltage) and α are negligible. During a typical voltage collapse incident, typically the angle variation is small (refer to Fig. 5.5). As shown in Fig. 5.5, α varies by 0.4 during the complete voltage collapse scenario. Usually, voltage instability and rotor angle instability are interrelated. However, voltage instability is observed when the rotor angle stability is not an issue [11]. However, rotor angle instability of a network can also lead to progressive drop of the busbar voltages.

According to these facts, the most sensitive variable to the energy margin is load bus voltage (i.e. V). Hence, energy margin can be used as a parameter to evaluate voltage instability.

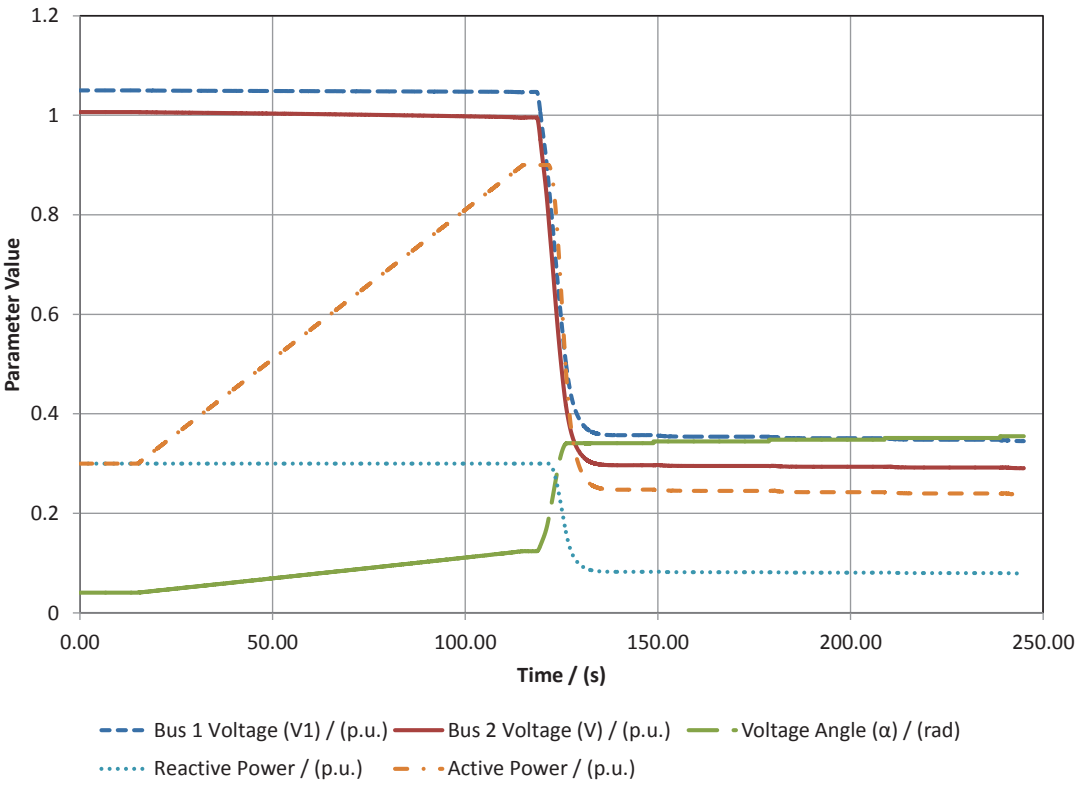

Figure 5.5: Variation of different variables with time

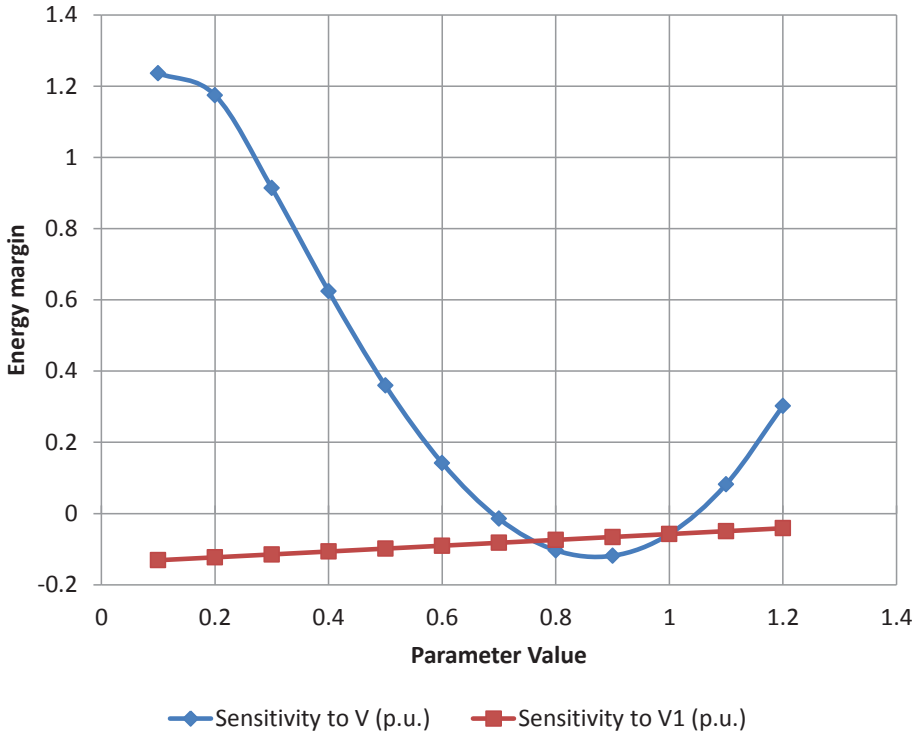

Figure 5.6: Sensitivity of energy margin to variables: *V, V1*

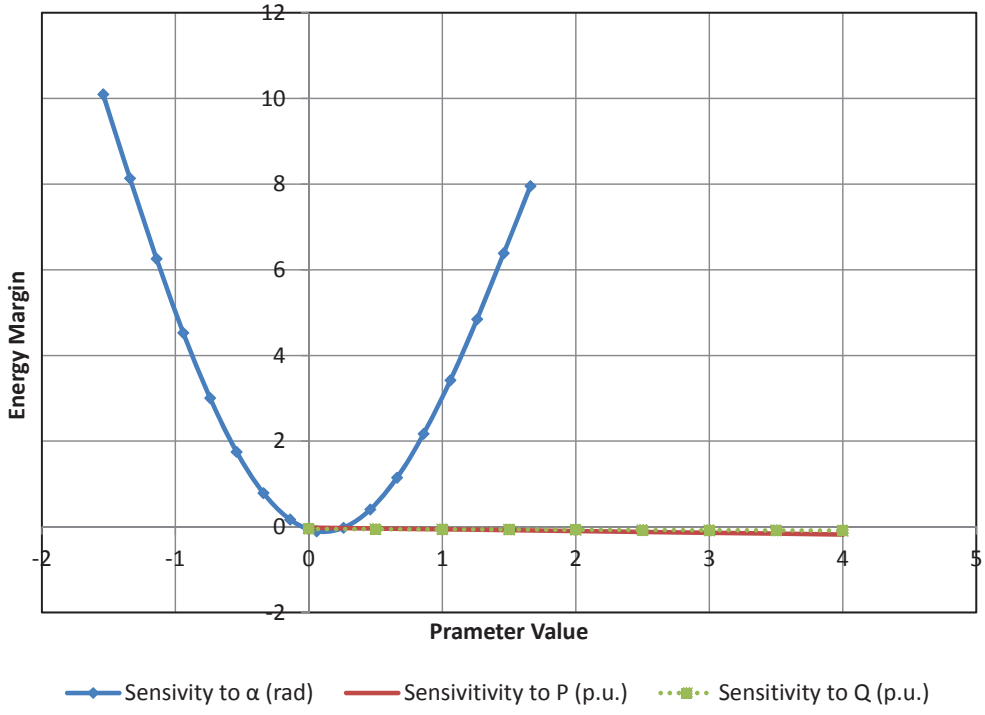

Figure 5.7: Sensitivity of energy margin to variables: P, Q, α

- **Comparison With the Conventional Method of Energy Function Analysis for Voltage Stability Analysis**

  As explained in Chapter 2, in the conventional energy function based method for voltage stability assessment, the energy distance between high and low voltage power power solutions is used as a proximity indicator for voltage collapse. The high and low voltage power flow solutions (stable and unstable solutions) coincides at the onset of voltage collapse, and hence the energy margin reaches zero at this point.

  However, in the methodology introduced in this chapter, the energy margin between a pre-determined stable operating point and any subsequent operating point is tracked to identify voltage instability. In this section, the energy margin is calculated using the conventional method for the scenario considered in this section, and it is compared with the methodology introduced in this chapter.

  For Bus 2 in the test system in Fig. 5.1,

$$P - jQ = V^* I \tag{5.25}$$

$$P - jQ = V\angle -\delta_2 \frac{(V_1\angle\delta_1 - V\angle\delta_2)}{jX} \tag{5.26}$$

$$P - jQ = \frac{VV_1}{X} sin\left(\delta_1 - \delta_2\right) - j\frac{VV_1}{X} cos\left(\delta_1 - \delta_2\right) + j\frac{jV^2}{X} \tag{5.27}$$

  Considering (5.27),

$$P^2 + \frac{\left(QX + V^2\right)^2}{X^2} = \frac{V^2 {V_1}^2}{X^2}\left(sin^2\left(\delta_1 - \delta_2\right) + cos^2\left(\delta_1 - \delta_2\right)\right) \tag{5.28}$$

$$V^4 + \left(2QX - {V_1}^2\right)V^2 + \left(P^2 + Q^2\right)X^2 = 0 \tag{5.29}$$

  Solving (5.28),

$$V^2 = \frac{-\left(2QX - {V_1}^2\right) \pm \sqrt{\left(2QX - {V_1}^2\right)^2 - 4\left(P^2 + Q^2\right)X^2}}{2} \tag{5.30}$$

The voltage magnitudes of high and low voltage power flow solutions can be found using (5.30).

Considering the real parts of (5.27),

$$P = \frac{VV_1}{X} sin\left(\delta_1 - \delta_2\right) \tag{5.31}$$

$$\delta_2 = \delta_1 - sin^{-}1\left(\frac{PX}{VV_1}\right) \tag{5.32}$$

Using (5.32), the voltage angles associated with the high and low voltage power flow solutions can be found.

Along the system trajectory shown in Fig. 5.2, the corresponding high an low voltage power flow solutions of Bus 2 voltage was numerically calculated using (5.30) and (5.32). Subsequently, the energy margin between high and low voltage power flow solutions at each snapshot was numerically calculated. Fig. 5.8 shows the variation of numerically calculated energy margin for each snapshot. It also shows the variation of energy margin using the proposed method, and the Bus 2 voltage profile with respect to time.

According to Fig. 5.8, the energy margin, which is numerically calculated using the conventional method has a value of about 3.4 in the pre-disturbance steady state while the energy margin calculated using the proposed method is zero. When the voltage collapse is initiated at about t= 118 s, the energy margin calculated using the conventional method starts to decrease rapidly and ultimately reaches zero at the onset of voltage collapse, while the energy margin calculated using the proposed method starts to decrease below zero at

the same time. Fig. 5.8 demonstrates that the results of the proposed method are consistent with the results of the conventional method.

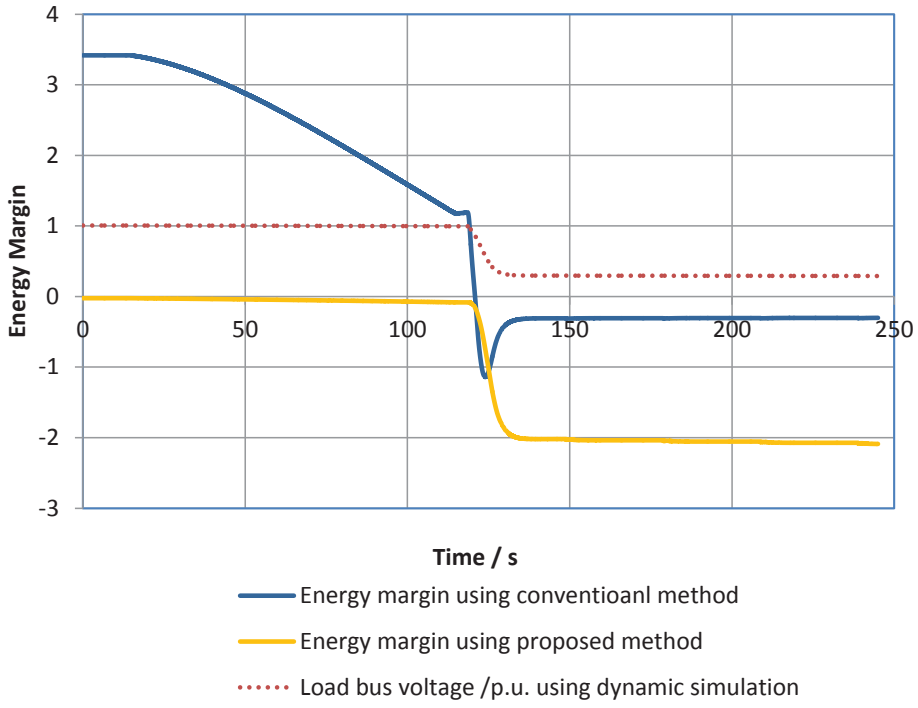

Figure 5.8: Variation of energy margin using the conventional method and the proposed method

To further confirm, the variation of the energy margin derived using the two methods is plotted with respect to active power demand of the system, as it is the conventional way of representing the energy margin in the literature. Fig. 5.9 shows resulting figure which confirms that the energy margin becomes zero at the onset of voltage collapse, which occurs when the active power demand reaches 0.9 p.u.

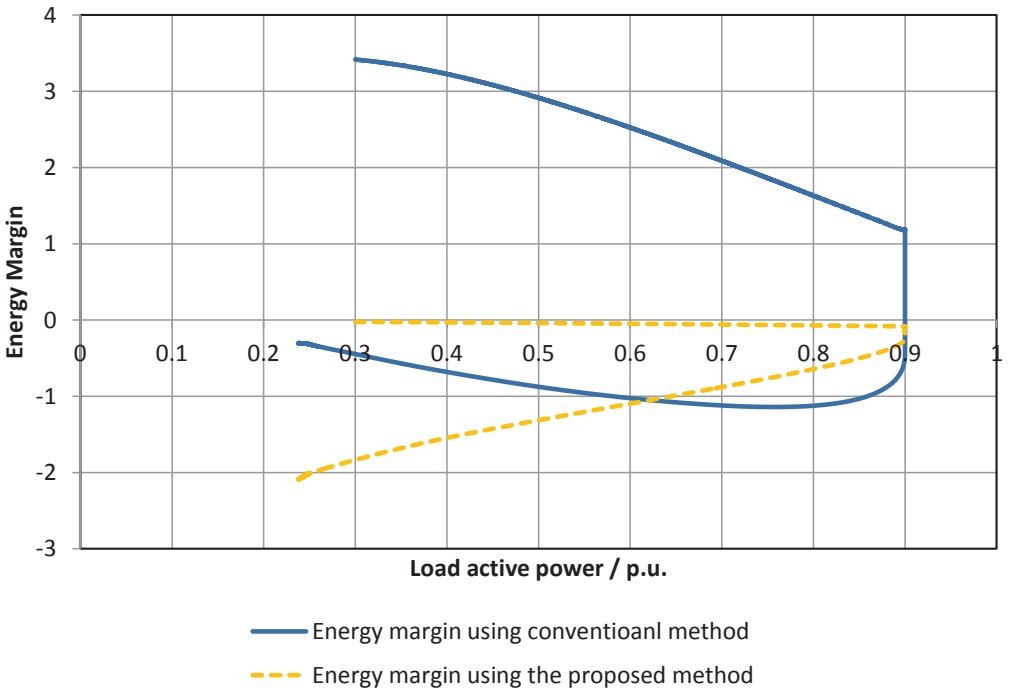

Figure 5.9: Comparison of energy margin calculated using the conventional method and the proposed method - variation of energy margin with the active power demand

5.3 Extension of the Methodology to a Large Network

5.3.1 Theoretical Derivation

In this section, the theoretical derivations for the extension of the proposed energy function method for large networks is explained. Energy function approach for multi-machine systems that follows the conventional approach is explained in [38,44]. Power flow equations for bus i in a network with n number of busbars are considered here. Assume that the voltage at the i^{th} bus is $V_i\angle\delta_i$ and the (i,j) element of admittance matrix is $Y_{ij}\angle\beta_{ij}$. Hence,

$$P_i = V_i \sum_{j=1}^{n} Y_{ij} V_j cos\left(\delta_i - \delta_j - \beta_{ij}\right) \tag{5.33}$$

$$Q_i = V_i \sum_{j=1}^{n} Y_{ij} V_j sin\left(\delta_i - \delta_j - \beta_{ij}\right) \tag{5.34}$$

Let, $\alpha_{\mathrm{i}} = \delta_{\mathrm{ref}}$ - δ_{i} and $\alpha_{\mathrm{j}} = \delta_{\mathrm{ref}}$ - δ_{j}, where, δ_{ref} is the angle of the reference bus. Hence,

$$P_i = V_i \sum_{j=1}^{n} Y_{ij} V_j cos\left(\delta_j - \delta_i + \beta_{ij}\right) = V_i \sum_{j=1}^{n} Y_{ij} V_j cos\left(\alpha_i - \alpha_j + \beta_{ij}\right) \tag{5.35}$$

$$Q_i = -V_i \sum_{j=1}^{n} Y_{ij} V_j sin\left(\delta_j - \delta_i + \beta_{ij}\right) = -V_i \sum_{j=1}^{n} Y_{ij} V_j sin\left(\alpha_i - \alpha_j + \beta_{ij}\right) \tag{5.36}$$

Following the procedure adopted in the derivations for the two bus network explained in Section 5.2, let,

$$f = V_i \sum_{j=1}^{n} Y_{ij} V_j cos\left(\alpha_i - \alpha_j + \beta_{ij}\right) - P_i \tag{5.37}$$

$$g = Q_i + V_i \sum_{j=1}^{n} Y_{ij} V_j sin\left(\alpha_i - \alpha_j + \beta_{ij}\right) \tag{5.38}$$

Therefore the energy margin,

$$E = \int_{\alpha_i^0, V_i^0}^{\alpha_i, V_i} f \, \mathrm{d}\alpha_i + \int_{\alpha_i^0, V_i^0}^{\alpha_i, V_i} V_i^{-1} g \, \mathrm{d}V_i \tag{5.39}$$

Using (5.37) and (5.38), the energy margin can be written as,

$$E = -V_i^0 \sum_{j=1}^{n} Y_{ij} V_j sin\left({\alpha_i}^0 - \alpha_j + \beta_{ij}\right) + V_i \sum_{j=1}^{n} Y_{ij} V_j sin\left(\alpha_i - \alpha_j + \beta_{ij}\right) - P_i\left(\alpha_i - {\alpha_i}^0\right) + Q_i ln \frac{V_i}{V_i^0} \tag{5.40}$$

Equation for energy margin (5.40) can be applied with respect to any selected bus bar (i) in a large interconnected network. The application of the methodology to a large network is demonstrated in Section 5.3.3.

5.3.2 Test Network

The Reliability and Voltage Stability (RVS) test system developed in DIgSILENT Power Factory is used to demonstrate the methodology demonstrated in the previous

section to a large network [75]. This test system is specifically developed in [75] for voltage stability and security assessment and it is derived from 1979 IEEE reliability test system. A single line diagram of this network is shown in Fig. 5.10. This test system contains 75 busbars, 32 generators, 145 branches, 17 loads. This test system comprises two network regions; a 230 kV network and 138 kV network. All test system data and the dynamic model data are in in Appendix D [75].

For the cases studied in this chapter all loads are modelled as constant current loads for active power and constant impedance loads for reactive power.

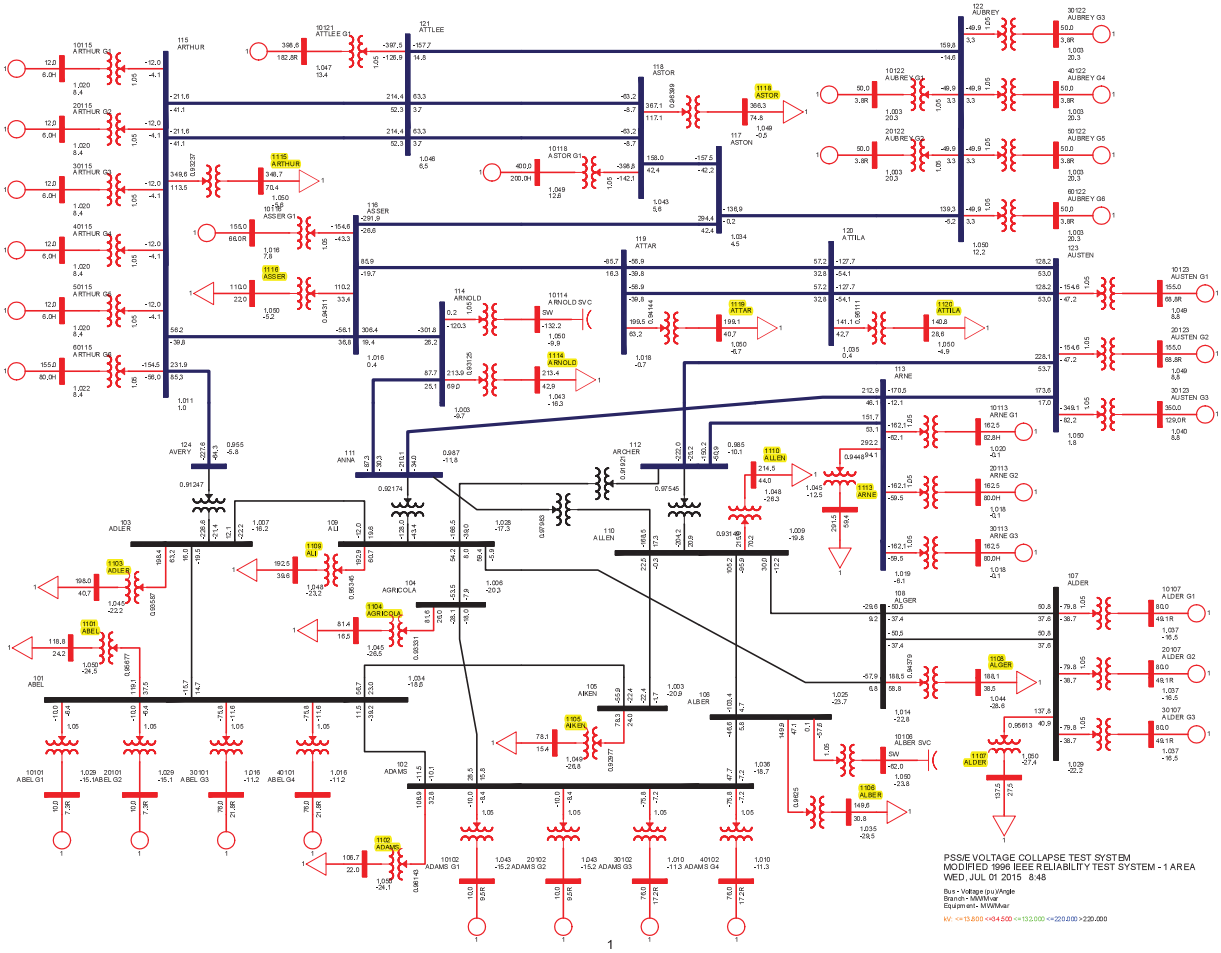

Figure 5.10: Single line diagram of RVS test system

5.3.3 Verification with RVS Network

As explained in Section 5.3.1, this methodology described in Section 5.3.1 can be applied with respect to a selected busbar of a network. Voltage instability is usually a local phenomenon, although it can lead to a system wide voltage collapse. Hence, it is suggested to apply the proposed method to selected busbars in the weak parts of a network in general. Therefore, the following steps can be followed to apply the proposed energy function method to large networks:

1. Identify weak areas in the network using QV modal analysis and/or VQ stability margins (as illustrated in Chapter 3)

2. Apply the proposed energy function method to selected busbars in the weak areas of the network

Therefore, as the first step, the VQ stability margins of all the load busbars in the RVS network were calculated using the VQ curves. Fig. 5.11 shows the VQ stability margins of all load busbars in 230 kV busbars in the network. Fig. 5.12 shows the VQ curves of all load busbars in 138 kV busbars in the network and Table 5.1 shows the VQ stability margins calculated using the VQ curves.

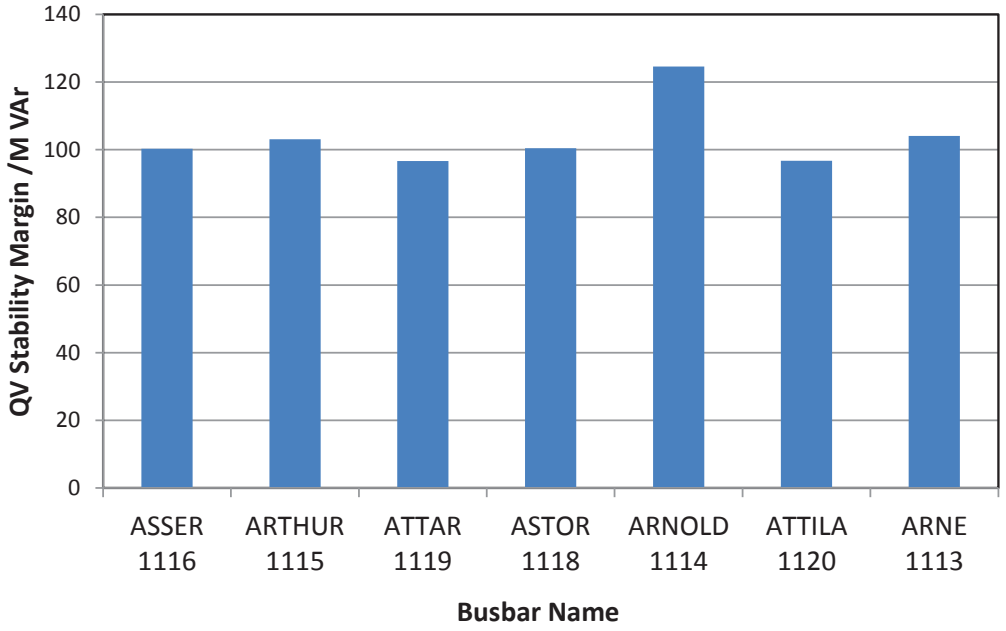

Figure 5.11: VQ stability margins of the 230 kV load busbars of the RVS network

According to the results obtained, 138 kV 1104 AGRICOLA load busbar has the lowest VQ stability margin and hence, it is the weakest busbar in the network. Hence, the extension of the energy function approach is demonstrated considering that busbar.

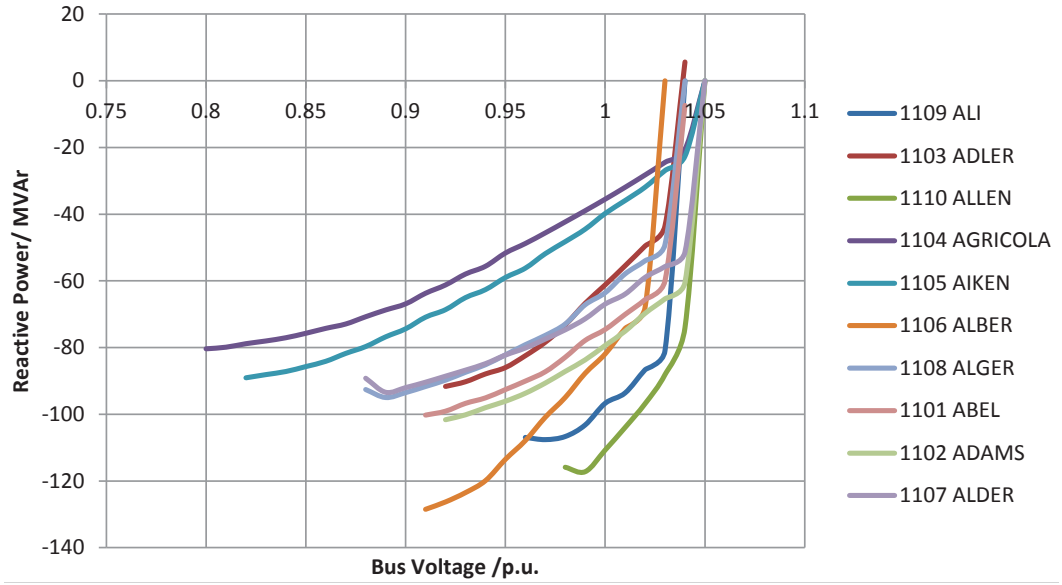

Figure 5.12: VQ curves of the 138 kV load busbars of the RVS network

Table 5.1: VQ stability margins of 138 kV busbars of the RVS network

Busbar Name	QV stability Margin / (MVAr)
1109 ALI	107.59
1103 ADLER	91.65
1110 ALLEN	117.21
1104 AGRICOLA	80.36
1105 AIKEN	89.06
1106 ALBER	128.49
1108 ALGER	94.97
1101 ABEL	100.24
1102 ADAMS	101.63
1107 ALDER	93.4

- Scenario 1 - Voltage Step Event

  In this case, two voltage step change events were simulated to observe the variation of energy margin. This event was simulated by switching a reactor at busbar 104 AGRICOLA. The energy margin was calculated for busbar 104 AGRICOLA. The following two cases are considered.

  - Case 1 - Switching a reactor with a capacity of 250 MVAr at t= 10 s
  - Case 2 - Switching a reactor with a capacity of 500 MVAr at t= 10 s

  Fig. 5.13 shows the variation of the busbar voltage, energy margin and rate of change of energy margin for the two cases. Results confirms that the voltage instability of the busbar is reflected by the variation of energy margin. The rate of change of energy margin also indicates the voltage instability. The higher the severity of voltage drop, the larger the decrease in the energy margin and hence, the rate of change of energy margin. The decrease in both energy margin and rate of change of energy margin are proportional to the level of voltage instability.

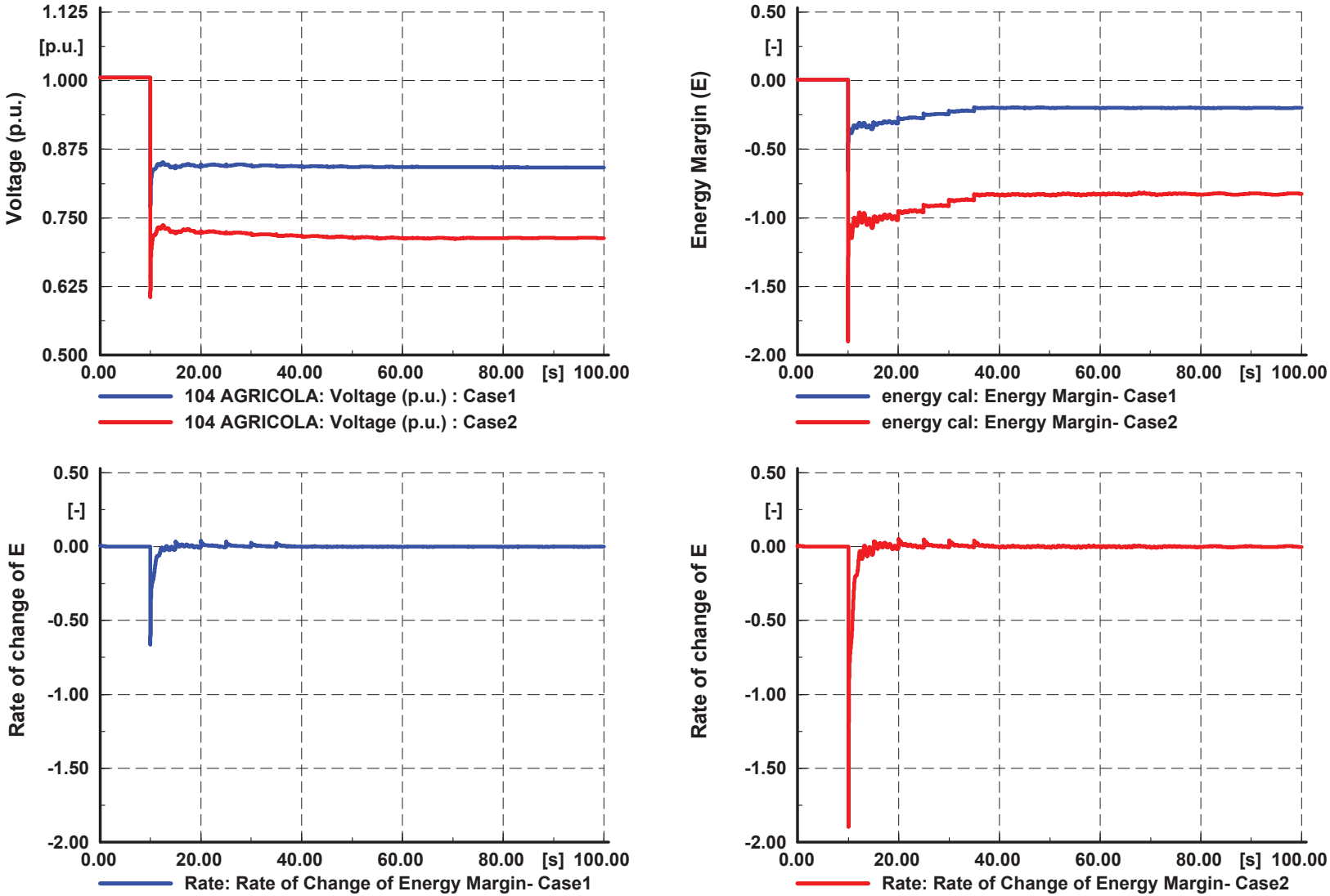

Figure 5.13: Results - Voltage Step Event

- Scenario 2 - Voltage Ramp Down

  In this scenario, a voltage ramp down event was simulated to observe the variation of the energy margin. The active power demand and the reactive power demand of the load connected to 1104 AGRICOLA busbar was progressively increased at a rate of 20% and 70% per second, respectively. The main aim of this scenario was to demonstrate the voltage instablity resulting from smooth load increase. The energy margin is calculated for busbar 104 AGRICOLA.

  Fig. 5.14 shows the variation of the 104 AGRICOLA busbar voltage, energy margin and rate of change of energy margin. It also shows the voltage variation of other nearby busbars. Although the voltages at the load busbar and the corresponding high voltage busbar are reduced to a low voltage due to the load ramp up event, the voltages at the nearby busbars are still within acceptable levels. The variation of the synchronous generator rotor angles was observed and it is noted that the rotor angle stability of the network is maintained during this voltage instability event. Fig. 5.15 shows the rotor angles of selected generators in the network.

  As shown in Fig. 5.14, the voltage instability of the busbar (1104 AGRICOLA) is reflected by the variation of energy margin. Both energy margin and the rate of change of energy margin decrease during the voltage instability event.

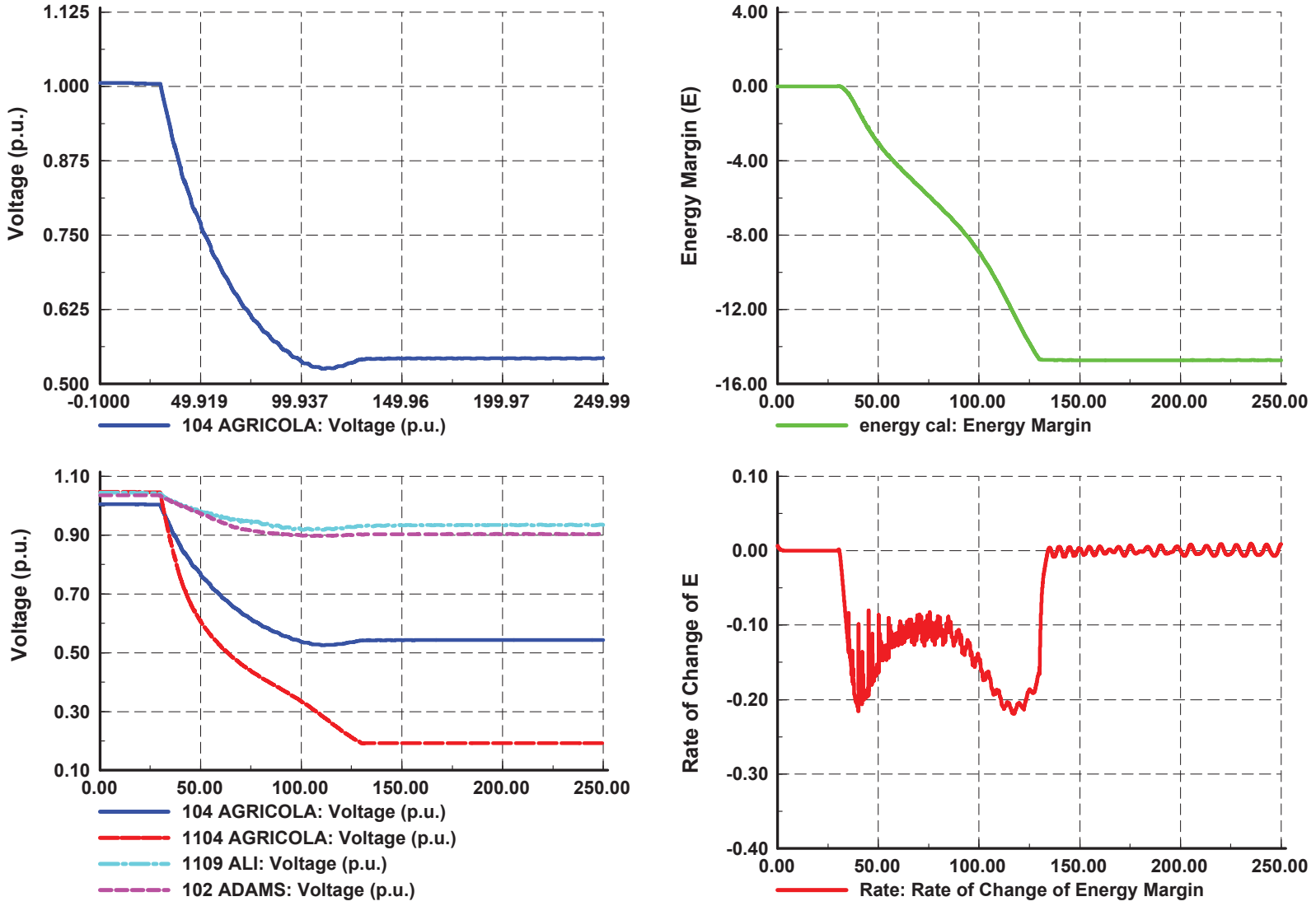

Figure 5.14: Results- Voltage Ramp Down

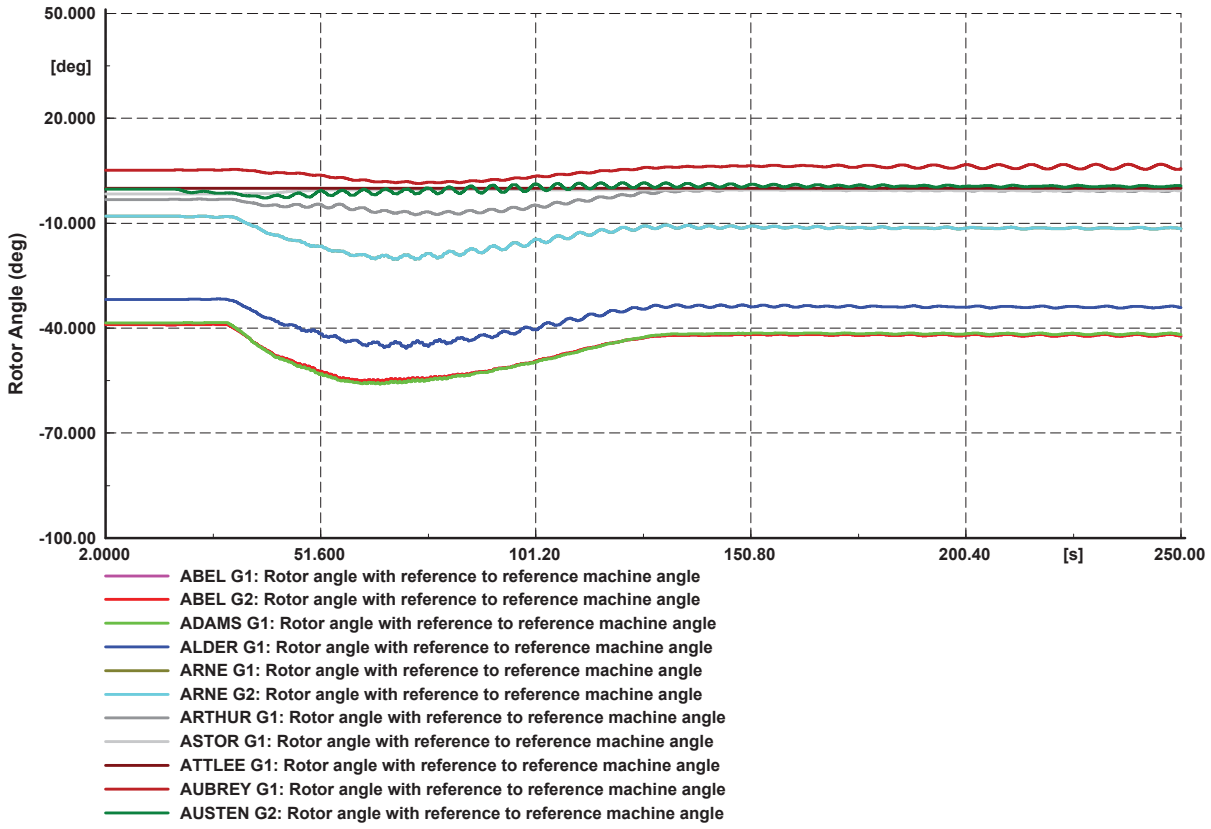

Figure 5.15: Variation of synchronous machine rotor angles during the voltage ramp down event

According to the observations of the two scenarios considered, the following criteria is suggested for voltage stability evaluation using the new proposed method: Assuming that the network voltages variation beyond 0.9 p.u.- 1. 1p.u. is not acceptable for stable operation of a network, the variation rate of change of energy margin below -0.1 is identified as a possible voltage instability event. Depending on the network operating guidelines of a particular network, a certain threshold for the rate of change of energy margin can be selected. This criteria can be evaluated for selected busbars in weak parts of the network to monitor the network voltage instability.

5.3.4 Future Extensions of the work

Network reduction techniques can be used to develop another approach for extension of the proposed energy function method to large networks. Such a reduction technique can be used to reduce the network with respect to the selected load busbar for the application of the proposed method. However, as the proposed energy function method is applied to various snapshots of time along the system trajectory, the network reduction tool must be able to capture the dynamics of the system. Such network reductions tools have been developed in the work in [76–78], where the methods have introduced for determination of real time Thevenin equivalent circuit parameters. These methods can be utilised to obtain the network equivalent along the system trajectory, if the network reduction approach is followed.

5.4 Applications of the proposed Energy Function Method

In this chapter, a new energy function based approach for long-term dynamic voltage stability assessment was introduced. This method needs less computational capacity compared to the conventional method. It was demonstrated that this new method can be used to monitor the dynamic voltage instability issues in networks.

Mainly due to the increasing penetration levels of renewable power generation in networks around the world, their behaviour has become more uncertain. Hence, the real-time security assessment is of vital importance in current power systems [79–81]. With the developments of wide-area measurements systems(WAMS) and PMU technologies, the practical limitations of application of real-time security assessment methods are getting eliminated.

As stated previously, voltage instability is a local phenomenon, which can lead to a system wide blackout. Hence, voltage instability is usually initiated in a weak part of the network and it can affect the other parts of network, as well. Hence, monitoring bus voltages itself is not sufficient to determine voltage instability of the network.

The energy function based method proposed in this chapter can be used for online voltage security assessment. The real time variation of energy margin and/or rate of change of energy margin can be used to detect the voltage instability issues in the network. Energy margin can be monitored for the selected busbars in weak parts of the network. The method only requires local measurements around the selected busbar. Network reduction techniques can also be used along with the method to identify the dynamic network equivalent at each snapshot of time.

5.5 Application of the Method to a Network with Wind Power Generation

In this section, the proposed energy function method is used to demonstrate the long-term voltage stability analysis of a network with wind generation. In this study, the test system (Fig. 4.6) and few case studies used in the long-term voltage stability analysis presented in Chapter 4 are used to demonstrate the application of the proposed energy function method. In this study, 3 cases were considered;

- Case 1 - The system is operated with no wind generation.
- Case 2 - The DFIG based wind generation with a total capacity of 97.5 MW (5 wind farms) is added to the network at Bus 1. The synchronous generation capacity in the existing network is not altered.
- Case 3 - The DFIG based wind generation with a capacity of 97.5 MW (5 wind farms) is added to the network at Bus 1. However, the synchronous generation capacity at Bus 1 is reduced in proportion to the added wind generation.

As demonstrated in Chapter 4, when wind generation is added to the network without altering the existing generation capacity in the network, it is favourable for improved network voltage stability. However, if the added wind generation leads to replacement of the synchronous generation in the system, it deteriorates the network voltage stability. These results are repeated in Figs. 5.16 (a) and (b).

The proposed energy function based method is applied to Bus 4 of the test network for all three cases, where Fig. 5.16 (c) shows the energy margin (E) and Fig. 5.16 (d) shows the rate of change of energy margin (dE/dt). It can be seen that the voltage instability is reflected in the energy margin. The rate of change of energy margin indicates the voltage instabilities and it is proportional to the level of instability. The energy margin and rate of change of energy margin is zero during the stable operation of the network. Even the first OXL operation after the load ramp event that was initiated at t= 40 s, is reflected in the rate of change of energy margin.

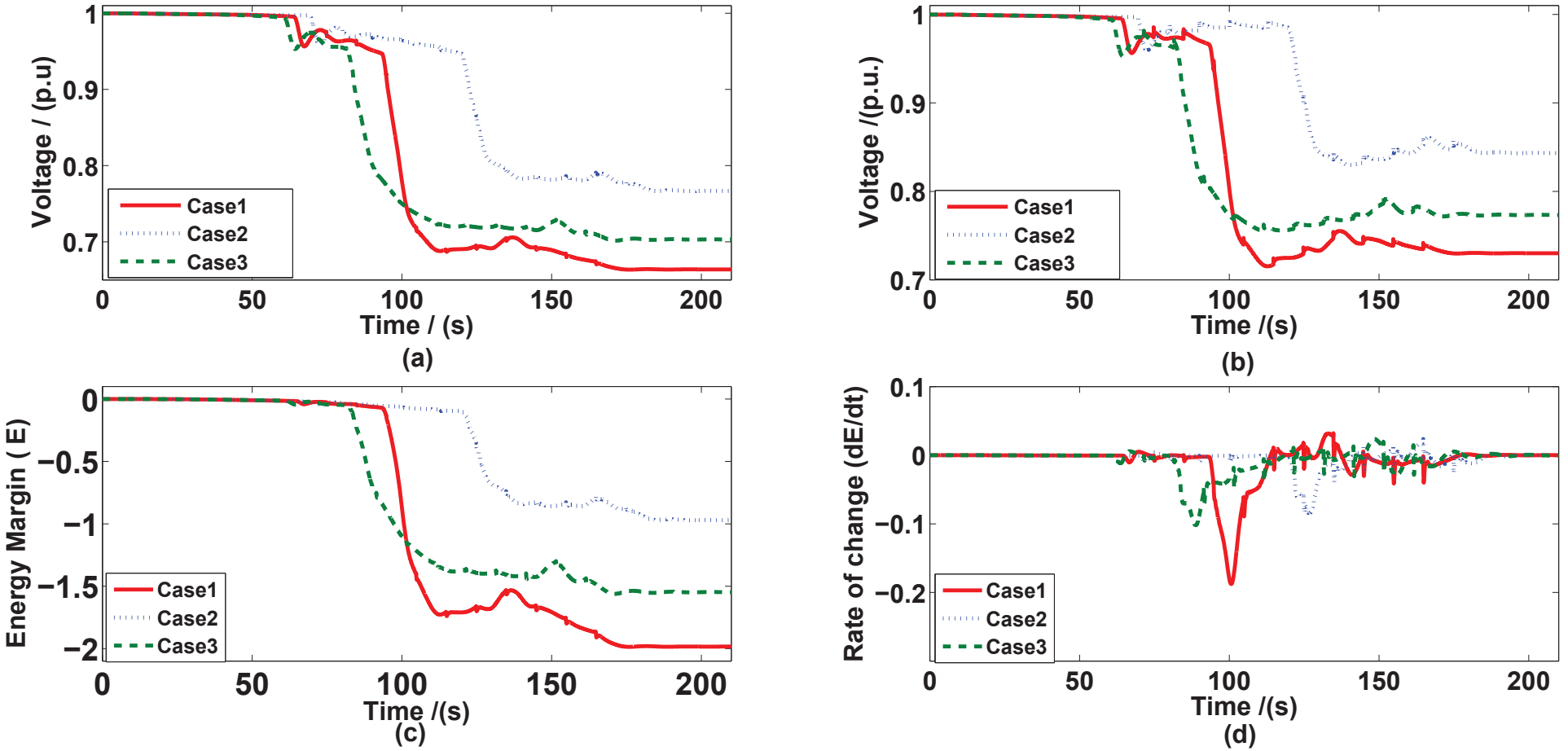

Figure 5.16: (a) Voltage profile of Bus 4 (b) Voltage profile of Bus 3 (c) Energy Margin (d) Rate of change of energy margin

5.6 Summary

In this chapter, a novel energy function based method to examine long-term dynamic voltage stability evaluation was introduced. The method was developed based on the conventional energy function based method for voltage stability evaluation. However, the proposed method eliminates the limitations in its practical application. The basic concept of the method was explained using a simple two bus network. The energy margin, which is the energy distance between a pre-determined stable operating point and any subsequent operating point, and the rate of change of energy margin can be used to assess the long-term dynamic voltage instability. The direct correlation between the energy margin and the voltage instability was demonstrated using sensitivity analysis and numerical computation using simulation studies.

The application of the method to a large interconnected network was demonstrated using the RVS test system developed in DIgSILENT Power Factory. It is suggested the energy margin be evaluated with respect to selected busbars from the weak areas of the power network to assess system wide-dynamic voltage instabilities.

One of the major applications of the proposed method is real-time voltage security assessment, which is very important for modern power systems with high penetration levels of renewable power generation. The method was applied to the test system (Chapter 4- Fig. 4.6) to examine long-term voltage stability to demonstrate the application for power networks with wind generation. The studies presented in this Chapter also provides additional verification for the studies conducted in Chapter 4.

Chapter 6

Short-term Voltage Stability Analysis of Power Systems in the Presence of Variable-Speed Wind Generators

6.1 Introduction

As explained in Chapter 2, dynamic voltage stability phenomenon is usually classified into two categories; short-term voltage stability and the long-term voltage stability. The main aim of this chapter is to investigate the impact of VSWGs on short-term voltage stability.

There are limited studies in the literature which analyse the short-term voltage stability associated with VSWGs, as explained in Chapter 2. Some of the drawbacks of those studies include: that they do not utilise suitable dynamic models of the VSWGs and other system components, and they do not consider different instability mechanisms, which are closely connected to short-term voltage instability of power systems. The aim of the analysis presented in this chapter is to conduct a comprehensive short-term voltage instability analysis of power systems which are

integrated with VSWGs.

The test system used in the simulation studies was explained in Section 6.2. As explained in Chapter 2, the major driving force of short-term voltage instability is the behaviour of dynamic loads, such as induction motors. In Chapter 2, different instability mechanisms which can lead a power network to short-term voltage instability were explained. In this Chapter, ST-1 and ST-2 type instability mechanisms are considered.

- **Type ST-1**: Loss of post-disturbance equilibrium of short-term dynamics

  Typical case of this type of instability corresponds to the induction motors stalling after a disturbance, which increases the total transmission impedance, such as loss of a supply transmission line. Due to the increase in system impedance, the motor mechanical and electrical torque speed curves will not be able to the intersect giving a stable post-disturbance equilibrium, which results the stalling of the motors and subsequent short-term voltage instability.

- **Type ST-2**: Lack of attraction towards the stable post-disturbance equilibrium of short-term dynamics

  A typical case of this type of instability is the stalling of induction motors after a short-circuit. Induction motors may not be able to re-accelerate after a short circuit fault, if they are heavily loaded or in the cases of slow fault clearing.

The impact of DFIG based wind generation on short-term voltage stability is investigated in Section 6.3 and Section 6.4 considering the aforementioned two instability mechanisms.

According to the reactive power capability charts of VSWGs explained in Chapter 2, the reactive power capability of VSWGs vary with their loading levels. In Section 6.5, the impact of VSWG loading level on short-term voltage stability is investigated. The impact of DFIG and FCWG based wind generation on short-term voltage stability is compared in Section 6.6.

6.2 Test System

The test system shown in Fig. 6.1 was used to analyse the short-term voltage stability [16]. The system parameters are listed in the Appendix C. All simulations were conducted using DIgSILENT Power Factory. The synchronous generator in the test system consists of a DC1A type excitation system [70]. The wind generation is integrated at Bus 1 through a transmission line (17 km) with a reactance of 0.58 Ω, as shown in Fig. 6.1. The aggregated wind farm model comprising of 13 wind turbines described in Chapter 4 is also used as the wind generation in the test system.

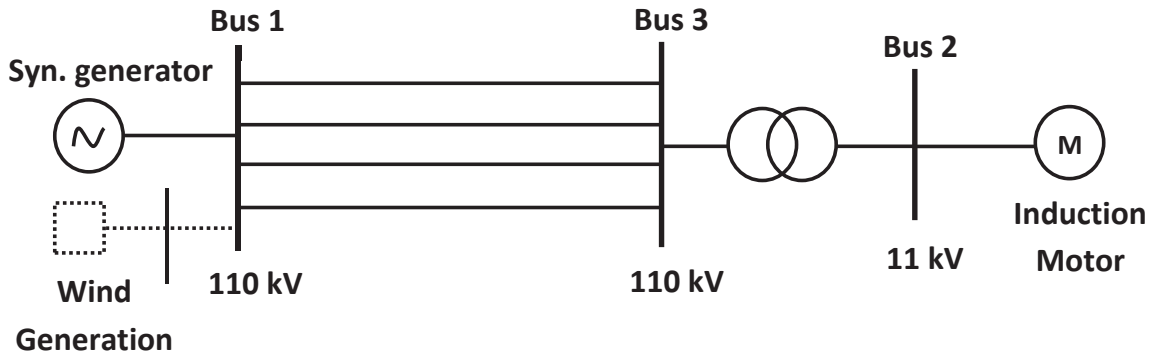

Figure 6.1: Test system used for short term voltage stability analysis.

6.3 Scenario 1 - Three Phase Short-Circuit Fault in a Network with Induction Motor Loads

In this scenario, ST-2 type short-term voltage instability is considered. The behaviour of a power network with induction motor loads after a short-circuit is typically considered in this type of stability investigations.

To illustrate the instability, a three phase short-circuit fault is simulated in one of the four transmission lines near Bus 3 at t = 1 s. The total load of the system is composed of four parallel connected induction motors.

Under normal voltage conditions of a power system, an induction motor will op-

erate at near synchronous speed (i.e., low slip). During fault conditions the network voltage can reduce to a low value and hence induction motors can decelerate, sometimes leading to the operation in the high slip region of the motor electromagnetic torque-speed curve (such operation cannot continue for a long period). If the network fault is cleared fast enough, motors can re-accelerate back to normal operating region of the motor torque-speed curve. However, if the prevailing network voltage is too low following a fault, motors do not produce sufficient electromagnetic torque to overcome the mechanical torque, causing induction motors to stall. It is well known that re-acceleration of induction motors located network wide can exacerbate the voltage instability phenomena, as they will be drawing excess currents in the process. Thus, it is important to ensure that network voltage recovers as fast as possible.

To illustrate the behaviour of the network and the connected induction motors, four cases are considered;

- Case A - The three phase short-circuit fault is cleared in 110 ms. There is no wind generation added to the system.

- Case B - The three phase short-circuit fault is cleared in 120 ms. There is no wind generation added to the system.

- Case C - DFIG wind generation with a capacity of 39 MW (2 farms) is integrated to the network at Bus 1 shown in Fig. 6.1. When the DFIG wind generation is added to the system, the existing synchronous generation capacity is reduced by an equivalent amount to the added wind generation to maintain the total system generation capacity constant. The three phase short-circuit fault is cleared in 110 ms.

- Case D - DFIG wind generation with a capacity of 97.5 MW (5 farms) is integrated to the network at Bus 1 shown in Fig. 6.1. When the DFIG wind generation is added to the system, the existing synchronous generation capacity is reduced by an equivalent amount to the added wind generation

to maintain the total system generation capacity constant. The three phase short-circuit fault is cleared in 110 ms.

As shown in Fig. 6.2 (continuous red curve), the load bus voltage recovers back to the pre-disturbance value in Case A, but it cannot recover back (continuous green curve) in Case B, in which the fault clearance is delayed compared to case A.

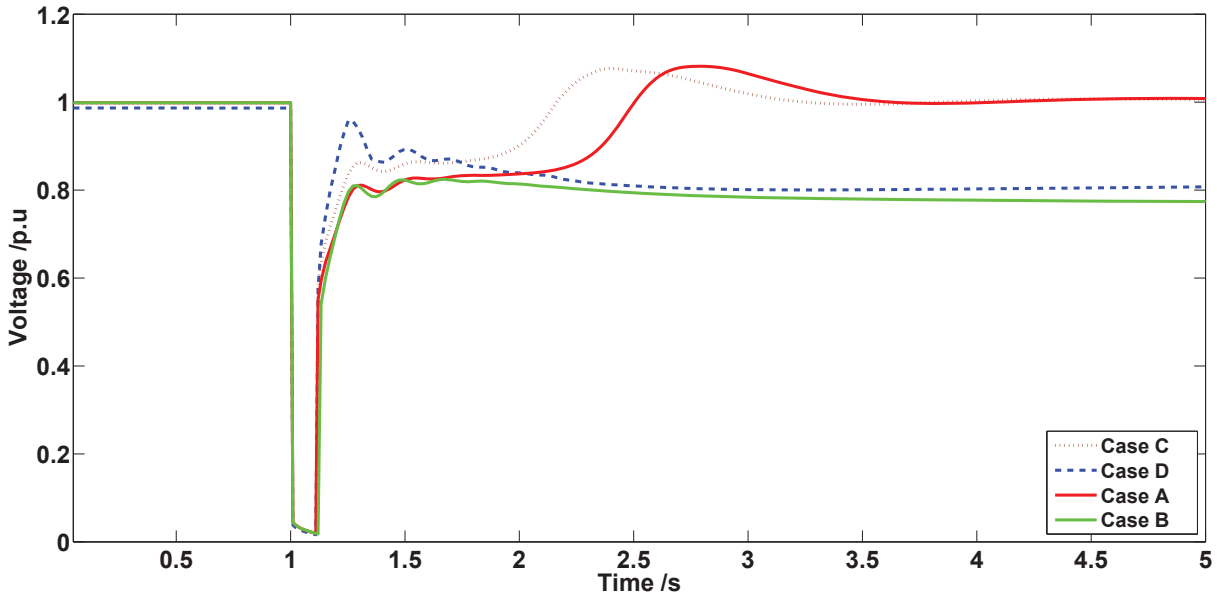

Figure 6.2: Bus 2 voltage for Scenario 1.

Fig. 6.3 shows the variation of induction motor slip for the two cases, and it confirms how the motor stalls in the Case B, when the voltage is not recovered back. In Case C and D, the impact of DFIG wind generation integrated at Bus 1 on short-term voltage instability is analysed. Fig. 6.2 also shows the voltage variation of Bus 2 for Case C and D, in which DFIG wind generation with capacities of 39 MW and 97.5 MW is added to Bus 1, respectively.

In Case C, system has the higher synchronous generation capacity compared to Case D. Therefore, the synchronous generator can provide more reactive power boost during the fault in Case C, as shown in Fig. 6.4. In Case C and D, the fault is cleared in 110 ms, and it is noted that the voltage could recover to the pre-disturbance voltage when the DFIG wind capacity is only 39 MW (dotted maroon

curve). However, when the DFIG wind generation is increased up to 97.5 MW the voltage could not recover although the fault was cleared in 110 ms (dashed blue curve).

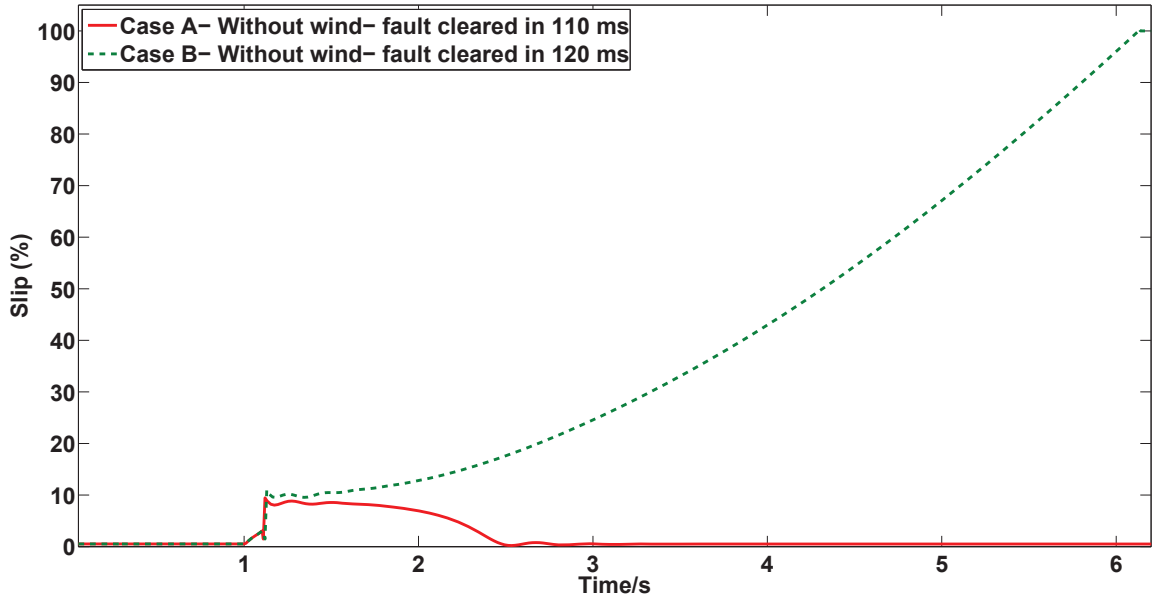

Figure 6.3: Variation of the induction motor slip.

Figs. 6.4 and 6.5 show the reactive power output of the synchronous generator and the reactive power output of the wind generator through RSC control and GSC control respectively. It shows that the DFIG supplies reactive power support to the system during the disturbance. If the DFIG wind capacity is only about 39 MW and there is a significant synchronous generator capacity in the system, the short-term voltage stability of the network can be maintained. However, when the DFIG capacity increases in the system, that system could not support the short-term voltage instability as much as a system with synchronous generation with the same capacity. As shown in Fig. 6.4, due to the less synchronous generation available in Case D, the synchronous generator cannot provide much reactive power boost during the fault recovery. Although the DFIG provides its full reactive power support at this instance as shown in Fig. 6.5, the network cannot recover back to the pre-disturbance voltage.

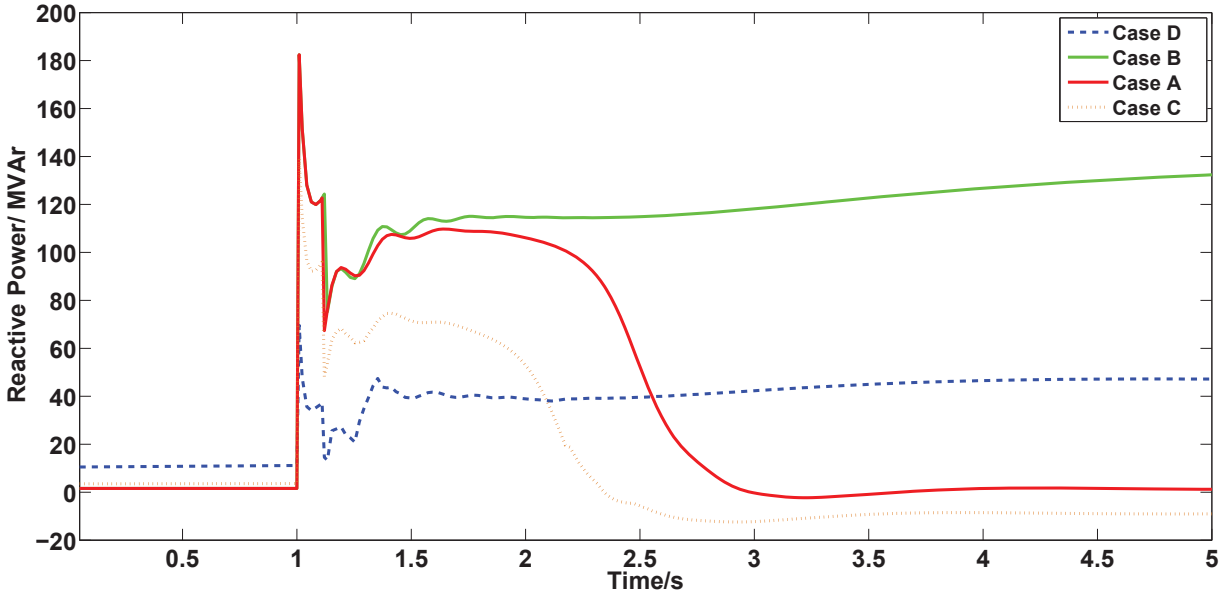

Figure 6.4: Reactive power output of synchronous generator.

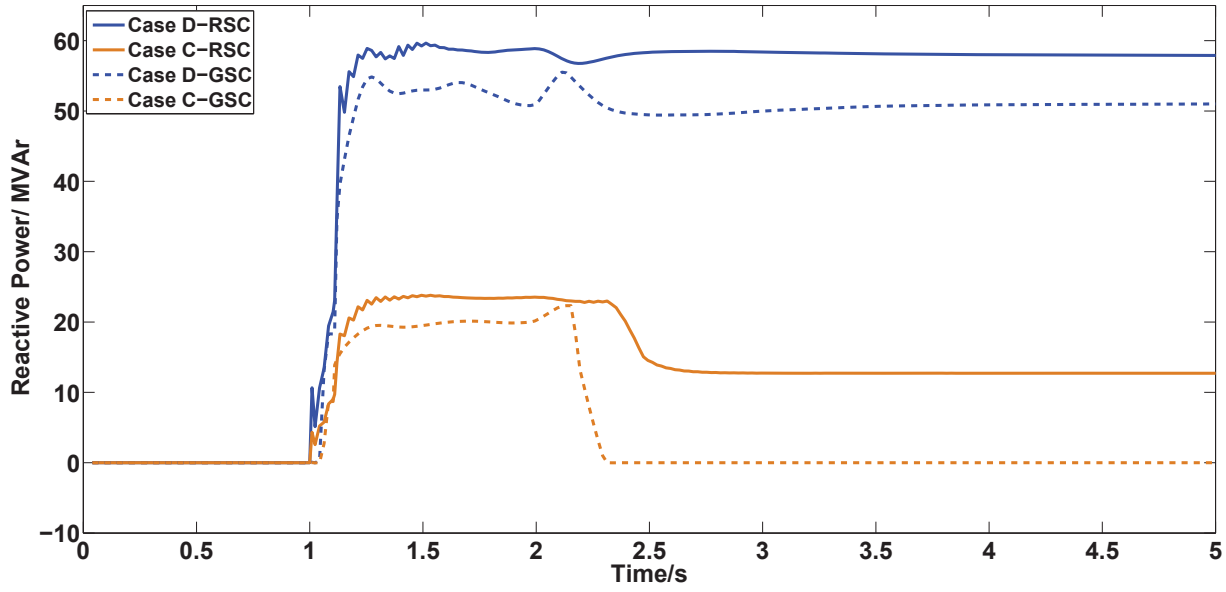

Figure 6.5: Reactive power output of DFIG wind generator through stator(RSC control) and GSC

6.4 Scenario 2 - Behaviour of Induction Motors After a Disturbance

In this scenario, ST-1 type short-term voltage instability is considered. The behaviour of a power network with induction motor loads after a disturbance is a typical example for this type of instability.

The test system explained in Fig. 6.1 is considered, where the total induction motor load is consists of 12 parallel connected induction motors. Two disturbances of tripping of two and three transmission lines out of four transmission lines at t= 1 s are considered.

Fig. 6.6 shows the variation of the Bus 2 voltage with the two disturbances. With two lines out, the voltage drops and settles at about 0.95 p.u. With three lines out, the voltage drops rapidly and system becomes unstable within about two seconds. Fig. 6.7 shows the variation of induction motor slip during the two disturbances, which illustrates the induction motor stalling following the outage of three lines.

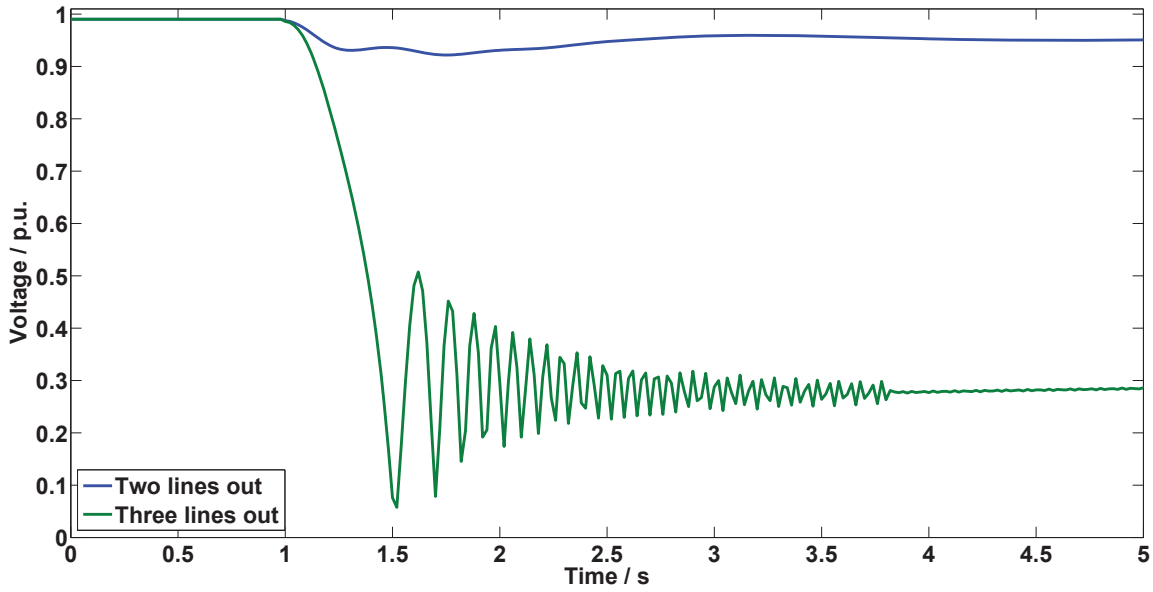

Figure 6.6: Bus 2 voltage profile with two and three lines out

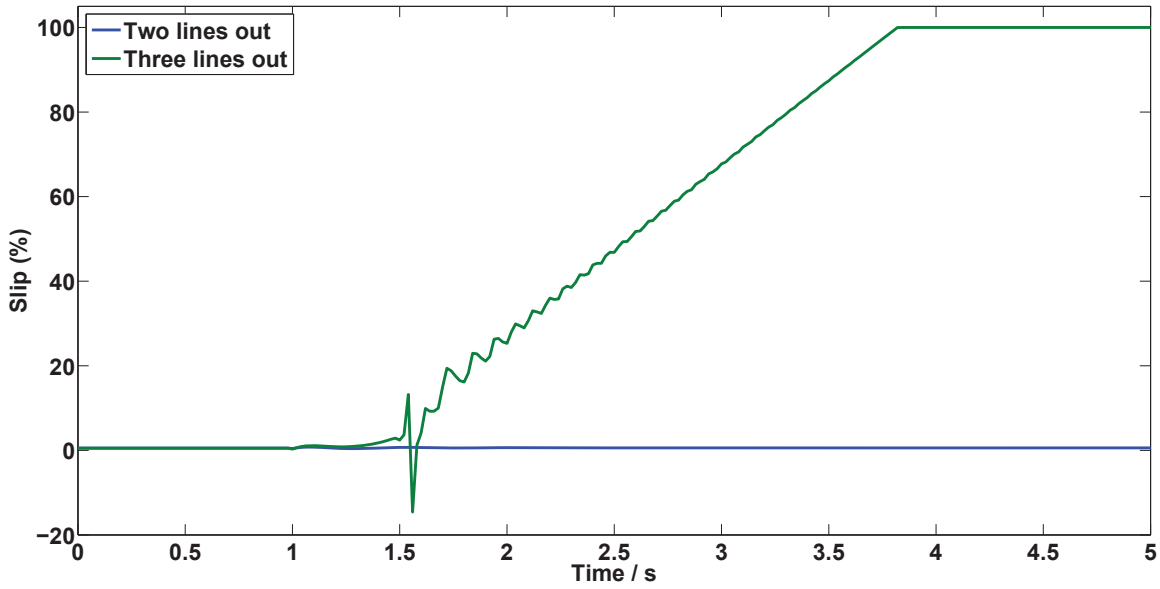

Figure 6.7: Variation of induction motor slip

As explained with (2.22) in Chapter 2.9.2, the electromagnetic torque of a induction motor is proportional to the square of the voltage. Therefore, the electromagnetic torque reduces, as the the voltage drops following a disturbance. Due to this, the torque-speed curve (electromagnetic torque) shifts down as shown in Fig. 6.8.

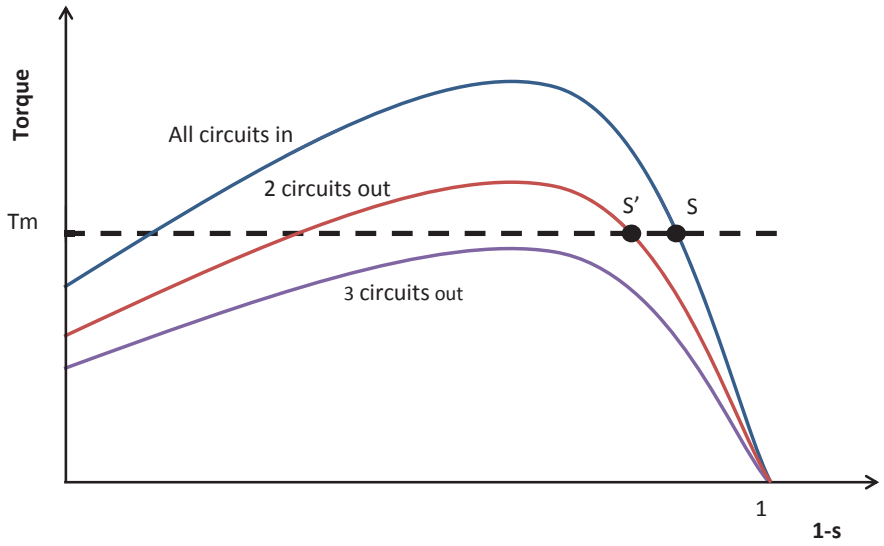

Figure 6.8: Variation of electromagnetic torque

After the outage of two lines, the stable operating point shifts from S to S'. However, after the outage of three lines, the voltage further drops and, the torque-speed curve moves further down. Therefore, there is no stable operating point when the three transmission lines are disconnected form the network, which results system instability.

In the next part of this scenario, the impact of DFIG based VSWGs on short-term voltage instability is assessed. DFIG based wind generation is integrated at Bus 1 while maintaining the total system generation capacity constant. As shown in Fig. 6.6, the Bus 2 voltage becomes unstable when three transmission lines are disconnected from the network even without having any wind generation in the system. Similarly, Bus 2 voltage becomes unstable with three lines out, when the wind generation is added to the system. Hence, the case with two line outages is considered for the comparison. Fig.6.9 shows the voltage profile with outages of two lines with and without DFIG wind generation. It is noted that with about 39.5 MW DFIG wind generation (about 22 % wind penetration) integrated at Bus 1, the voltage variation following the two line outages looks simlilar to the case with no wind generation. In other words, the voltages settle at a acceptable voltage after the disturbance. However, under the same disturbance, when the wind generation capacity is increased to 97.5 MW (i.e. about 54 % wind penetration), the volatge at Bus 2 becomes unstable.

These results demonstrate a similar trend to the scenario 1 considered in Section 6.3. When the wind penetration level is low, the system behaviour during short-term voltage instability is similar to the case with having synchronous generators with similar capacities. However, when the wind penetration level of the system is increased, the voltage becomes unstable. In other words, under high wind penetration levels, the system short-term voltage stability deteriorated compared to a system with synchronous generators of similar capacities.

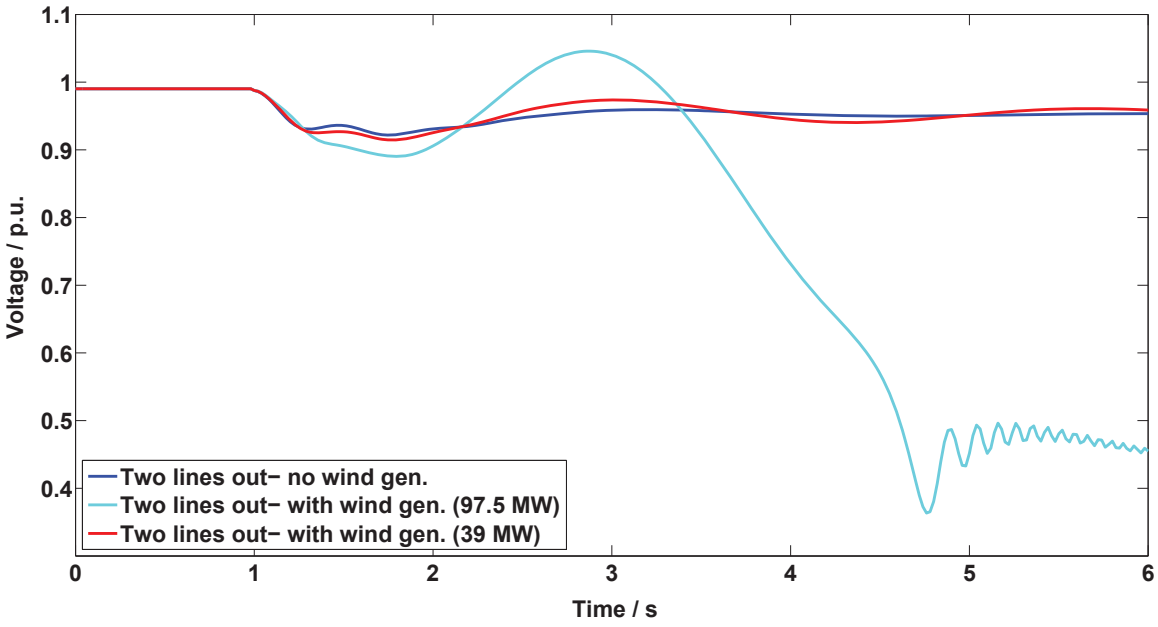

Figure 6.9: Bus 2 voltage profile with DFIG wind generation

6.5 Impact of Loading Levels of VSWGs on Short-term Voltage Stability

In this section, the impact of loading levels of VSWGs on short-term voltage stability is investigated using Scenario 1 considered in Section 6.3. Loading level of a VSWG is calculated as the ratio of the power output of the VSWG and the rated/maximum power of the VSWG.

According to the reactive power capability charts of the VSWGs explained in Chapter 2, the DFIG and FCWG based VSWGs have a larger reactive power capability at lower loading levels. The aim of this section is to investigate how the loading level of the VSWGs affect the short-term voltage stability.

In this case DFIG based wind generation with a capacity of 39 MW(2 farms) is integrated to the network at Bus 1 similar to the scenario considered in Section 6.3. The existing synchronous generation in the network is reduced by an equivalent amount to the added wind generation to maintain the total network generation capacity constant. A three phase short circuit fault is simulated near Bus 3 in one

of the four transmission lines at t= 1 s and the fault is cleared after 110 ms.

The DFIG is operated at 3 different loading levels 50%, 65% and 80%. The active power output of the DFIG under the three loading levels is shown in Fig. 6.10. Fig. 6.11 shows the variation of voltage at Bus 2 during the fault when the DFIG is operated under the three different loading levels. According to the response, it can be seen that the fault recovery is better when the DFIG is operated at the higher loading level. When the loading level is 50%, the voltage cannot recover back to the pre-disturbance voltage. When the loading level is increased up to 65%, the voltage recovers back to the pre-disturbance voltage. When the loading level is further increased up to 80%, the voltage recovery is quicker.

Fig. 6.12, shows the variation of the reactive power output of the synchronous generator under the three different cases. It should be noted that the synchronous generation capacity of the network is the same in the three cases. Immediately, after the fault occurs, the synchronous generator supplies a large reactive power boost. The reactive power response of the synchronous generator during the fault look similar under the three loading levels of the DFIG. Due to the fact that synchronous generators can be overloaded in short-term, they can provide a large reactive power boost during the fault duration which is about 110 ms.

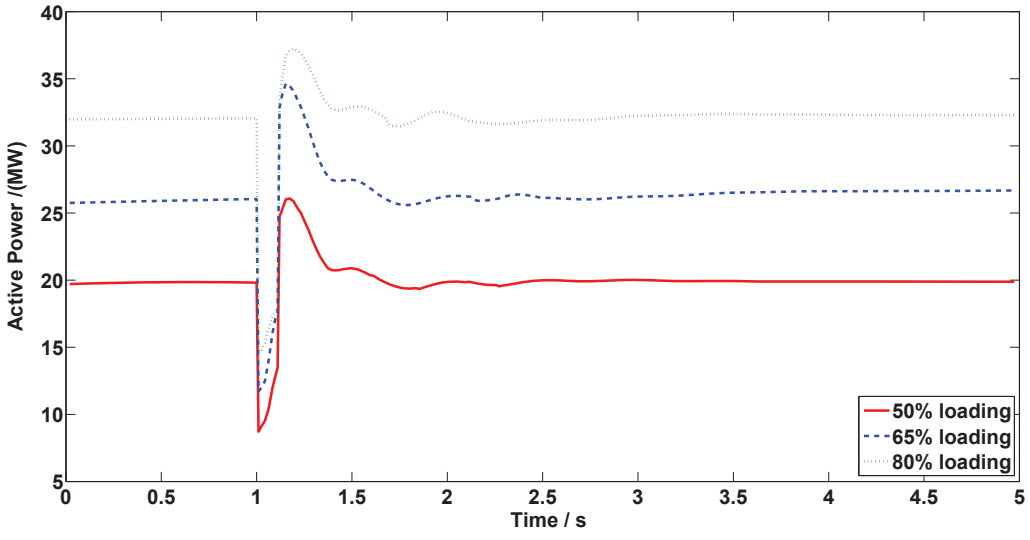

Figure 6.10: Active power output of DFIG

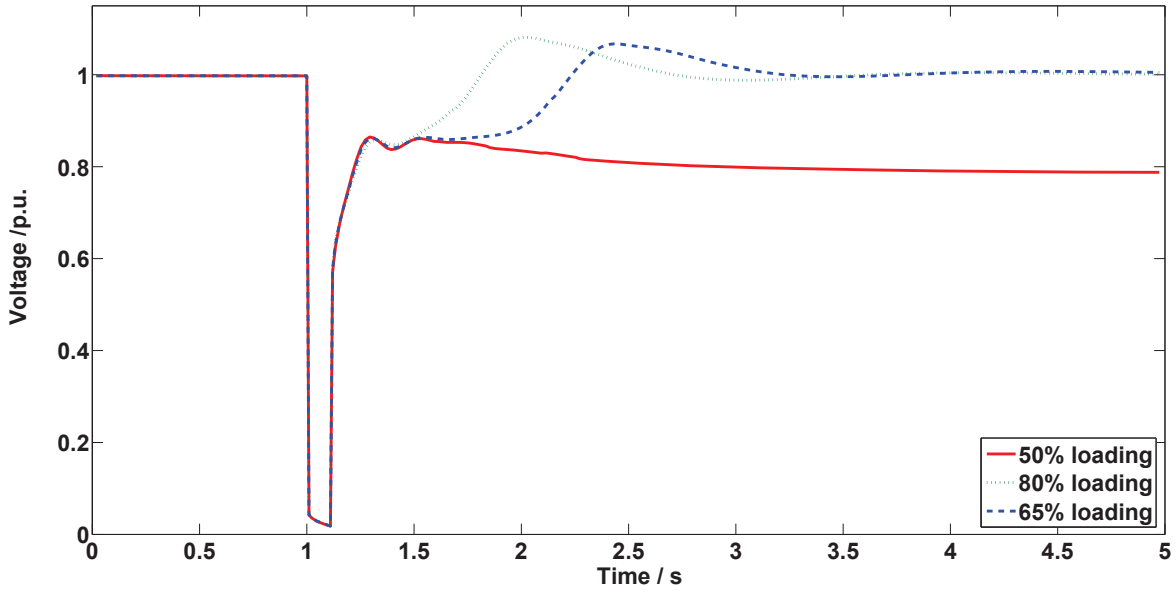

Figure 6.11: Bus 2 voltage profile with different loading levels of DFIG

When the loading level of the DFIG is low, the synchronous generator loading is increased to provide the additional active power demand of the network. However, it does not affect the short-term response of the synchronous generator during the fault and during the initial fault recovery. Therefore, the voltage variation during the fault and during the initial fault recovery looks similar under the three cases.

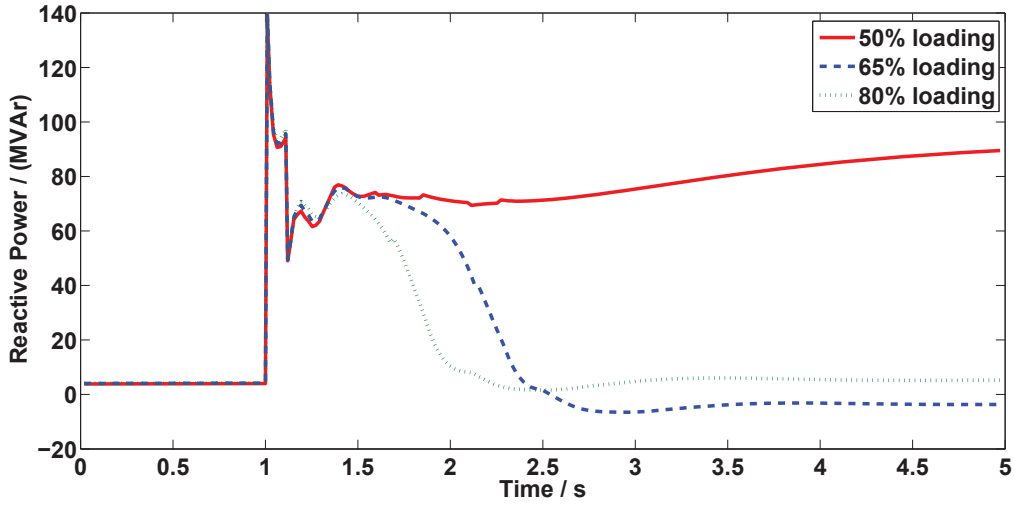

Figure 6.12: Synchronous generator reactive power output

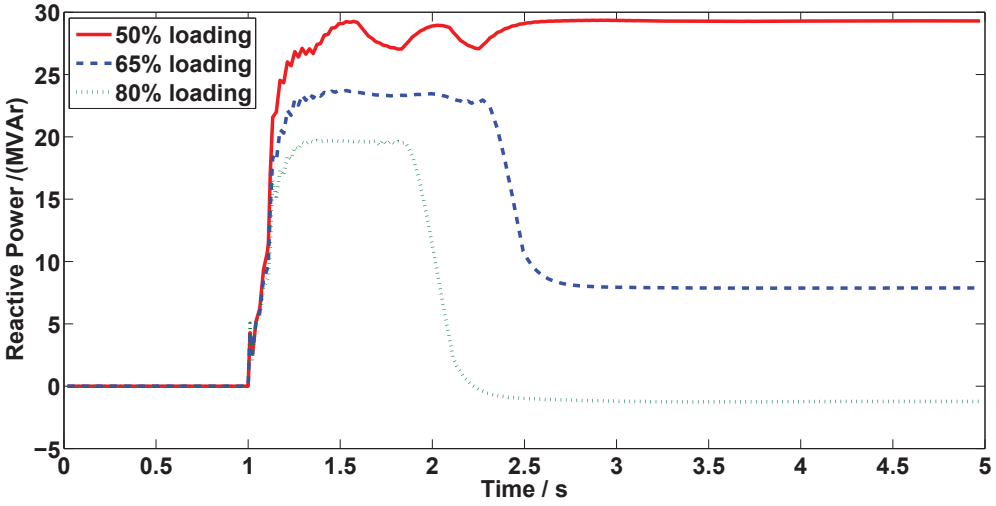

Figure 6.13: DFIG reactive power output (RSC control)

The increased loading level of synchronous generator due to the lightly loaded DFIG, reduces the capability of synchronous generator to provide more reactive power. Although it does not affect its short-term capability, it affects the subsequent fault recovery. Therefore, when the DFIG is lightly loaded, the synchronous generator cannot provide more reactive power during the subsequent fault recovery, which leads the voltage to drop and the induction motor to stall. Due to the large reactive power absorption of the induction motor after stalling, the bus voltage cannot recover back to the pre-disturbance voltage.

These observations further confirms that the available synchronous generation in the network can largely affect the short-term voltage stability. Although, lightly loaded VSWGs have a higher reactive power capability, when the synchronous generation capacity in the network is unchanged, VSWGs cannot support more during a short-term voltage instability. These results show that the network short-term voltage stability is affected at increased penetration levels of VSWGs when less synchronous generation is available in the network.

6.6 Short-term Voltage Stability with FCWG

In this section, the impact of DFIG and FCWG base wind generation on short-term voltage stability is compared using Scenario 1 considered in Section 6.3.

In Case 1 of this section, DFIG based wind generation with a capacity of 39 MW(2 farms) is integrated to the network at Bus 1 similar to the scenario considered in Section 6.3. The existing synchronous generation in the network is reduced by an equivalent amount to the added wind generation to maintain the total network generation capacity constant. A three phase short circuit fault is simulated near Bus 3 in one of the four transmission lines at t= 1 s and the fault is cleared after 110 ms.

In Case 2 of this section, the DFIG wind generation in Case 1 is replaced with FCWG based wind generation with the same capacity. The FCWG is operated at the same loading level as the DFIG generation. The same disturbance is simulated as in Case 1 and the results are compared.

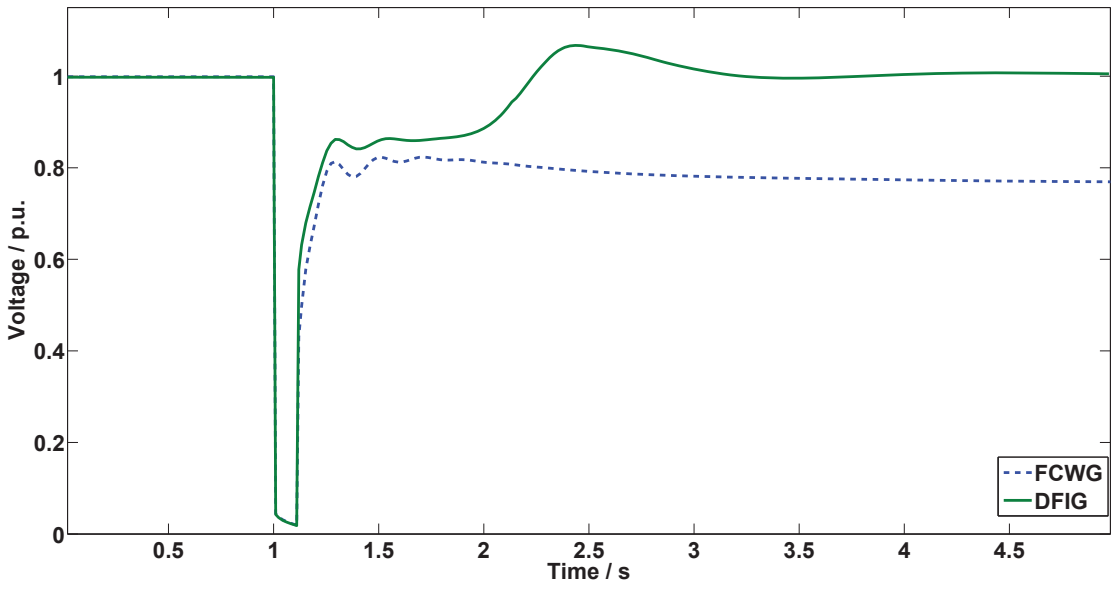

Figure 6.14: Bus 2 voltage profile with FCWG and DFIG

Fig. 6.14 shows the voltage profile of Bus 2 for the two cases. As shown, the voltage recovers back to the pre-disturbance in the case with DFIG based wind gen-

eration. However, the voltage does not recover back to the pre-disturbance voltage in the case with FCWG. In these two cases synchronous generator and each VSWG are loaded to the same levels and hence, the less reactive power capability of the FCWG wind generation affects the latter part of fault recovery, which results in reduced voltage after the fault recovery.

6.7 Summary

In this chapter, the impact of VSWGs on short-term voltage stability was investigated considering two different instability mechanisms which usually lead power networks to short-term voltage instability. DFIG based VSWGs were used in the studies. The study was conducted using a simple two bus test network developed in DIgSILENT Power Factory. The main driving force of short-term voltage instability is the behaviour of dynamic loads, such as induction motors. Therefore, the load in the test network was composed of induction motors, and it can be considered as an aggregated industrial load.

The DFIG based wind generation was added to the network while maintaining the total system generation capacity constant. It allows the comparison of the response of the synchronous generation and DFIG wind generation during short-term voltage instability. According to the two instability mechanisms studied in this chapter, it was noted that the short-term voltage stability of the network can be maintained by having significant penetration level of the wind generation in the system. However, under large penetration levels of the wind generation in the system, the system leads to short-term voltage instability. Under this condition, the synchronous generation capacity in the system is small. Therefore, the network short-term voltage stability is affected by high wind penetration levels in the network, where the existing synchronous generation capacity is small.

According to the reactive power capability charts of VSWGs explained in Chapter 2, the VSWGs have a larger reactive power capability when they are lightly loaded. Therefore, the impact of the wind generator loading level on short-term

voltage stability was also investigated considering ST-2 type short-term voltage instability and DFIG based wind generation. According to the results, improved voltage recovery was observed when the DFIG wind generator loading is larger. The observations further confirm that the available synchronous generation in the network can largely affect the short-term voltage stability. Although, lightly loaded VSWGs have a higher reactive power capability, when the synchronous generation capacity in the network is unchanged, VSWGs cannot support more during a short-term voltage instability.

The impact of DFIG and the FCWG based wind generation on short-term voltage stability was compared using ST-2 type short-term voltage instability. According to the results, better short-term voltage stability was observed with the DFIG compared to the FCWG. In the two cases considered, synchronous generator and each VSWG were loaded to the same levels. It was noted that the less reactive power capability of the FCWG wind generation affects during the latter part of voltage recovery and, subsequently resulted a deteriorated short-term voltage stability.

Chapter 7

Conclusions and Recommendations for Future Work

7.1 Conclusions

With the increasing penetration levels of renewable power generation in power systems around the world, it is imperative to understand the impact of these generators on the connected networks. Existing literature claims that the increased penetration levels of renewable power generators, particularly wind power generators can affect power system stability in all aspects. Through a critical review of existing literature related to this topic, it was identified that there are significant research gaps related to voltage stability in wind rich networks. Considering these gaps, the main objective of this thesis was to investigate the voltage stability of power systems with high wind power penetration levels considering both static and dynamic aspects of voltage stability.

In the first part of this thesis, the preliminary investigations of the impact of VSWGs on power system voltage stability was investigated using steady-state analysis. The importance of accurate representation of the reactive power capability of wind generators in voltage stability studies was emphasised in the analysis. Stud-

ies using DFIG based wind generators revealed that operating VSWGs in voltage control mode is favourable for steady-state voltage stability of a network compared to the operation in power factor control mode, due to the fact that the reactive power capability of the VSWGs can be appropriately utilised to support the network voltage stability. Moreover, the impact of conventional synchronous generators and, DFIG and FCWG based VSWGs on the steady-state voltage stability was compared. It was illustrated that the VSWGs have the capability to improve the steady-state voltage stability. Although, synchronous generators have a better reactive power capability at all loading conditions, the reactive power capability of VSWGs significantly vary with the generator loading level. If a synchronous generator in a network is replaced with an equivalent FCWG, it can improve the voltage stability even at heavily loaded conditions. If the synchronous generator is replaced with an equivalent DFIG, latter cannot significantly improve the voltage stability, if the GSC is operated at unity power factor. However, if the reactive power capability of the GSC of the DFIG is also utilised, DFIG can also improve the voltage stability depending on the loading level.

In the next phase of steady-state analysis, QV modal analysis was used to identify strong and weak areas of a power network in terms of voltage stability. It was found that by integration of VSWGs in weak areas in a network, which were identified by the QV modal analysis, can support the voltage stability. Due to the reactive power capability of power electronic converter based VSWGs, they can support to maintain a larger reactive power margins in weak parts of the networks, and hence it is beneficial for the overall voltage stability of network. The inherent reactive power capability of the VSWGs was considered in the studies. However, it is noted that there are some other site-specific factors, such as wind farm internal impedances which can affect reactive power capability available at the connection points of large wind farms.

Steady-state voltage stability analysis is not sufficient to derive accurate results in voltage stability analysis, and hence dynamic voltage stability analyis is

imperative. In the next phase of this thesis, the impact of VSWGs on long-term dynamic voltage stability was investigated. Results revealed that the VSWGs added to a network without altering the existing system generation capacity, improves the long-term voltage stability of the network. The DFIG and FCWG based VSWGs have the capability to provide reactive power to a power network, in addition to the active power. However, with the increasing penetration levels of the renewable power generators in networks, some of the existing synchronous generators will be retired or decommissioned. Therefore, VSWGs will be replacing some of the existing synchronous generator based power generation in networks. This factor has been extensively considered in the long-term voltage stability analysis presented in this thesis. The results demonstrated that the capability of the VSWGs to support a network, under such conditions is less compared to an equivalent synchronous generator capacity.

The results of long-term voltage stability analysis also revealed that the connection point of a wind farm is an important factor which affects long-term voltage stability. Usually, the reactive power support to the loads are provided by the nearby generators. Therefore, the local generation is crucial for load centres. The replacement of synchronous generation close to a load center, with wind generators can have detrimental effects on long-term voltage stability. However, if the wind generation is added without making any changes to the existing generation, it becomes favourable for the long-term voltage stability. When the reactive power capability characteristics of the DFIG and FCWG are compared, DFIG has a larger reactive power capability compared to a FCWG, when the reactive power support from the GSC of the DFIG is also considered. Furthermore, by comparing the response of these two types of generators during a long-term voltage instability event, it was shown that the DFIG has a better capability to support the system compared to a FCWG.

Under light loading conditions, during low wind speed conditions, VSWGs have higher reactive power capabilities. This factor has also been considered in the studies

in the long-term voltage stability analysis. According to the results, in the cases where the VSWGs have to replace the synchronous generators, although the VSWGs have higher reactive power capability during light loading conditions, detrimental effects on long-term voltage stability can be observed, due to the low active power output of the VSWGs. Long-term voltage instability in networks with significant induction motor loads was also examined in the long-term voltage stability analysis. Using a scenario with significant amount of induction motors in the test system, the unfavourable response of the DFIGs compared to synchronous generators during a long-term voltage instability event was noted.

It should be noted that the best possible voltage control strategy was used in the long-term voltage stability analysis utilising the maximum possible reactive power support of DFIG and FCWG based generation. However, the response of VSWGs in relation to the long-term voltage stability was not favourable in some conditions. VSWGs have no (or little) dynamic overload capability compared to conventional synchronous generators, and it is one of the major factors which influences this unfavourable response. Due to these reasons, additional reactive power support devices, preferably dynamic reactive power support such as STATCOMs have to used along with the VSWGs, particularly in networks with very high wind power penetration levels, where the existing synchronous generator capacity is not significant.

Conducting complete dynamic simulations for large interconnected networks demands considerable effort and computational capability. By using direct methods, system stability can be evaluated without explicitly solving the differential equations of the system. In the next part of this thesis, a novel energy function based method for long-term dynamic voltage stability evaluation was introduced. This method was developed based on the conventional energy function based method for voltage stability evaluation. However, the proposed method overcomes the limitations of the energy function methods in practical applications. The basic concept of the new method was explained using a simple two bus network. The energy margin, which is the energy distance between a pre-determined stable operating point and any

subsequent operating point, and the rate of change of energy margin, can be used to assess the long-term dynamic voltage instability. The direct correlation between the energy margin and the voltage instabilities was demonstrated using sensitivity analysis and numerical computation using simulations.

The application of the method to a large interconnected network was demonstrated using the Reliability and Voltage Stability (RVS) test system developed in DIgSILENT Power Factory. It was suggested to evaluate the energy margin with respect to selected busbars from the weak areas of the network to assess the system wide-dynamic voltage instability issues. One of the major applications of the proposed method is real-time voltage security assessment, which is very important in modern power systems with high penetration levels of renewable power generation. The method was applied to the test system which used in Chapter 4 to examine long-term voltage stability analysis with VSWGs to demonstrate the application for networks with wind generation. The associated results provides an additional verification for the studies conducted in Chapter 4.

The last part of this thesis focused on the impact of VSWGs on short-term voltage stability, which is the second category of dynamic voltage stability. The main driving force of short-term voltage instability is the behaviour of dynamic loads. Therefore, the load in the test system constituted induction motors. According to the two instability mechanisms studied, it was revealed that the short-term voltage stability of the network can be maintained in the presence of significant penetration levels of VSWGs in the system. However, under large penetration levels of VSWGs, the system leads to short-term voltage instability. Therefore, the network short-term voltage stability is affected by high wind penetration levels in the network, where the existing synchronous generation capacity is small. The impact of the VSWG loading level on short-term voltage stability is also investigated and an improved voltage stability was observed when the VSWG loading is larger. Although, lightly loaded VSWGs have a higher reactive power capability, when the synchronous generation capacity in the network is unchanged, VSWGs cannot support more during a

short-term voltage instability. The observations further confirmed that the available synchronous generation in the network is crucial for the short-term voltage stability. The impact of DFIG and the FCWG based wind generation on short-term voltage stability was compared using ST-2 type short-term voltage instability. A better short-term voltage stability was observed with the DFIG compared to the FCWG.

7.2 Recommendations for Future work

In dynamic voltage stability assessment with VSWGs conducted in this thesis, it was identified that the dynamic voltage stability of networks can be affected by the added VSWGs, particularly when the wind penetration level is high and the synchronous generation capacity available in the network is small. One important study to be considered in future work could be the detailed investigation of the strategies to improve the dynamic voltage instability identified in this research. A comparative analysis of possible mitigation methods, such as reactive power compensation devices, for example, STATCOMs, synchronous condensers and energy storage to identify the most suitable strategies to improve the dynamic voltage instability will be important.

In Chapter 5 of this thesis, a new direct method using energy function method was developed to examine long-term dynamic voltage stability. The possibility of utilising this method for real-time voltage security assessment was explained. Future work can undertake the application of this methodology using real-time PMU data to verify the practical application of the method. It was also revealed that real-time network reduction methods can be used in the implementation stage of this method. Future work can also include identification of a suitable real-time network reduction method. A comparative evaluation of the application of the method using strategies developed Chapter 5 and with the utilisation of the aforementioned real-time network reduction methods can identify the most efficient method for practical implementation.

Bibliography

[1] REN21 Steering Commitee. Renewables 2016- global status report. Technical report, REN21, 2016.

[2] Renewable energy statistics, http://www.ec.europa.eu/eurostat/statistics-explained, November 2016.

[3] Energy trends: September 2016, special feature article - renewable electricity in scotland, wales, northern ireland and the regions of england in 2015, November 2016.

[4] The australian renewable energy race: Which states are winning or losing? Technical report, Climate Council of Austrlain Limited, 2014.

[5] Wind in power- 2015 European statistics. Technical report, The European Wind Energy Association, 2016.

[6] E. Vittal, M. O'Malley, and A. Keane. A steady-state voltage stability analysis of power systems with high penetrations of wind. *IEEE Trans. Power Syst.*, 25(1):433–442, Feb 2010.

[7] V. Vittal and R. Ayyanar. *Grid Integration and Dynamic Impact of Wind Energy*. Kluwer international series in engineering and computer science: Power electronics & power systems. Springer, 2012.

[8] D. Gautam, V. Vittal, and T. Harbour. Impact of increased penetration of DFIG-based wind turbine generators on transient and small signal stability of power systems. *IEEE Trans. Power Syst.*, 24(3):1426–1434, 2009.

[9] B. Fox, L. Bryans, D. Flynn, N. Jenkins, D. Milborrow, M. O'Malley, R. Watson, and O. Anaya-Lara. *Wind Power Integration: Connection and System Operational Aspects*. IET Renewable Energy Series 14. Institution of Engineering and Technology, 2 edition, 2014.

[10] P. Kundur, J. Paserba, V. Ajjarapu, G. Andersson, A. Bose, C. Canizares, N. Hatziargyriou, D. Hill, A. Stankovic, C. Taylor, T. Van Cutsem, and V. Vittal. Definition and classification of power system stability ieee/cigre joint task force on stability terms and definitions. *IEEE Trans. Power Syst.*, 19(3):1387–1401, 2004.

[11] P. Kundur, N.J. Balu, and M.G. Lauby. *Power System Stability and Control*. The EPRI power system engineering series: Electrical engineering. McGraw-Hill Education, 1994.

[12] B.H. Chowdhury and C.W. Taylor. Voltage stability analysis: V-Q power flow simulation versus dynamic simulation. *IEEE Trans. Power Syst.*, 15(4):1354–1359, 2000.

[13] Turbine components, http://www.mstudioblackboard.tudelft.nl/duwind, November 2016.

[14] Wind turbine, https://www.au.mathworks.com/help/physmod, November 2016.

[15] V. Ajjarapu. *Computational techniques for voltage stability assessment and control*. Kluwer international series in engineering and computer sciences: Power electronics & power systems. Springer Science + Business Media, LLC, 2006.

[16] T. Van Cutsem and C. Vournas. *Voltage Stability of Electric Power Systems*. Kluwer International Series in Engineering and Computer Science. Springer, 1998.

[17] T. Van Cutsem. Voltage instability: phenomena, countermeasures, and analysis methods. *Proceedings of the IEEE*, 88(2):208–227, Feb 2000.

[18] Modelling of voltage collapse including dynamic phenomena. Technical report, Task Force 38.02.10, CIGRE, 1993.

[19] V. Ajjarapu and C. Christy. The continuation power flow: a tool for steady state voltage stability analysis. *IEEE Trans. Power Syst.*, 7(1):416–423, 1992.

[20] Carson W. Taylor. *Power System Voltage Stability*. McGRAW-Hill, Inc., 1994.

[21] B. Gao, G. K. Morison, and P. Kundur. Voltage stability evaluation using modal analysis. *IEEE Trans. Power Syst.*, 7(4):1529–1542, Nov 1992.

[22] V. S. Sravan Kumar, K. Krishna Reddy, and D. Thukaram. Coordination of reactive power in grid-connected wind farms for voltage stability enhancement. *IEEE Trans. Power Syst.*, 29(5):2381–2390, Sept 2014.

[23] I. S. Naser, A. Garba, O. Anaya-Lara, and K.L. Lo. Voltage stability of transmission network with different penetration levels of wind generation. In *45th International Universities Power Engineering Conference (UPEC),Cardiff, Wales*, pages 1–5, 2010.

[24] Yongning Chi, Yanhua Liu, Weisheng Wang, and Huizhu Dai. Voltage stability analysis of wind farm integration into transmission network. In *International Conference on Power System Technology, 2006(PowerCon 2006), Chongqing*, pages 1–7, 2006.

[25] M.P. Palsson, T. Toftevaag, K. Uhlen, and J. O G Tande. Large-scale wind power integration and voltage stability limits in regional networks. In *IEEE Power Engineering Society Summer Meeting*, volume 2, pages 762–769, 2002.

[26] M. J. Hossain, H.R. Pota, M.A. Mahmud, and R.A. Ramos. Investigation of the impacts of large-scale wind power penetration on the angle and voltage stability of power systems. *IEEE Systems Journal*, 6(1):76–84, 2012.

[27] M. J. Hossain, H.R. Pota, M. A. Mahmud, and R.A. Ramos. Impacts of large-scale wind generators penetration on the voltage stability of power systems. In *IEEE Power and Energy Society General Meeting*, pages 1–8, 2011.

[28] M. Ntshangase, S. K. Kariuki, S. Chowdhury, and S. P. Chowdhury. Voltage stability analysis of electricity networks with dfig-based wind power plants. In *IEEE Power and Energy Society General Meeting*, pages 1–8, July 2012.

[29] O. E. Fadhel Loubaba Bekri and M. K. Fellah. Placement of wind farms for enhancing voltage stability based on continuation power flow technique. In *2015 3rd International Renewable and Sustainable Energy Conference (IRSEC)*, pages 1–6, Dec 2015.

[30] A. Jalali and M. Aldeen. Placement and operation of statcom-storage for voltage stability enhancement of power systems with embedded wind farms. In *2016 IEEE Innovative Smart Grid Technologies - Asia (ISGT-Asia)*, pages 948–953, 2016.

[31] Ala Tamimi. *Voltage stability limitis for weak power systems with high wind penetration*. PhD thesis, Department of Electrical and Computer Engineering, Kansas State University, 2011.

[32] A.A. Tamimi, A. Pahwa, and S. Starrett. Effective wind farm sizing method for weak power systems using critical modes of voltage instability. *IEEE Trans. Power Syst.*, 27(3):1610–1617, Aug 2012.

[33] F. P. de Mello and J. W. Feltes. Voltage oscillatory instability caused by induction motor loads. *IEEE Trans. Power Syst.*, 11(3):1279–1285, Aug 1996.

[34] W. R. Lachs and D. Sutanto. The dynamics of system voltage instability. In *1995 International Conference on Energy Management and Power Delivery*, volume 1, pages 331–336, Nov 1995.

[35] W. R. Lachs and D. Sutanto. Voltage instability in interconnected power systems: a simulation approach. *IEEE Trans. Power Syst.*, 7(2):753–761, May 1992.

[36] T. Van Cutsem and C. D. Vournas. Voltage stability analysis in transient and mid-term time scales. *IEEE Trans. Power Syst.*, 11(1):146–154, Feb 1996.

[37] C. L. DeMarco and T. J. Overbye. An energy based security measure for assessing vulnerability to voltage collapse. *IEEE Trans. Power Syst.*, 5(2):419–427, May 1990.

[38] T. J. Overbye and C. L. De Marco. Voltage security enhancement using energy based sensitivities. *IEEE Trans. Power Syst.*, 6(3):1196–1202, Aug 1991.

[39] T. J. Overbye and C. L. DeMarco. Improved techniques for power system voltage stability assessment using energy methods. *IEEE Trans. Power Syst.*, 6(4):1446–1452, Nov 1991.

[40] T. J. Overbye. Use of energy methods for on-line assessment of power system voltage security. *IEEE Trans. Power Syst.*, 8(2):452–458, May 1993.

[41] Claudio A. Canizares. *Voltage collapse and transient energy function analyses of ac/dc systems*. PhD thesis, University of Wisconsin-Madison, 1991.

[42] K. L. Praprost and K. A. Loparo. An energy function method for determining voltage collapse during a power system transient. *IEEE Trans. Circuits and Systems I: Fundamental Theory and Applications*, 41(10):635–651, Oct 1994.

[43] Voltage stability assessment: Concepts, practises and tools. Technical report, Power system dynamic performance committee, Power system stability subcommittee, IEEE Power & Energy Society, 2002.

[44] A. Y. Abdelaziz, M. M. Abu-Elnaga, M. A. Elsharkawy, and K. M. Elbahrawy. Voltage stability assessment of multi-machine power systems using energy function and neural networks techniques. *Electric Power Components and Systems*, 34(12):1313–1330, 2006.

[45] K.R. Padiyar. *Structure Preserving Energy Functions in Power Systems: Theory and Applications*. Taylor & Francis, 2013.

[46] E. Valenca De Lorenci, A.C. Zambroni de Souza, and B.I. Lima Lopes. Energy function applied to voltage stability studies - discussion on low voltage solutions with the help of tangent vector. *Electric Power Systems Research*, 141:290 – 299, 2016.

[47] Q. Y. Liu, C. C. Liu, and Q. F. Liu. Coordinated voltage control with online energy margin constraints. *IEEE Trans. Power Syst.*, 31(3):2064–2075, May 2016.

[48] K. Ben-Kilani and M. Elleuch. Structural analysis of voltage stability in power systems integrating wind power. *IEEE Trans. on Power Syst.*, 28(4):3785–3794, Nov 2013.

[49] L. Meegahapola and T. Littler. Characterisation of large disturbance rotor angle and voltage stability in interconnected power networks with distributed wind generation. *IET Renewable Power Generation*, 9(3):272–283, 2015.

[50] J. Schmall, S. H. Huang, Ying Li, J. Billo, J. Conto, and Yang Zhang. Voltage stability of large-scale wind plants integrated in weak networks: An ERCOT case study. In *2015 IEEE Power Energy Society General Meeting*, pages 1–5, July 2015.

[51] N.R. Ullah and T. Thiringer. Variable speed wind turbines for power system stability enhancement. *IEEE Trans. Energy Conv.*, 22(1):52–60, March 2007.

[52] R.J. Konopinski, P. Vijayan, and V. Ajjarapu. Extended reactive capability of DFIG wind parks for enhanced system performance. *IEEE Trans. Power Syst.*, 24(3):1346–1355, Aug 2009.

[53] S. De Rijcke, H. Ergun, D. Van Hertem, and J. Driesen. Grid impact of voltage control and reactive power support by wind turbines equipped with direct-drive synchronous machines. *IEEE Trans. Sust. Energy*, 3(4):890–898, Oct 2012.

[54] R.R. Londero, C.M. Affonso, and J.P.A. Vieira. Long-term voltage stability analysis of variable speed wind generators. *IEEE Trans. Power Syst.*, 30(1):439 – 447, 2014.

[55] R. R. Londero, C. M. Affonso, J. P. A. Vieira, and U. H. Bezerra. Impact of different dfig wind turbines control modes on long-term voltage stability. In *2012 3rd IEEE PES Innovative Smart Grid Technologies Europe (ISGT Europe)*, pages 1–7, Oct 2012.

[56] X. Wang, H. D. Chiang, J. Wang, H. Liu, and T. Wang. Long-term stability analysis of power systems with wind power based on stochastic differential equations: Model development and foundations. *IEEE Trans. Sust. Energy*, 6(4):1534–1542, Oct 2015.

[57] M. Bakhtvar and A. Keane. Allocation of wind capacity subject to long term voltage stability constraints. *IEEE Trans. Power Syst.*, 31(3):2404–2414, May 2016.

[58] Austrailian Energy Market Operator (AEMO). Black system south australia 28 september 2016 - final report. Technical report, March, 2017.

[59] Torsten Lund, Poul Sorensen, and Jarle Eek. Reactive power capability of a wind turbine with doubly fed induction generator. *Wind Energy*, 10(4):379–394, 2007.

[60] Lasantha Meegahapola, Tim Littler, and Sarath Perera. Capability curve based enhanced reactive power control strategy for stability enhancement and network voltage management. *International Journal of Electrical Power & Energy Systems*, 52:96 – 106, 2013.

[61] D. J. Hill. Nonlinear dynamic load models with recovery for voltage stability studies. *IEEE Trans. Power Syst.*, 8(1):166–176, Feb 1993.

[62] A. Borghetti, R. Caldon, A. Mari, and C. A. Nucci. On dynamic load models for voltage stability studies. *IEEE Trans. Power Syst.*, 12(1):293–303, Feb 1997.

[63] J. B. Ekanayake, L. Holdsworth, XueGuang Wu, and N. Jenkins. Dynamic modeling of doubly fed induction generator wind turbines. *IEEE Trans. Power Syst.*, 18(2):803–809, May 2003.

[64] J. Hu, Y. Huang, D. Wang, H. Yuan, and X. Yuan. Modeling of grid-connected DFIG-based wind turbines for dc-link voltage stability analysis. *IEEE Trans. Sust. Energy*, 6(4):1325–1336, Oct 2015.

[65] Markus Pller and Sebastian Achilles. Direct drive synchronous machine models for stability assessment of wind farms, http://www.digsilent.de/, November 2015.

[66] Anca D. Hansen. Evaluation of power control with different electrical and control concept of wind farm. Technical report, Project UpWind, Riso National Laboratory for Sustainable Energy, 2010.

[67] T. Saha, M. Nadarajah, J. Hossain, and S. Aziz, T.and Dahal. Control methodologies of distributed generation for enhanced network stability and control. Technical report, Intelligent Grid, Research Cluster- Project 1, 2009.

[68] M. A. Poller. Doubly-fed induction machine models for stability assessment of wind farms. In *2003 IEEE Bologna Power Tech Conference Proceedings,*, volume 3, page 6, June 2003.

[69] Lasantha Meegahapola, Brendan Fox, Tim Littler, and Damian Flynn. Multi-objective reactive power support from wind farms for network performance enhancement. *International Transactions on Electrical Energy Systems*, 23:135–150, 2013.

[70] IEEE recommended practice for excitation system models for power system stability studies. *IEEE Std 421.5-1992*, 1992.

[71] H.D. Chiang. *Direct Methods for Stability Analysis of Electric Power Systems: Theoretical Foundation, BCU Methodologies, and Applications*. Wiley, 2011.

[72] A. Pai. *Energy Function Analysis for Power System Stability*. Power Electronics and Power Systems. Springer US, 1989.

[73] P.M. Anderson, A.A.A. Fouad, Institute of Electrical, and Electronics Engineers. *Power system control and stability*. IEEE Press power engineering series. IEEE Press, 2003.

[74] E. Kreyszig. *Advanced Engineering Mathematics*. John Wiley & Sons, 2010.

[75] Test systems for voltage stability analysis and security assessment. Technical report, Power system dynamic performance committee, Power system stability subcommittee, Test systems for volatge stability and security assessment task force, IEEE Power & Energy Society, 2015.

[76] S. Corsi and G. N. Taranto. A real-time voltage instability identification algorithm based on local phasor measurements. *IEEE Trans. Power Syst.*, 23(3):1271–1279, Aug 2008.

[77] S. M. Abdelkader and D. J. Morrow. Online tracking of thevenin equivalent parameters using pmu measurements. *IEEE Trans. Power Syst.*, 27(2):975–983, May 2012.

[78] S. M. Abdelkader and D. J. Morrow. Online thevenin equivalent determination considering system side changes and measurement errors. *IEEE Trans. Power Syst.*, 30(5):2716–2725, Sept 2015.

[79] M. Glavic and T. Van Cutsem. Wide-area detection of voltage instability from synchronized phasor measurements. part i: Principle. *IEEE Trans. Power Syst.*, 24(3):1408–1416, Aug 2009.

[80] M. Glavic and T. Van Cutsem. Wide-area detection of voltage instability from synchronized phasor measurements. part ii: Simulation results. *IEEE Trans. Power Syst.*, 24(3):1417–1425, Aug 2009.

[81] H. Y. Su and C. W. Liu. Estimating the voltage stability margin using pmu measurements. *IEEE Trans. Power Syst.*, 31(4):3221–3229, July 2016.

Appendix A

Test System Data related to Chapter 3

A.1 Five Bus Test System Parameters

Component	Parameters
G1	400 MVA, 15 kV
G2	800 MVA, 15 kV
TF1-5	400 MVA,15/345 kV
TF3-4	800 MVA,345/15 kV
Bus1	15 kV, Slack bus
Bus2, Bus4, Bus5	345 kV, Load bus
Bus3	15 kV, PV bus
L1	40 MVAr,80 MW
L2	280 MVAr,800 MW

A.2 IEEE 14 Bus Test System Parameters

Bus No	**Bus Data**	**Load(MW, MVAr)**
1	Slack bus, Control Voltage- 1.04 p.u., Nominal voltage- 110 kV	0
2	PV bus, Control Voltage- 1.02 p.u., Nominal voltage- 110 kV, Gen- 40 MW, Qmin- -40 MVAr, Qmax- 50 MVAr	21.7, 12.7
3	PV bus, Control voltage-1 p.u., Nominal voltage- 110 kV, Qmin- 0, Qmax-40 MVAr	94.2, 19
4	PQ bus, Nominal voltage- 110 kV	47.8, -3.9
5	PQ bus, Nominal voltage- 110 kV	7.6, 1.6
6	PV bus, control voltage - 1.04 p.u., Nominal voltage- 33 kV	11.2, 7.5
7	PQ bus, Nominal voltage- 22 kV	0
8	PV bus, Control Voltage- 1 p.u., Nominal voltage- 11 kV	0
9	PQ bus, Nominal voltage- 33 kV Q compensation- 19 MVAr	29.5, 16.6
10	PQ bus, Nominal voltage- 33 kV	9.0, 5.8
11	PQ bus, Nominal voltage- 33 kV	3.5, 1.8
12	PQ bus, Nominal voltage- 33 kV	6.1, 1.6
13	PQ bus, Nominal voltage- 33 kV	13.5, 5.8
14	PQ bus, Nominal voltage- 33 kV	14.9, 5.0

Branch	**Resistance (p.u.)**	**Reactance (p.u.)**	**Suceptance (p.u.)**
1-2	0.01938	0.05917	0.0528
1-5	0.05403	0.22304	0.0492
2-3	0.04699	0.19797	0.0438
2-4	0.05811	0.17632	0.0340
2-5	0.05695	0.17388	0.0346
3-4	0.06701	0.17103	0.0128
4-5	0.01335	0.04211	0.0
4-7	0.0	0.20912	0.0
4-9	0.0	0.55618	0.0
5-6	0.0	0.25202	0.0
6-11	0.09498	0.19890	0.0
6-12	0.12291	0.25581	0.0
6-13	0.06615	0.13027	0.0
7-8	0.0	0.17615	0.0
7-9	0.0	0.11001	0.0
9-10	0.03181	0.08450	0.0
9-14	0.12711	0.27038	0.0
10-11	0.08205	0.19207	0.0
12-13	0.22092	0.19988	0.0
13-14	0.17093	0.34802	0.0

Appendix B

Test System Data related to Chapter 4

B.1 Five Bus Test System

Component	Parameters
G1	X_d - 2 p.u. , X_q - 2 p.u. , H- 10 s
G2	X_d - 2.1 p.u. , X_q - 2.1 p.u. , H- 3.5 s
Line 1-4	Line reactance-0.0277 p.u.
Load	725 MW, 325 MVAr
Capacitor bank	225 MVAr
Transformer 3-4 LTC	min position- -20, max position- 10, dead band- 0.99 p.u.-1.01 p.u., tap changer delay- 10s, voltage per step -0.01 p.u.
Induction motor	8000 kW, 11 kV, 1492 rpm, 50 Hz, R_1- 0.022 p.u. , X_m- 4.36 p.u., X_1- 0.01 p.u. X_2- 0.01 p.u. , H- 1.13 s

Appendix C

Test System Data related to Chapter 5

C.1 Test System Parameters

Synchronous Generator- 180 MVA, X_d-2.642 p.u.,

X_q-2.346 p.u., H-7.344 s

Induction Motor-8000 kW, 11 kV, 1492 rpm, 50 Hz

R_1- 0.022 p.u., X_m- 4.36 p.u.

X_1- 0.01 p.u., X_2- 0.01 p.u., J- 734 kg.m^2

Line reactance (per line)- 0.6 Ω /km (100 km)

Appendix D

The Reliability and Voltage Stability Test system Data [75]

Table D.1: Busbar data

Bus no	Bus name	Base Voltage (kV)	Bus Type	Voltage Magnitude (pu)	Voltage Angle (degrees)
101	ABEL	138.00	PQ	1.0342	-18.6
102	ADAMS	138.00	PQ	1.0358	-18.7
103	ADLER	138.00	PQ	1.0072	-16.2
104	AGRICOLA	138.00	PQ	1.0055	-20.3
105	AIKEN	138.00	PQ	1.0030	-20.9
106	ALBER	138.00	PQ	1.0250	-23.7
107	ALDER	138.00	PQ	1.0286	-22.2
108	ALGER	138.00	PQ	1.0136	-22.8
109	ALI	138.00	PQ	1.0280	-17.3
110	ALLEN	138.00	PQ	1.0088	-19.8
111	ANNA	230.00	PQ	0.9872	-11.8
112	ARCHER	230.00	PQ	0.9851	-10.1
113	ARNE	230.00	PQ	1.0191	-6.1
114	ARNOLD	230.00	PQ	1.0033	-9.7
115	ARTHUR	230.00	PQ	1.0111	1.0
116	ASSER	230.00	PQ	1.0164	0.4
117	ASTON	230.00	PQ	1.0338	4.5
118	ASTOR	230.00	PQ	1.0425	5.6
119	ATTAR	230.00	PQ	1.0180	-0.7
120	ATTILA	230.00	PQ	1.0349	0.4
121	ATTLEE	230.00	PQ	1.0459	6.5
122	AUBREY	230.00	PQ	1.0500	12.2
123	AUSTEN	230.00	PQ	1.0499	1.8
124	AVERY	230.00	PQ	0.9550	-5.8
1101	ABEL	13.800	PQ	1.0497	-24.5
1102	ADAMS	13.800	PQ	1.0496	-24.1
1103	ADLER	13.800	PQ	1.0446	-22.2
1104	AGRICOLA	13.800	PQ	1.0450	-26.5
1105	AIKEN	13.800	PQ	1.0488	-26.8
1106	ALBER	13.800	PQ	1.0350	-29.5
1107	ALDER	13.800	PQ	1.0497	-27.4
1108	ALGER	13.800	PQ	1.0442	-28.6
1109	ALI	13.800	PQ	1.0477	-23.2
1110	ALLEN	13.800	PQ	1.0484	-26.3
1113	ARNE	13.800	PQ	1.0453	-12.5
1114	ARNOLD	13.800	PQ	1.0433	-16.3
1115	ARTHUR	13.800	PQ	1.0497	-5.6
1116	ASSER	13.800	PQ	1.0496	-5.2
1118	ASTOR	13.800	PQ	1.0492	-0.5
1119	ATTAR	13.800	PQ	1.0498	-6.7
1120	ATTILA	13.800	PQ	1.0497	-4.9

Table D.2: Busbar data

Bus no	Bus name	Base Voltage (kV)	Bus Type	Voltage Magnitude (pu)	Voltage Angle (degrees)
10101	ABEL G1	18.000	PV	1.0290	-15.1
10102	ADAMS G1	18.000	PV	1.0430	-15.2
10106	ALBER SVC	18.000	PQ	1.0500	-23.8
10107	ALDER G1	18.000	PV	1.0370	-16.5
10113	ARNE G1	18.000	PV	1.0198	-0.1
10114	ARNOLD SVC	18.000	PQ	1.0500	-9.9
10115	ARTHUR G1	18.000	PV	1.0204	8.4
10116	ASSER G1	18.000	PV	1.0159	7.8
10118	ASTOR G1	18.000	PV	1.0487	12.6
10121	ATTLEE G1	18.000	slack	1.0468	13.4
10122	AUBREY G1	18.000	PV	1.0034	20.3
10123	AUSTEN G1	18.000	PV	1.0491	8.8
20101	ABEL G2	18.000	PV	1.0290	-15.1
20102	ADAMS G2	18.000	PV	1.0430	-15.2
20107	ALDER G2	18.000	PV	1.0370	-16.5
20113	ARNE G2	18.000	PV	1.0181	-0.1
20115	ARTHUR G2	18.000	PV	1.0204	8.4
20122	AUBREY G2	18.000	PV	1.0034	20.3
20123	AUSTEN G2	18.000	PV	1.0491	8.8
30101	ABEL G3	18.000	PV	1.0155	-11.2
30102	ADAMS G3	18.000	PV	1.0096	-11.3
30107	ALDER G3	18.000	PV	1.0370	-16.5
30113	ARNE G3	18.000	PV	1.0181	-0.1
30115	ARTHUR G3	18.000	PV	1.0204	8.4
30122	AUBREY G3	18.000	PV	1.0034	20.3
30123	AUSTEN G3	18.000	PV	1.0401	8.8
40101	ABEL G4	18.000	PV	1.0155	-11.2
40102	ADAMS G4	18.000	PV	1.0096	-11.3
40115	ARTHUR G4	18.000	PV	1.0204	8.4
40122	AUBREY G4	18.000	PV	1.0034	20.3
50115	ARTHUR G5	18.000	PV	1.0204	8.4
50122	AUBREY G5	18.000	PV	1.0034	20.3
60115	ARTHUR G6	18.000	PV	1.0220	8.4
60122	AUBREY G6	18.000	PV	1.0034	20.3

Table D.3: Generator data

Bus no	Bus name	S MVA	P MW	Q Mvar	Q_{max} Mvar	Q_{min} Mvar
10115	ARTHUR G1	14	12	6	6	0
20115	ARTHUR G2					
30115	ARTHUR G3					
40115	ARTHUR G4					
50115	ARTHUR G5					
10101	ABEL G1	24	10	7.3689	10	0
20101	ABEL G2					
10102	ADAMS G1	24	10	9.5355	10	0
20102	ADAMS G2					
10122	AUBREY G1	53	50	3.7514	16	-10
20122	AUBREY G2					
30122	AUBREY G3					
40122	AUBREY G4					
50122	AUBREY G5					
60122	AUBREY G6					
30101	ABEL G3	89	76	21.7756	30	-25
40101	ABEL G4					
30102	ADAMS G3					
40102	ADAMS G4					
10107	ALDER G1	118	80	49.1462	60	0
20107	ALDER G2					
30107	ALDER G3					
60115	ARTHUR G6	182	155	80	80	-50
10116	ASSER G1	182	155	65.9791	80	-50
10123	AUSTEN G1	182	155	68.8361	80	-50
20123	AUSTEN G2					
10113	ARNE G1	232	162.5	82.7791	82.7791	0
20113	ARNE G2	232	162.5	80	80	0
30113	ARNE G3					
30123	AUSTEN G3	412	350	128.9053	150	-25
10118	ASTOR G1	471	400	200	200	-50
10121	ATTLEE G1	471	398.6392	182.7737	200	-50

Table D.4: Generator data- controlled voltages

generator				controlled bus		
Bus no	Bus name	Base Voltage (kV)	Scheduled Voltage (pu)	Bus no	Bus name	Base Voltage (kV)
10101	ABEL G1	18.000	1.0342	101	ABEL	138.00
20101	ABEL G2	18.000	1.0342	101	ABEL	138.00
30101	ABEL G3	18.000	1.0342	101	ABEL	138.00
40101	ABEL G4	18.000	1.0342	101	ABEL	138.00
10102	ADAMS G1	18.000	1.0358	102	ADAMS	138.00
20102	ADAMS G2	18.000	1.0358	102	ADAMS	138.00
30102	ADAMS G3	18.000	1.0358	102	ADAMS	138.00
40102	ADAMS G4	18.000	1.0358	102	ADAMS	138.00
10107	ALDER G1	18.000	1.0286	107	ALDER	138.00
20107	ALDER G2	18.000	1.0286	107	ALDER	138.00
30107	ALDER G3	18.000	1.0286	107	ALDER	138.00
10113	ARNE G1	18.000	1.0200	113	ARNE	230.00
20113	ARNE G2	18.000	1.0200	113	ARNE	230.00
30113	ARNE G3	18.000	1.0200	113	ARNE	230.00
10115	ARTHUR G1	18.000	1.0113	115	ARTHUR	230.00
20115	ARTHUR G2	18.000	1.0113	115	ARTHUR	230.00
30115	ARTHUR G3	18.000	1.0113	115	ARTHUR	230.00
40115	ARTHUR G4	18.000	1.0113	115	ARTHUR	230.00
50115	ARTHUR G5	18.000	1.0113	115	ARTHUR	230.00
60115	ARTHUR G6	18.000	1.0113	115	ARTHUR	230.00
10116	ASSER G1	18.000	1.0164	116	ASSER	230.00
10118	ASTOR G1	18.000	1.0432	118	ASTOR	230.00
10121	ATTLEE G1	18.000	1.0468	121	ATTLEE	230.00
10122	AUBREY G1	18.000	1.0500	122	AUBREY	230.00
20122	AUBREY G2	18.000	1.0500	122	AUBREY	230.00
30122	AUBREY G3	18.000	1.0500	122	AUBREY	230.00
40122	AUBREY G4	18.000	1.0500	122	AUBREY	230.00
50122	AUBREY G5	18.000	1.0500	122	AUBREY	230.00
60122	AUBREY G6	18.000	1.0500	122	AUBREY	230.00
10123	AUSTEN G1	18.000	1.0499	123	AUSTEN	230.00
20123	AUSTEN G2	18.000	1.0499	123	AUSTEN	230.00
30123	AUSTEN G3	18.000	1.0499	123	AUSTEN	230.00

Table D.5: Load data

Bus no	Bus name	Base Voltage (kV)	Active Power (MW)	Reactive Power (Mvar)
1101	ABEL	13.8	118.8	24.2
1102	ADAMS	13.8	106.7	22.0
1103	ADLER	13.8	198.0	40.7
1104	AGRICOLA	13.8	81.4	16.5
1105	AIKEN	13.8	78.1	15.4
1106	ALBER	13.8	149.6	30.8
1107	ALDER	13.8	137.5	27.5
1108	ALGER	13.8	188.1	38.5
1109	ALI	13.8	192.5	39.6
1110	ALLEN	13.8	214.5	44.0
1113	ARNE	13.8	291.5	59.4
1114	ARNOLD	13.8	213.4	42.9
1115	ARTHUR	13.8	348.7	70.4
1116	ASSER	13.8	110.0	22.0
1118	ASTOR	13.8	366.3	74.8
1119	ATTAR	13.8	199.1	40.7
1120	ATTILA	13.8	140.8	28.6

Table D.6: 138 kV line data

from bus		to bus					
Bus no	Bus name	Bus no	Bus name	circuit no	R (pu)	X (pu)	B (pu)
101	ABEL	102	ADAMS	1	0.0030	0.0140	0.4610
101	ABEL	103	ADLER	1	0.0550	0.2110	0.0570
101	ABEL	105	AIKEN	1	0.0220	0.0850	0.0230
102	ADAMS	104	AGRICOLA	1	0.0330	0.1270	0.0340
102	ADAMS	106	ALBER	1	0.0500	0.1920	0.0520
103	ADLER	109	ALI	1	0.0310	0.1190	0.0320
104	AGRICOLA	109	ALI	1	0.0270	0.1040	0.0280
105	AIKEN	110	ALLEN	1	0.0230	0.0880	0.0240
106	ALBER	110	ALLEN	1	0.0140	0.0610	2.4590
107	ALDER	108	ALGER	1	0.0080	0.0300	0.0085
107	ALDER	108	ALGER	2	0.0080	0.0300	0.0085
108	ALGER	109	ALI	1	0.0430	0.1650	0.0450
108	ALGER	110	ALLEN	2	0.0430	0.1650	0.0450
all values expressed in (pu) of system MVA (100 MVA)							

Table D.7: 138 kV line data

from bus		to bus			Rate	Rate	Rate	Line
Bus no	Bus name	Bus no	Bus name	circuit no	A (MVA)	B (MVA)	C (MVA)	Length (km)
101	ABEL	102	ADAMS	1	175.0	193.0	200.0	3.0
101	ABEL	103	ADLER	1	175.0	208.0	220.0	55.0
101	ABEL	105	AIKEN	1	175.0	208.0	220.0	22.0
102	ADAMS	104	AGRICOLA	1	175.0	208.0	220.0	33.0
102	ADAMS	106	ALBER	1	175.0	208.0	220.0	50.0
103	ADLER	109	ALI	1	175.0	208.0	220.0	31.0
104	AGRICOLA	109	ALI	1	175.0	208.0	220.0	27.0
105	AIKEN	110	ALLEN	1	175.0	208.0	220.0	23.0
106	ALBER	110	ALLEN	1	175.0	193.0	200.0	16.0
107	ALDER	108	ALGER	1	87.5	104.0	110.0	16.0
107	ALDER	108	ALGER	2	87.5	104.0	110.0	16.0
108	ALGER	109	ALI	1	175.0	208.0	220.0	43.0
108	ALGER	110	ALLEN	2	175.0	208.0	220.0	43.0

Table D.8: 230 kV line data

from bus		to bus					
Bus no	Bus name	Bus no	Bus name	circuit no	R (pu)	X (pu)	B (pu)
111	ANNA	113	ARNE	1	0.0060	0.0480	0.1000
111	ANNA	114	ARNOLD	1	0.0050	0.0420	0.0880
112	ARCHER	113	ARNE	1	0.0060	0.0480	0.1000
112	ARCHER	123	AUSTEN	1	0.0120	0.0970	0.2030
113	ARNE	123	AUSTEN	1	0.0110	0.0870	0.1820
114	ARNOLD	116	ASSER	1	0.0050	0.0590	0.0820
115	ARTHUR	116	ASSER	1	0.0020	0.0170	0.0360
115	ARTHUR	121	ATTLEE	1	0.0060	0.0490	0.1030
115	ARTHUR	121	ATTLEE	2	0.0060	0.0490	0.1030
115	ARTHUR	124	AVERY	1	0.0070	0.0520	0.1090
116	ASSER	117	ASTON	1	0.0030	0.0260	0.0550
116	ASSER	119	ATTAR	1	0.0030	0.0230	0.0490
117	ASTON	118	ASTOR	1	0.0020	0.0140	0.0300
117	ASTON	122	AUBREY	1	0.0140	0.1050	0.2210
118	ASTOR	121	ATTLEE	1	0.0030	0.0260	0.0550
118	ASTOR	121	ATTLEE	2	0.0030	0.0260	0.0550
119	ATTAR	120	ATTILA	1	0.0050	0.0400	0.0830
119	ATTAR	120	ATTILA	2	0.0050	0.0400	0.0830
120	ATTILA	123	AUSTEN	1	0.0030	0.0220	0.0460
120	ATTILA	123	AUSTEN	2	0.0030	0.0220	0.0460
121	ATTLEE	122	AUBREY	1	0.0090	0.0680	0.1420
all values expressed in (pu) of system MVA (100 MVA)							

Table D.9: 230 kV line data

from bus		to bus						
Bus no	Bus name	Bus no	Bus name	circuit no	Rate A (MVA)	Rate B (MVA)	Rate C (MVA)	Line Length (km)
111	ANNA	113	ARNE	1	500.0	600.0	625.0	33.0
111	ANNA	114	ARNOLD	1	500.0	600.0	625.0	29.0
112	ARCHER	113	ARNE	1	500.0	600.0	625.0	33.0
112	ARCHER	123	AUSTEN	1	500.0	600.0	625.0	67.0
113	ARNE	123	AUSTEN	1	500.0	600.0	625.0	60.0
114	ARNOLD	116	ASSER	1	500.0	600.0	625.0	27.0
115	ARTHUR	116	ASSER	1	500.0	600.0	625.0	12.0
115	ARTHUR	121	ATTLEE	1	500.0	600.0	625.0	34.0
115	ARTHUR	121	ATTLEE	2	500.0	600.0	625.0	34.0
115	ARTHUR	124	AVERY	1	500.0	600.0	625.0	36.0
116	ASSER	117	ASTON	1	500.0	600.0	625.0	18.0
116	ASSER	119	ATTAR	1	500.0	600.0	625.0	16.0
117	ASTON	118	ASTOR	1	500.0	600.0	625.0	10.0
117	ASTON	122	AUBREY	1	500.0	600.0	625.0	73.0
118	ASTOR	121	ATTLEE	1	500.0	600.0	625.0	18.0
118	ASTOR	121	ATTLEE	2	500.0	600.0	625.0	18.0
119	ATTAR	120	ATTILA	1	500.0	600.0	625.0	27.5
119	ATTAR	120	ATTILA	2	500.0	600.0	625.0	27.5
120	ATTILA	123	AUSTEN	1	500.0	600.0	625.0	15.0
120	ATTILA	123	AUSTEN	2	500.0	600.0	625.0	15.0
121	ATTLEE	122	AUBREY	1	500.0	600.0	625.0	47.0

Table D.10: 138 kV generator step-up transformer data

from bus		to bus					
Bus no	Bus name	Bus no	Bus name	R (pu)	X (pu)	Rating (MVA)	HV tap (pu)
101	ABEL	10101	ABEL G1	0.003	0.15	24	1.05
101	ABEL	20101	ABEL G2	0.003	0.15	24	1.05
101	ABEL	30101	ABEL G3	0.003	0.15	89	1.05
101	ABEL	40101	ABEL G4	0.003	0.15	89	1.05
102	ADAMS	10102	ADAMS G1	0.003	0.15	24	1.05
102	ADAMS	20102	ADAMS G2	0.003	0.15	24	1.05
102	ADAMS	30102	ADAMS G3	0.003	0.15	89	1.05
102	ADAMS	40102	ADAMS G4	0.003	0.15	89	1.05
107	ALDER	10107	ALDER G1	0.003	0.15	118	1.05
107	ALDER	20107	ALDER G2	0.003	0.15	118	1.05
107	ALDER	30107	ALDER G3	0.003	0.15	118	1.05
106	ALBER	10106	ALBER SVC	0.003	0.15	100	1.05
all impedances expressed in (pu) of transformer MVA all transformers represented with 5 tap positions (2.5%), no LTC							

Table D.11: 230 kV generator step-up transformer data

from bus		to bus					
Bus no	Bus name	Bus no	Bus name	R (pu)	X (pu)	Rating (MVA)	HV tap (pu)
113	ARNE	10113	ARNE G1	0.003	0.15	232	1.05
113	ARNE	20113	ARNE G2	0.003	0.15	232	1.05
113	ARNE	30113	ARNE G3	0.003	0.15	232	1.05
115	ARTHUR	10115	ARTHUR G1	0.003	0.15	14	1.05
115	ARTHUR	20115	ARTHUR G2	0.003	0.15	14	1.05
115	ARTHUR	30115	ARTHUR G3	0.003	0.15	14	1.05
115	ARTHUR	40115	ARTHUR G4	0.003	0.15	14	1.05
115	ARTHUR	50115	ARTHUR G5	0.003	0.15	14	1.05
115	ARTHUR	60115	ARTHUR G6	0.003	0.15	182	1.05
116	ASSER	10116	ASSER G1	0.003	0.15	182	1.05
118	ASTOR	10118	ASTOR G1	0.003	0.15	471	1.05
121	ATTLEE	10121	ATTLEE G1	0.003	0.15	471	1.05
122	AUBREY	10122	AUBREY G1	0.003	0.15	53	1.05
122	AUBREY	20122	AUBREY G2	0.003	0.15	53	1.05
122	AUBREY	30122	AUBREY G3	0.003	0.15	53	1.05
122	AUBREY	40122	AUBREY G4	0.003	0.15	53	1.05
122	AUBREY	50122	AUBREY G5	0.003	0.15	53	1.05
122	AUBREY	60122	AUBREY G6	0.003	0.15	53	1.05
123	AUSTEN	10123	AUSTEN G1	0.003	0.15	182	1.05
123	AUSTEN	20123	AUSTEN G2	0.003	0.15	182	1.05
123	AUSTEN	30123	AUSTEN G3	0.003	0.15	412	1.05
114	ARNOLD	10114	ARNOLD SVC	0.003	0.15	200	1.05
all impedances expressed in (pu) of transformer MVA all transformers represented with 5 tap positions (2.5%), no LTC							

Table D.12: 230 kV/138 kV transformer data

138 kV bus		230 kV bus					
Bus no	Bus name	Bus no	Bus name	R (pu)	X (pu)	Rating (MVA)	HV tap (pu)
103	ADLER	124	AVERY	0.002	0.084	400	0.9125
109	ALI	111	ANNA	0.002	0.084	400	0.9217
109	ALI	112	ARCHER	0.002	0.084	400	0.9192
110	ALLEN	111	ANNA	0.002	0.084	400	0.9798
110	ALLEN	112	ARCHER	0.002	0.084	400	0.9755
all impedances expressed in (pu) of transformer MVA							

Table D.13: 230 kV/138 kV transformer LTC data

138 kV bus		230 kV bus		voltage range	
Bus no	Bus name	Bus no	Bus name	max (pu)	min (pu)
103	ADLER	124	AVERY	1.01458	0.99573
109	ALI	111	ANNA	1.03278	1.01359
109	ALI	112	ARCHER	1.03278	1.01359
110	ALLEN	111	ANNA	1.01951	1.00057
110	ALLEN	112	ARCHER	1.01951	1.00057
voltage range at 138 kV buses					

Table D.14: Load step-down transformer data

HV bus		LV bus					
Bus no	Bus name	Bus no	Bus name	R (pu)	X (pu)	Rating (MVA)	HV tap (pu)
101	ABEL	1101	ABEL	0.003	0.15	150	0.9568
102	ADAMS	1102	ADAMS	0.003	0.15	150	0.9614
103	ADLER	1103	ADLER	0.003	0.15	250	0.9359
104	AGRICOLA	1104	AGRICOLA	0.003	0.15	100	0.9333
105	AIKEN	1105	AIKEN	0.003	0.15	100	0.9298
106	ALBER	1106	ALBER	0.003	0.15	200	0.9625
107	ALDER	1107	ALDER	0.003	0.15	200	0.9561
108	ALGER	1108	ALGER	0.003	0.15	250	0.9438
109	ALI	1109	ALI	0.003	0.15	250	0.9534
110	ALLEN	1110	ALLEN	0.003	0.15	250	0.9315
113	ARNE	1113	ARNE	0.003	0.15	350	0.9448
114	ARNOLD	1114	ARNOLD	0.003	0.15	250	0.9313
115	ARTHUR	1115	ARTHUR	0.003	0.15	400	0.9324
116	ASSER	1116	ASSER	0.003	0.15	150	0.9431
118	ASTOR	1118	ASTOR	0.003	0.15	450	0.9640
119	ATTAR	1119	ATTAR	0.003	0.15	250	0.9414
120	ATTILA	1120	ATTILA	0.003	0.15	200	0.9611
all impedances expressed in (pu) of transformer MVA							

Table D.15: Load step-down transformer data LTC data

Bus name	HV Bus no	LV Bus no	voltage range (at load LV bus) max (pu)	min (pu)
ABEL	101	1101	1.05	1.03982
ADAMS	102	1102	1.05	1.03974
ADLER	103	1103	1.05	1.04
AGRICOLA	104	1104	1.05	1.03974
AIKEN	105	1105	1.05	1.03967
ALBER	106	1106	1.045	1.025
ALDER	107	1107	1.05	1.03983
ALGER	108	1108	1.05	1.03996
ALI	109	1109	1.05	1.03998
ALLEN	110	1110	1.05	1.03999
ARNE	113	1113	1.05	1.04003
ARNOLD	114	1114	1.05	1.04
ARTHUR	115	1115	1.05	1.04006
ASSER	116	1116	1.05	1.03979
ASTOR	118	1118	1.05	1.04005
ATTAR	119	1119	1.05	1.03997
ATTILA	120	1120	1.05	1.03984

Table D.16: SVC data

Bus no	Bus name	Base Voltage (kV)	Scheduled Voltage (pu)	Inductive Range (Mvar)	Capacitive Range (Mvar)
10106	ALBER SVC	18.000	1.0500	−50.00	100.00
10114	ARNOLD SVC	18.000	1.0500	−50.00	200.00

Table D.17: Line shunt data

Bus no	Bus name	Base Voltage (kV)	Line Reactor (Mvar)
106	ALBER	138.00	75.00
110	ALLEN	138.00	75.00